A MICROSTRUCTURAL STUDY OF HAZ CRACKING IN CONVENTIONALLY AND DIRECTIONALLY CAST POLYCRYSTALLINE AND SINGLE CRYSTAL IN-738 LC

BY

JINAL N. SANGHVI

A thesis submitted to Faculty of Graduate Studies in partial fulfillment of the requirement for the degree of

MASTER OF SCIENCE

Department of Mechanical and Manufacturing Engineering
University of Manitoba
Winnipeg, Manitoba.
2014

ABSTRACT

IN 738, a precipitation hardened nickel based superalloy, containing substantial amounts of Al + Ti contents, is very difficult to weld due to its high susceptibility to HAZ cracking, during welding via conventional fusion welding techniques and subsequent PWHT. The cracking in IN 738 is mainly intergranular in nature and associated with liquation of secondary solidification products (such as MC carbides, γ - γ' eutectic phases), and solid state reaction products (γ' precipitate particles) that are present along the grain boundaries in the pre-weld material. The current research presents the results of a study of weld cracking observed in the laser welds produced autogenously on conventionally solidified polycrystalline (CS) and directionally solidified polycrystalline (DS), and single crystal (SC) IN 738 LC subjected to two different pre weld heat treatments (NHT - new heat treatment and UMT University of Manitoba treatment). Weldability was assessed by measuring the total crack lengths in HAZ region. The following two approached were made in order to understand their influence on weldability of IN-738 LC.

The first approach was to study the effect of grain boundaries on the weldability. HAZ intergranular cracking was observed in all the three cast forms and the extent of which was observed to be considerably reduced due to the reduction in number of grain boundaries. The SC alloy did not crack at all both in FZ and HAZ despite the presence of stray grains in the fusion zone. Therefore, for a SC IN-738 LC, weldability was drastically improved which is attributed to absence of grain boundaries in the material.

The second approach, further investigated the effect of pre-weld heat treatment on weldability of IN-738 LC. It was observed in the current work that HAZ cracking was significantly reduced using the a recently developed over aging pre-weld heat treatment, NHT in DS and CS alloys

when compared to UMT treated samples. Microstructural study of welded samples and gleeble thermo-mechanical simulations showed that the improvement in weldability of NHT treated samples was primarily due to reduction in the amount of liquation and also by reducing the sub-solidus non-equilibrium segregation of boron atoms on the grain boundaries liberated during dissociation of boride particles. There was also a marginal change in cracking after PWHT.

Therefore, the current research shows that reducing the grain boundaries improves the weldability of IN-738 LC. Also the use of NHT pre-weld heat treatment over the commonly used UMT could also prove to be beneficial for the overall reduction in HAZ cracking in this alloy.

ACKNOWLEDGEMENT

I would like to take this opportunity to express my sincerest gratitude to my professors, Prof. M. C. Chaturvedi, and Prof. O. A. Ojo for giving me the opportunity to work with them on my Masters research project and also helping me financially during the course of my work. I am very grateful to my supervisors for their continual support throughout my Masters program. I would like to acknowledge both for providing me with their valuable guidance, timely advice and their encouragements to accomplish my end goal. I acknowledge and sincerely thank Dr. K. R. Vishwakarma for her endless support and guidance technically and emotionally.

I am grateful to NSERC for supporting this research financially. I would also like to thank Mr. John Van Dorp, Mr. Don Mardis, Mr. Mike Boskwick and Mr. Trevor Smith of the Mechanical engineering department for their technical assistance.

I would like to thank all my friends including Osoba Lawrence, Jianqi Zhang, Johnson Aina, Ola Dele, who have made my time at the University of Manitoba enjoyable and also helped me technically. Finally, I am grateful to my family for their understanding and wonderful support throughout my masters and especially to my father who always wished that I study further and be successful in life. And lastly I would also like to thank my son for being so understanding at his age.

Dedicated to

My

Husband

Nishant Dhruve

TABLE OF CONTENTS

LIST OF FIGURES

LIST OF TABLES

Copyright Permissions

Figure 2-2: Source – "Welding Metallurgy" (2nd Ed) by Sindo Kuo. Reprinted with permission from Copyright Clearance Centre, John Wiley & Sons, Inc. (16th June, 2014)

Figure 2-3: Source – "Welding Metallurgy" (2nd Ed) by Sindo Kuo. Reprinted with permission from Copyright Clearance Centre, John Wiley & Sons, Inc. (16th June, 2014)

Figure 2-4: Source – "Welding Metallurgy" (2nd Ed) by Sindo Kuo. Reprinted with permission from Copyright Clearance Centre, John Wiley & Sons, Inc. (16th June, 2014)

Figure 2-5: Source – "Welding Metallurgy" (2nd Ed) by Sindo Kuo. Reprinted with permission from Copyright Clearance Centre, John Wiley & Sons, Inc. (16th June, 2014)

Figure 2-6a: Source– JOM Journal of the Minerals, Metals and Materials Society by S.A. David Reprinted with permission from Copyright Clearance Centre. (12th June, 2014)

Figure 2-7: Source – "Welding Metallurgy" (2nd Ed) by Sindo Kuo. Reprinted with permission from Copyright Clearance Centre, John Wiley & Sons, Inc. (16th June, 2014)

Figure 2-8: Source – "Superalloy: A Technical Guide" by E.F. Bradley. Reprinted with permission (26th June, 2014)

Figure 2-9: Source – "Welding Journal. Reprinted with permission. (28th August, 2014)

Figure 2-10: Source – Welding Journal. Reprinted with permission. (28th August, 2014)

Figure 2-11: Source – Maney Publishing author Institute of Metals. Reprinted from P.N. Quested, S. Osgerby, Mater.Sci.Technol. 2 (1986) 461-475, with permission from Copyright Clearance Centre. (24th June, 2014)

Figure 4-24: Source – Metallurgical and Materials Transactions A. Reprinted from O.A. Ojo, N.L. Richards, M.C. Chaturvedi, Metall Mat Trans A Phys Metall Mat Sci. 37 (2006) 421-433, with permission from Copyright Clearance Centre. (24th June, 2014)

Chapter 1.Introduction

1.1 General Overview

Nickel based superalloys are used in the industrial and aero based gas turbine engines, specifically in the hot section components. These materials posses outstanding high temperature properties such as creep, tensile strength, fracture toughness and corrosion resistance that are required to withstand aggressive conditions encountered during operation [1]. Many nickel based superalloys have been developed which includes both solid solution strengthened and precipitation hardened alloys to meet the specific requirements.

Conventionally solidified poly crystalline IN-738 LC (CS), a precipitation hardened nickel base superalloy, is widely used as blade materials in the hot section components. With the purpose of meeting the demands of higher operating temperature and improving the performance of the alloy, significant progress has been made in advance processing techniques. Directional solidification processing generates alloys with reduced number of grain boundaries (directionally solidified, DS) and can even completely eliminate grain boundaries (single crystal, SC) and further improving the creep rupture, high temperature ductility, fatigue and hot corrosion properties.

However, cost effective and viable manufacturing and repair of new components, damaged components is dependent upon the ability to fabricate by fusion welding techniques in a satisfactory manner. Laser welding technique is one of the most attractive fusion welding techniques for fabrication and repair of superalloys, as it offers several advantages over conventional welding methods which include high production rate as well as, flexibility to weld

intricate shapes. Laser welding produces low-heat input welds due to concentrated heat source with reduced heat affected zone and physical distortion. Rapid solidification during laser welding improves weld performance and component service life.

Welding of IN-738 LC is difficult and challenging due to presence of significant volume fraction of γ' (Ni_3 (Al, Ti)) precipitate particles, the primary strengthening phase. Weldability problem could be more pronounced in DS and SC cast forms of IN-738 LC due to coarse microstructure and increased level of elemental segregation. IN 738 superalloy is extremely susceptible to heat affected zone (HAZ) cracking during welding and subsequent post-weld heat treatment (PWHT). HAZ cracking in this alloy is mainly attributed to intergranular liquation occurring during the weld thermal cycle due to constitutional liquation of various phases as well as grain boundaries due to segregation of low melting point alloying elements.

1.2 Research Objective

The main objectives of the present research were:

- To study the effect of number of grain boundaries on HAZ microfissuring in IN-738 LC during laser beam welding.
- To study the effect of pre-weld heat treatment on reduction of HAZ cracking during laser beam welding of DS and CS IN-738 LC.

1.3 Methodology

With the aim of achieving above mentioned objectives, laser welding was done on different cast forms of IN-738 LC and prior to welding the test coupons were subjected to NHT (New heat treatment) and UMT (University of Manitoba heat treatment) pre-weld heat treatments. Gleeble

simulations of the thermal cycle experienced in the HAZ of CS IN-738 LC alloy during welding were performed by Gleeble thermo-mechanical simulation system. Microstructural analysis of the welded samples and Gleeble simulated samples was carried out to assess the weldability of the materials and the factors responsible for enhancing the susceptibility to cracking were also identified.

1.4 Major Findings

Microstructural analysis of the weld sections of SC, DS and CS IN-738 LC subjected to UMT pre-weld heat treatment has shown that, a reduction in the number of grain boundaries intersecting the fusion boundary, leads to a reduction in the extent of HAZ microfissuring. In DS IN-738 LC, substantially less amount of HAZ cracking was observed when compared to CS IN-738 LC alloy, while, SC IN-738 LC did not crack in both HAZ and fusion zone. Susceptibility to HAZ microfissuring was extensively influenced by presence of grain boundaries.

A comparative study of HAZ microfissuring in NHT to UMT pre-weld heat treatments revealed that the extent of HAZ microfissuring drastically reduced in weld of DS IN-738 LC subjected to NHT heat treatment. The Gleeble simulation study further revealed that non-equilibrium liquation of various secondary phases that were present in the alloy extensively contributed to intergranular liquation in HAZ. In addition to this, it was found that the onset of liquation in UMT samples took place at a much lower temperature than NHT samples, which could have resulted in extensive HAZ intergranular cracking during welding of UMT samples.

It was also observed that, the effect of grain boundary on HAZ microfissuring after PWHT followed the same pattern i.e. SC < DS < CS. And, also NHT heat treatment was observed to be

effective in reducing cracking in DS and CS IN-738 LC alloy during welding and subsequent PWHT.

1.5 Thesis Organisation

This thesis consists of 6 chapters and is organized as follows:

- **Chapter 1** contains a brief background, problem description, objectives of the study, methodology used and major findings.
- **Chapter 2** is the literature review which consists of a general overview of nickel based superalloys and their welding metallurgy, welding techniques used on these alloys, and the problems associated with welding. Lastly, the scope and objectives of this research were laid out.
- **Chapter 3** gives details on the methodology and instruments used in the research.
- **Chapter 4** provides results of the experimental work carried out and its analysis.
- **Chapter 5** contains a summary of the major findings and conclusions.
- **Chapter 6** presents recommendations for future work.

Chapter 2.Literature Review

2.1 Physical Metallurgy of IN 738

IN 738, a nickel (Ni) based superalloy which was first developed by the Paul D. Merica Research Laboratory of the International Nickel Company Inc., is ideal for most demanding high temperature applications, including components of turbine engines, such as turbine blades and hot section components of modern power generation turbines. This alloy is processed by vacuum melting, investment cast, and later subjected to a hot isostatic press in order to reduce the amount of micro porosities in the solidifying ingot [2]. It is a Ni-chromium (Cr)-cobalt (Co) based superalloy designed to combine the strength of IN 713C, and oxidation and sulphidation resistance of Udimet 500. Depending on the carbon content, there exists two different forms of IN 738 alloys; a low carbon version (C ~ 0.09-0.13 wt %) designated as IN-738 LC, and a high carbon version (C ~ 0.15-0.20 wt %) designated as IN 738C. The zirconium (Zr) levels in the former are lowered in order to obtain superior casting quality of sections with larger dimensions [3]. Table 2-1 lists the nominal composition of IN-738 LC used in this particular study [3]. The major alloying constituents are Cr, Co, aluminum (Al), titanium (Ti), and small amounts of tungsten (W), niobium (Nb), molybdenum (Mo), tantalum (Ta), and traces of boron (B), Zr, and carbon.

Table 2-1: Nominal composition of alloy IN 738 [3]

Elements	**IN-738 C (wt%)**	**IN-738 LC (wt %)**
Carbon	0.17	0.11
Cobalt	8.50	8.50
Chromium	16.00	16.00
Molybdenum	1.75	1.75
Tungsten	2.60	2.60
Tantallum	1.75	1.75
Niobium	0.90	0.90
Aluminium	3.40	3.40
Titanium	3.40	3.40
Boron	0.010	0.010
Zirconium	0.05	0.05
Iron	VL*	VL*
Manganese	VL*	VL*
Silicon	VL*	VL*
Sulphur	VL*	VL*
Nickel	Bal*	Bal*

* Very Low

** Balance

These alloying elements increase the strength of the alloy by solid solution strengthening and precipitation hardening. In addition to this, carbides directly impart strength by stabilising the grain boundaries at high temperatures. The gamma phase (γ) is a fcc austenitic phase formed by the solid solution of various elements which includes Ni, Co, Cr, Mo, and W. The atomic radius of the elements Co, Cr, Mo, and W is similar to that of Ni, and prefer to partition to the austenitic γ solid solution because they contribute to its stabilisation, and as well, act as solid solution strengtheners. Al and Ti are the basis for precipitation hardening. Al, Ti, and Ta have atomic radii greater than that of Ni and partition to form a face centered cubic (FCC) intermetallic compound (Ni_3 (Al, Ti)) known as gamma prime (γ′). The high temperature strength is mainly derived from the coherent precipitation of an ordered $L1_2$ intermetallic γ′ phase [4]. The service temperatures can be as high as 980^0C which impart excellent corrosion and creep resistance [3]. Cr and Al impart high temperature oxidation resistance by forming protective layers of Cr_2O_3 and Al_2O_3. The presence of traces of B, Zr and carbon helps to reduce the tendency of the grain boundaries to crack. The major phases present in cast IN 738 are discussed in the following section [5].

2.2 Microstructure of As-cast IN 738

The major phases present in cast IN 738 includes the gamma prime precipitates (γ′), gamma - gamma prime eutectics (γ-γ′), carbides and borides distributed in the gamma matrix (γ) [6]. A brief discussion of the phases formed is done in the following sections.

2.2.1 Gamma Phase (γ)

The matrix phase, γ, exhibits a FCC crystal structure. This Ni based austenitic phase contains high percentages of elements, such as Cr, Co, Al, Ti, W and Mo that imparts solid solution

strengthening to the matrix. Most of these alloying elements belong to d-block. The difference in atomic diameter of these elements with respect to Ni is in the range of 1-15% and owing to their similar sizes they form substitutional solid solutions. The distortion of the atomic lattice caused by the misfit of the atomic radius inhibits dislocation movement with spherically symmetrical strain fields [7]. This also lowers the stacking fault energy primarily due to the inhibition of dislocations from cross slipping. These are the main deformation modes at elevated temperatures. Another mechanism which contributes to the strength of Ni based superalloys is atomic clustering or the short range order in which the dislocation movements are significantly impeded. The strengthening due to atomic clustering significantly decreases above 0.6 T_m, where T_m is the actual melting temperature. Slow diffusing elements, like W and Mo, help to reduce creep and strength at high temperatures as they are strongly influenced by diffusion at high temperatures [8].

2.2.2 Gamma Prime (γ') Phase

The most important high temperature strengthening phase of Ni based superalloys is derived from the precipitation of the γ' phase. This results from the dispersion of second phase particles of type A_3B. γ' is a $L1_2$ type of intermetallic compound ($Ni_3(Al, Ti)$) with an ordered FCC crystal structure. It is generally formed in alloys that contain Al and Ti in amounts that exceed its solubility in Ni matrix. γ' precipitates are usually coherent with the γ matrix. Figure 2-1 below shows a unit cell of $L1_2$ crystal structure where the Al and Ti atoms occupy the corner of the cube and the Ni atoms at the center of the cube [9]. There are many other elements present in addition to Ni, Al and Ti, such as Nb, Ta, Cr and Co, in trace amounts. The chemical composition of γ' in IN 738 as suggested by Garosshen and McCarthy [10] is given below:

$$(Ni_{0.92}Co_{0.58}Cr_{0.017}Mo_{0.002}W_{0.002})(Al_{0.518}Ti_{0.352}Ta_{0.046}W_{0.014}Cr_{0.020})$$

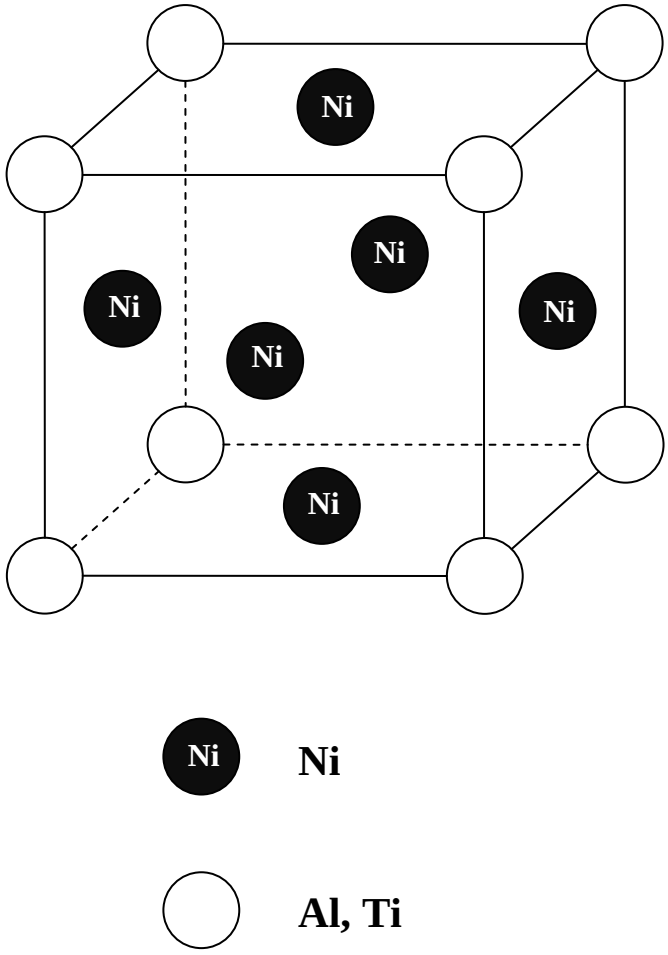

Figure 2-1: Illustration of γ' precipitate unit cell - an ordered FCC crystal structure

γ' precipitates are formed by homogenous precipitation with a low surface energy. The coherency between γ and γ' is maintained up to very high temperatures and are extraordinarily stable. The precipitates and matrix are crystallographically coherent, so the composition of the phase influences the lattice parameters and precipitate matrix misfit. The misfit results in initial internal stresses, and together with a high degree of elastic anisotropy, will strongly influence precipitate shape and resultant mechanical properties. γ' precipitate morphologies have been observed by Hagel and Beattie [11], and have reported that γ' particles are spherical for 0 to ±0.2% mismatches, and become cuboidal for mismatches of about ±0.5% to ±1% and plate-like at mismatches above about ±1.25%.

2.2.3 Gamma - Gamma Prime (γ-γ′) Eutectic Phase

The γ - γ' eutectic is a mixture of γ' phase and thin lamellae of the γ phase and it forms within the interdendritic regions due to continuous enrichment (i.e. elemental microsegregation) of Al and Ti in the solidifying liquid. As discussed above Al and Ti are strong γ' forming elements.

2.2.4 Carbide Phase

Carbides are formed in Ni based super alloys when carbon in amounts of about 0.02 to 0.2 wt% is combined with reactive elements such as Ti, Ta, Nb, Cr, and W and form metal carbides (MC) [12]. The important carbide phases formed in Ni based super alloys are MC, $M_{23}C_6$ and M_6C. Carbides are a potential phase of Ni based superalloys for grain boundary strengthening. However, their role is complex since they can either enhance or deteriorate alloy properties based on their location, composition and shape [4].

Carbides are randomly distributed in the γ matrix and can form within the grains as well as on the grain boundaries. These carbides when properly formed, strengthen the grain boundaries, and

reduce stress along the grain boundaries. Their most important function is to prevent or retard the creep mechanism of grain boundary sliding during high temperature service. Since carbides are harder and more brittle than the alloy matrix, their distribution along grain boundaries will affect high temperature strength and creep performance. Therefore, if a continuous film of carbides is present along grain boundaries, this gives rise to an easy path for crack propagation. Furthermore, if no carbides are present along the grain boundaries, voids are formed, which contribute to excessive grain boundary sliding. The precipitation of these carbides indirectly imparts strengthening by removing reactive elements, which include Mo, W, and Ti, that would otherwise partition to γ or to γ′ thus promoting phase instability during service. The carbides will then hinder grain boundary sliding without adversely affecting the ductility [4,8,13].

MC type carbides are the most refractory carbides with an FCC crystal structure that forms in superalloys during ingot solidification just below the melting point of the alloys (freezing). These carbides formed are discrete blocky particles and have a complex formula [10]:

$$(Ti_{0.5}Ta_{0.2}Nb_{0.2}W_{0.04}Mo_{0.03}Cr_{0.02})C$$

MCs tend to decompose into $M_{23}C_6$ or M_6C carbides by the following reactions [7]:

$$MC + \gamma \longrightarrow \gamma' + M_{23}C_6$$

$$MC + \gamma \longrightarrow \gamma' + M_6C$$

$M_{23}C_6$ is low temperature carbide and readily forms in alloys that contain moderate to high Cr content. It is formed during low temperature heat treatment or exposure to service temperatures of about approximately 760°C to 816°C (1400°F to 1500°F) [4]. $M_{23}C_6$ is primarily formed at grain boundaries. In general, the morphology of this carbide is globular, irregular, and discontinuous, with blocky script-like particles. $M_{23}C_6$ plays an important role, and depending on

its location along grain boundaries, enhances the stress-rupture strength in the alloy by inhibiting grain boundary sliding, except when it occurs in cellular formation which is distinctly deleterious by initiating premature rupture failures.

M_6C is intermediate temperature carbide as it is formed at higher temperatures. In Ni based superalloys, the tendency of the formation of M_6C requires higher concentrations of Mo and W, and higher temperatures of approximately 815^0C to 980^0C (1500^0F to 1800^0F) [4]. Like $M_{23}C_6$ carbides, M_6C carbides can also precipitate at the grain boundaries in a blocky form.

In general, these secondary carbides formed during heat treatment or during exposure to service temperatures, provide significant beneficial effects that includes pinning the dislocations and hardening the alloy, stabilising the grain boundaries against excessive shear, thus improving stress rupture strength.

2.2.5 Boride Phase

Small concentrations of boron present in Ni based superalloys essentially improve creep rupture resistance. Boron segregates to grain boundaries and low density boride particles M_3B_2 are formed. The presence of boron in Ni based superalloy acts to modify the initial grain boundary carbides and also help tie up deleterious elements, such as sulphur and lead. Borides have the beneficial effect of hindering the onset of grain boundary tearing. Borides tend to have high concentrations of Mo, Ti, Ni, Cr, and forms a tetragonal crystal structure with shapes that vary from blocky to half-moon in appearance [14]. These borides formed at the grain boundaries are brittle in nature and melt at lower temperatures than equilibrium solidus which results in reduction in ductility and hot workability of the alloy [15].

2.2.6 Topological Closed Packed Phases

In some superalloys where the composition is not controlled, undesirable phases could form either during heat treatment or service. Many elements, such as Cr, Mo, W, rhenium (Re), etc., are added for their desirable properties; however, excessive quantities promote the precipitation of undesirable intermetallic phases known as topological closed pack (TCP) phases. These phases are generally detrimental, often nucleating on grain boundary carbides. Common TCP phases formed in Ni based superalloy are σ, μ and Laves phases. TCP phases are usually plate- or needle-like phases that form in some compositions and under certain conditions. Ductility and mechanical properties are severely affected by the formation of these phases [4].

2.3 Fusion Welding Process

Fusion welding is a joining process extensively used in many industries that include ship building, aerospace, automotive, chemical, petrochemical, electrical, and power generation. Gas turbine components extensively manufactured and repaired by fusion welding processes [16,17]. Fusion welding process is highly localized process where the total heat energy of a system is concentrated on to a very small region and involves the melting and solidification of adjacent areas of two parts with the application of heat, pressure or both. Fusion welding affects the metallurgical bonds between the respective components. It can be performed in different procedures, one of them is autogenously i.e. by simply melting the edges of two work pieces and allowing them to fuse together upon cooling. Other procedures involve the use of external materials during the process for the fusion to take place, like electrodes or filler materials. The filler material used could be of the same/similar compositions of the base alloy or environmentally and mechanically compatible with those of the material being joined. However, the welded area encompasses a cast structure of variable size and properties that in turn depends

on the materials being welded and welding technique used. Fusion welding can be sub categorized based on the heat source used for fusion of the base material. A variable heat source are used which includes a mixture of gas in the oxy-acetylene gas welding process, an electric arc in arc welding processes and high energy density beam in energy beam welding process [16,17]. Fusion welding has been successfully used to weld many superalloys with little or no difficulties with the exception of those that contain a high percentage of gamma prime, i.e. high Al and Ti content; for example IN 738. A few widely used fusion welding techniques are discussed below.

2.3.1 Oxy-Acetylene Gas Welding Process

The oxy-acetylene gas welding process is the simplest and most frequently used oxy-fuel gas welding process. It is a manual welding process in which the metal surface to be joined is progressively melted by heat from a flame generated by a mixture of gases with or without filler material, and solidifies without application of pressure. The principal gas used is oxygen, for combustion of fuel gases and acetylene, which, contribute to the heat intensity, and atmosphere needed for welding. The combustion of a mixture of the fuel gas and oxygen generates a high temperature flame. As an instrument, its main advantage is that it is portable and inexpensive. On the other hand, due to its limited power density, low speed, and high heat input, it results in severe distortion and larger HAZ. Metals like Al and Ti with high tendency towards oxidation are difficult to weld using this process because of its limited atmospheric protection [17].

2.3.2 Arc Welding Process

The arc welding process is a conventional fusion welding process that uses an electric arc as a heat source to melt and join materials. The arc struck between the work piece and the tip of the

electrode when manually or mechanically moved along the joints. The electrode used is either consumable wire or rod that also serves as the filler material, or non-consumable carbon or tungsten rods. The main purpose of the electrode is to carry the current and sustain the electric arc between its tip and the work piece. Shielding gases or flux-cored electrodes used during arc welding processes to protect the hot weld from oxidation [16,17]. Successful welding of the superalloys is made possible by using a wide variety of arc welding processes, which include: gas tungsten arc welding (GTAW), submerged arc welding (SAW), gas metal arc welding (GMAW), and shielded metal arc welding (SMAW).

Shielded Metal Arc Welding

SMAW is a manual welding process, also known as stick welding. In this process, a weld is produced when an arc is generated between a consumable flux covered electrode and the work piece. The filler metal deposited from the core of the electrode conducts the electric current to the arc and the electrode covering decomposes to form a gaseous shield that protects the electrode tip, molten weld pool, and the arc generated. This covering provides fluxing elements for protection of weld metal droplets and the weld pool from the atmosphere. As the weld pool solidifies, the fluxing elements solidify into a slag layer on top of the weld metal. The major advantage of this process is that it is portable and inexpensive in terms of equipment. The disadvantages includes, the inability to be automated, difficulty in flux removal, slow rates of deposition, difficulty in welding thin sections, and slow production rates due to recurrent electrode changes. SMAW processes are used in joining of solid solution strengthened Ni based superalloys, but rarely for the welding of precipitation strengthened superalloys.

Gas-Metal Arc Welding

GMAW, also commonly known as metal inert gas (MIG) welding, is a process that joins work pieces together by heating them with an arc established between a consumable electrode and the work piece together with a shielding gas or a gas mixture, which protects the arc and the weld pool from the external atmosphere. Figure 2-2 gives a schematic of the GMAW process [16]. The shielding obtained from using inert gases such as helium and argon. A consumable electrode continuously fed in a form of a wire. The GMAW process operates in semi-automatic and automatic modes. The major advantages of this process include continuous feeding of electrodes thus enabling deposition of long welds without interruption, and higher deposition and travel speeds. The limitations that restrict its implementation are complex equipment, less portability in comparison, as the GMAW torch is bulky, and its inability to reach small corners.

Gas-Tungsten Arc Welding

GTAW also referred to as tungsten inert gas (TIG) or HeliArc welding. This is a welding process, in which the joining of work pieces takes place by heat generated from an arc struck between a non-consumable tungsten electrode and the work piece. The shielding obtained from inert gas or a mixture of inert gases, which includes argon and helium, provides a twofold advantage i.e. protection of the electrode, weld pool arc, and adjacent heated areas of the work piece from atmospheric contamination and as well the gases used act as a conducting path for the arc current. Figure 2-3 is a schematic of the GTAW process [16].

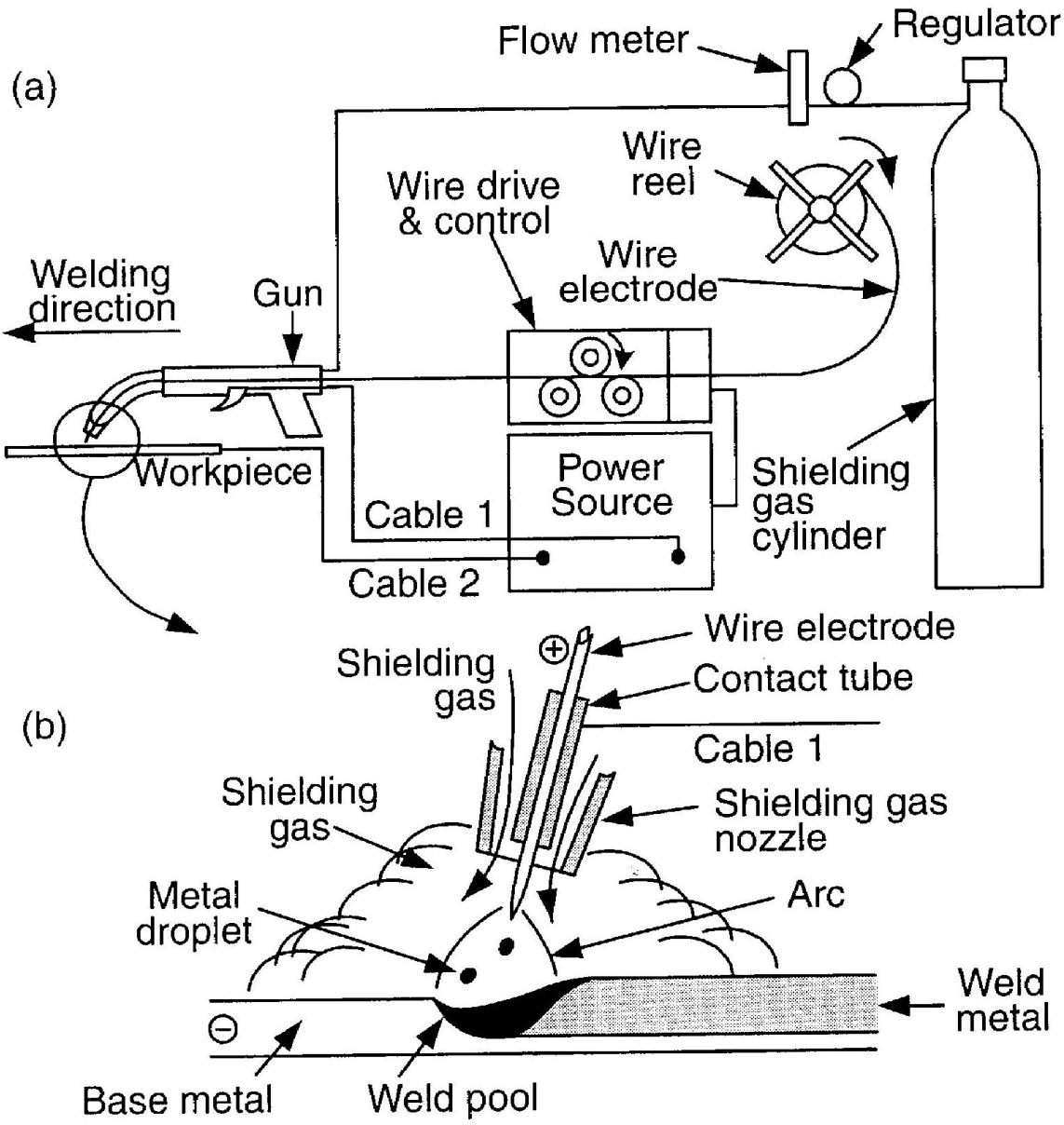

Figure 2-2: An adapted schematic diagram of GMAW showing: a) setup; b) working [16]

Source: "Welding Metallurgy" (2nd Ed) by Sindo Kuo.

Many Ni based superalloys are welded with GTAW process, as these materials require protection from atmospheric contamination and high weld quality. The advantages of GTAW include precise control of heat input, which results in high quality and low distortion welds, suitability for joining thin sections, and use with or without filler wires. The disadvantages associated with this process are lower deposition rates, and possibility of inclusions of brittle tungsten in the weld pool.

2.3.3 Electron Beam Welding

Electron beam welding (EBW) is a fusion welding process that melts and joins the work piece by impinging high energy electrons onto the material to be welded. These electrons are accelerated to velocities ranging from 30% to 70% of the speed of light at 25 to 200 kV, respectively. The kinetic energy of electrons is instantaneously transformed into thermal energy as they impact the surface and penetrates into the material, and producing a required joint. A schematic diagram showing the working of EBW and key-hole mode generation is shown in Figure 2-4 [16]. In EBW, the electron beam generating system uses an electron beam gun which consists of a cathode with a negatively charged filament. The filament emits electrons via thermoionic emission mechanism which are then accelerated towards the anode in an electro-static field generated by a cathode and the anode itself. Further, the electrons flow through a hole in the anode in the form of a collimated tube. Electromagnetic coils are used to focus the electron beam onto the sample surface, where the total kinetic energy of the electrons is concentrated onto a small area on the work piece, and the resultant power densities achieved are as high as 10^8 W/cm^2 (10^7 W/in.^{2}) [16].

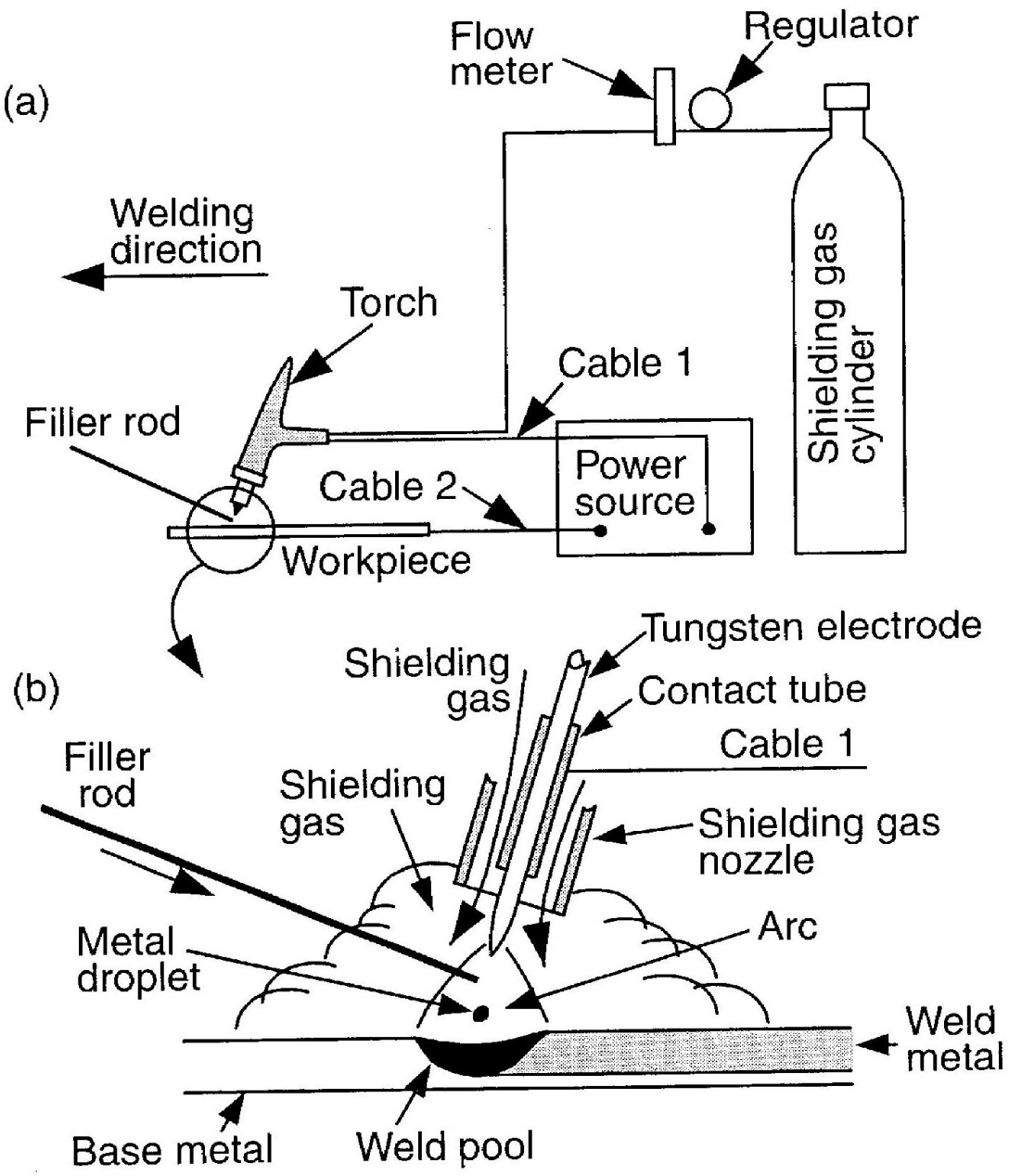

Figure 2-3: An adapted schematic diagram of GTAW showing: a) setup; b) working [16]

Source: "Welding Metallurgy" (2nd Ed) by Sindo Kuo.

A high intensity electron beam instantly penetrates into the work piece, which results in local melting and vaporisation of the material, and forms a capillary vapor known as a key hole, which in turn, is surrounded by molten metal beads on the work piece. Thus electron beams produce welds with an excellent depth to width ratio which is one of their main advantages. EBW can weld thick joints at higher speeds in a single pass, thus resulting in narrow HAZs and less distortions. The EBW process facilitates the welding of most hardened alloys, refractory materials, reactive metals, and the combination of many dissimilar metals that cannot be joined by the arc welding process. Limitations of this process include high equipment and production costs due to the need for high vacuum [16,18].

2.3.4 Laser Beam Welding

Laser beam welding (LBW) is a fusion welding process in which the coalescence of the material is achieved with heat obtained from a concentrated beam of coherent, monochromatic light. The word laser is an acronym for “light amplification by stimulated emission of radiation". Laser can be generated by different mediums, and categorised as solid state and gas lasers. In solid state lasers synthetic rubies and crystals are used to generate the laser beam, for example, Nd:YAG and diode lasers. In gas lasers a mixture of gases (helium, nitrogen or carbon dioxide) are excited to generate the laser beam, for example, CO2 lasers. Solid state lasers generates a laser beam of lower frequency and wavelengths than gas lasers, and thus have much lower power outputs. A schematic of a laser welding system exhibiting the process operation and setup is shown in Figure 2-5 [16].

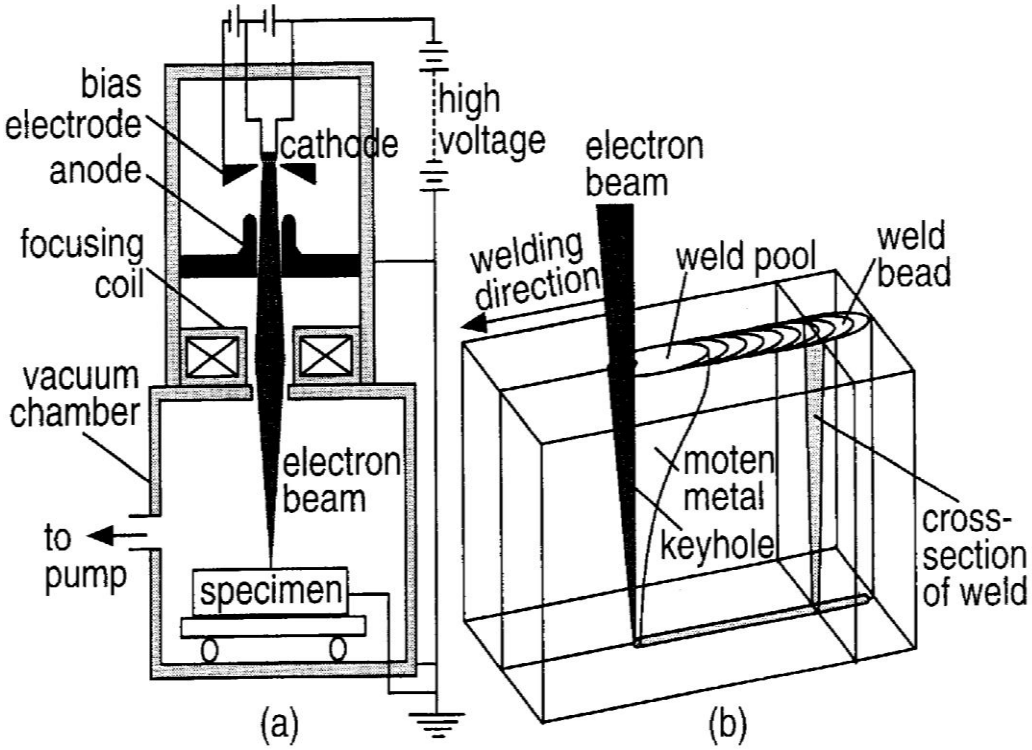

Figure 2-4: An adapted schematic diagram of EBW process a) setup; b) Keyhole mode [16]

Source: "Welding Metallurgy" (2nd Ed) by Sindo Kuo .

The mixture of gases is electrically excited in order to produce the laser beam in a gas laser. The main features of lasers include high-energy concentration and power transfer rate from the source to the work piece. The power densities generated that are greater than 106 W/in2, are a primary factor for its potential in welding. Conductive distribution of heat on the sample surface takes place in a low power density lasers. Whereas, when a high power density lasers are used, a focused laser beam transferred onto the surface, melts the surface and even vaporizes the metal. As a result of this a hole filled with ionized metallic gas forms and this is characterized as keyhole [16,18]. The advantage of the keyhole is that, with its formation, heat energy will be more effectively absorbed and this significantly enhances the welding process, especially by means of penetration. Thus, higher welding speeds could be achieved and much greater depth to width ratios (i.e. good weld penetration through thickness). One of the major advantages of this process is that precise welds with narrow heat affected zones are produced, which is the most critical factor for welding quality. Thus, heat induced distortions are also minimized. As laser beams readily focused, aligned, and redirected by optical/reflecting mirror systems, they can weld in areas that are not easily accessible. Another most important advantage of the laser is that, thick sections can be welded with the single pass laser welding method and without any use of filler metal. Fabrication or repair of difficult to weld materials is possible by using this process. The limiting factors of this process firstly, are high investment costs, and secondly, high reflection at metallic surfaces, and lastly, with respect to work piece, proper alignment, and joint fit-up is a prerequisite for a high weld quality.

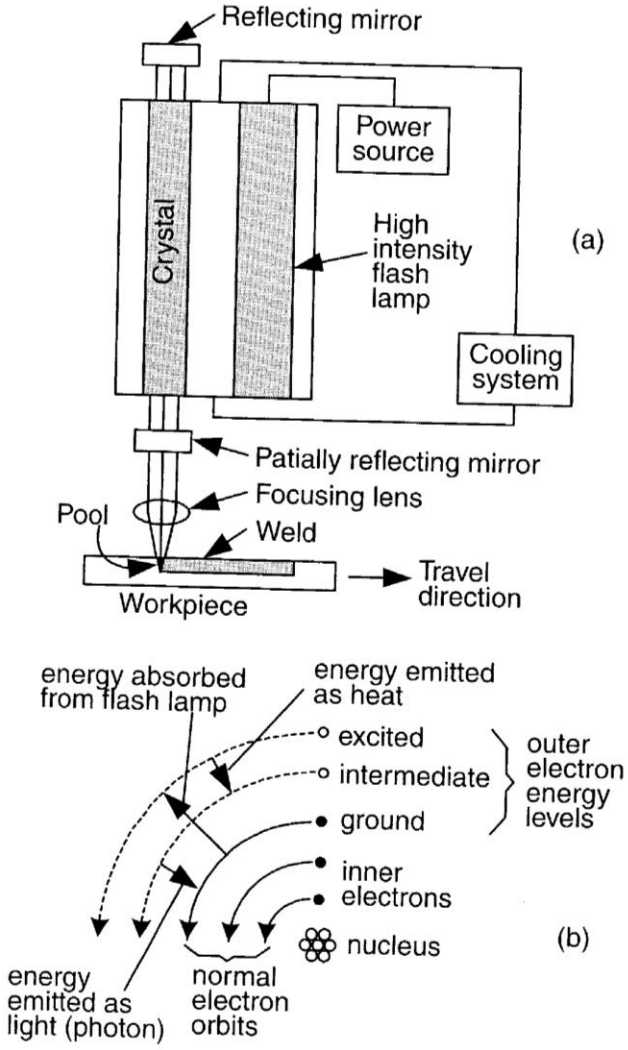

Figure 2-5: Laser beam welding process a) setup; b) working [16]

Source: "Welding Metallurgy" (2nd Ed) by Sindo Ku..

2.4 Microstructure of Weld

During welding, the interaction of the heat source with the material results in melting and solidification (illustrated in Figure 2-6a [19]). A very high temperature gradient within a small region is generated with peak temperatures at the center of the fusion. A typical fusion weld consists of three distinct regions, as shown in Figure 2-6b. They are the fusion zone (FZ), which undergoes melting and solidification, the heat affected zone (HAZ), which experiences significant thermal exposure and undergoes solid-solid phase transformations, and lastly, the unaffected base metal (BM) [16]. The FZ is also known as mini casting as there exists complete localised melting and solidification, and hence the resultant microstructure significantly changes as the temperatures are above liquidus temperatures. The HAZ is the region adjacent to the FZ, which is separated by a fusion boundary. In HAZ, the original microstructure has been altered by the heat generated during welding. In this region, the peak temperatures experienced are below the solidus line. A narrow zone exists at the weld interface that undergoes partial melting of the base material; this zone is known as partially melted zone (PMZ). This region surrounds the weld pool, and the peak temperature experienced lies between the liquidus and the solidus, i.e. the eutectic temperature of the base metal. In high energy density beam welding, like laser welding, the HAZ region is very narrow. The unaffected BM zone surrounds the HAZ which experiences high residual stresses, and does not undergo any microstructural changes [16].

a)

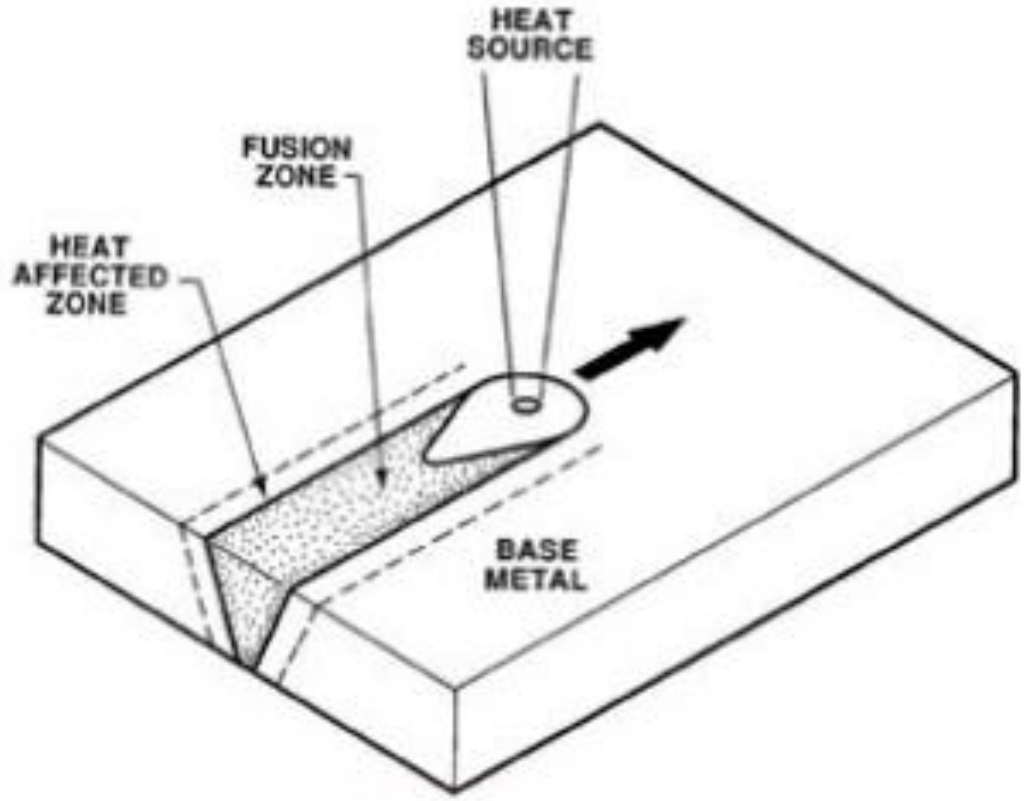

b)

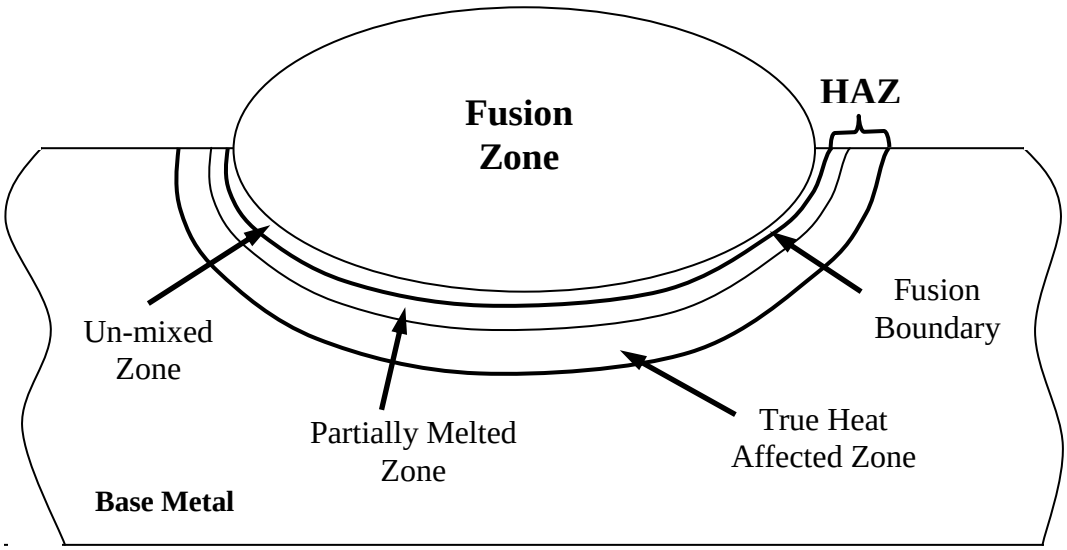

Figure 2-6: Schematic of laser welding: a) Interaction with material [19] b) cross section view of the weld zone

2.4.1 Fusion Zone

The FZ experiences peak temperatures well above the liquidus temperature, thus causing it to completely melt and then solidify [16,19]. The microstructure of the FZ depends on the solidification behavior of the weld pool. The solidification of weld metals and structural formation are influenced by the chemical composition, welding process and welding conditions [20]. The size and shape of the grains, segregation, and the distribution of inclusions and porosities in the weldment is controlled by the principles of solidification. During welding, the interaction of the heat source with the base material causes many changes to occur in the weld zone, which include physical state changes, metallurgical transformation and transient thermal stresses and distortion which complicate the microstructure development in the FZ [21].

The solidification of metals and alloys normally occur in the planar or cellular interface at the fusion boundary. The weld bead shape varies with the type of welding process, heat source, shielding gas used and the conducting properties of the metal being welded. The size and shape of the melt depends on the heat energy being supplied in terms of the moving heat source, i.e. welding speed, and the rate at which heat is transmitted into the surrounding of the metal [21]. When the heat input and welding speed are very low, the shape of the molten weld pool is generally elliptical in shape and the columnar structure grows by curving in the welding direction. When the heat input rate is higher, the weld pool assumes a tear drop shape. Sometimes nearer to the center, equiaxed crystals form along the cellular dendrite or columnar dendrite interface morphology. These are readily formed in alloys with higher solute content and heat input.

In autogenous welding, solidification in the weld pool often occurs without a nucleation barrier, and spontaneously occurs through epitaxial growth on partially melted grains at the fusion line and without altering their existing crystallographic orientation. Moreover, the growth of solid phases in the FZ occurs through a heterogeneous nucleation process. The rejection of the solute ahead of the growing planar interface results in a solute rich liquid at the interface. The stability of the solid/liquid interface is determined by the thermal and constitutional gradient that exists in the near vicinity of the interface, and this is also critical in determining the microstructural characteristic of a weld. Depending on these conditions, the interface growth may occur by planar, cellular or dendritic growth. The significant effects of composition and thermal gradient on the solidification front are described by the concept of the constitutional supercooling criterion and can be mathematically stated as [19,22,23]:

$$\frac{G_L}{R} \geq \frac{\Delta T}{\mathrm{D_L}}$$

This is the steady state form of the criterion for planar growth. Planar instability will occur and the condition for constitutional supercooling where cellular dendritic growth occurs is stated by:

$$\frac{G_L}{R} < \frac{\Delta T}{\mathrm{D_L}}$$

where,

D_L - Diffusion coefficient of the solute in the liquid.

$\Delta T = T_L - T_s$, equilibrium freezing range, which is the temperature difference across the boundary layer.

G_L - Temperature gradient in the liquid

R- Growth rate at the solidification front.

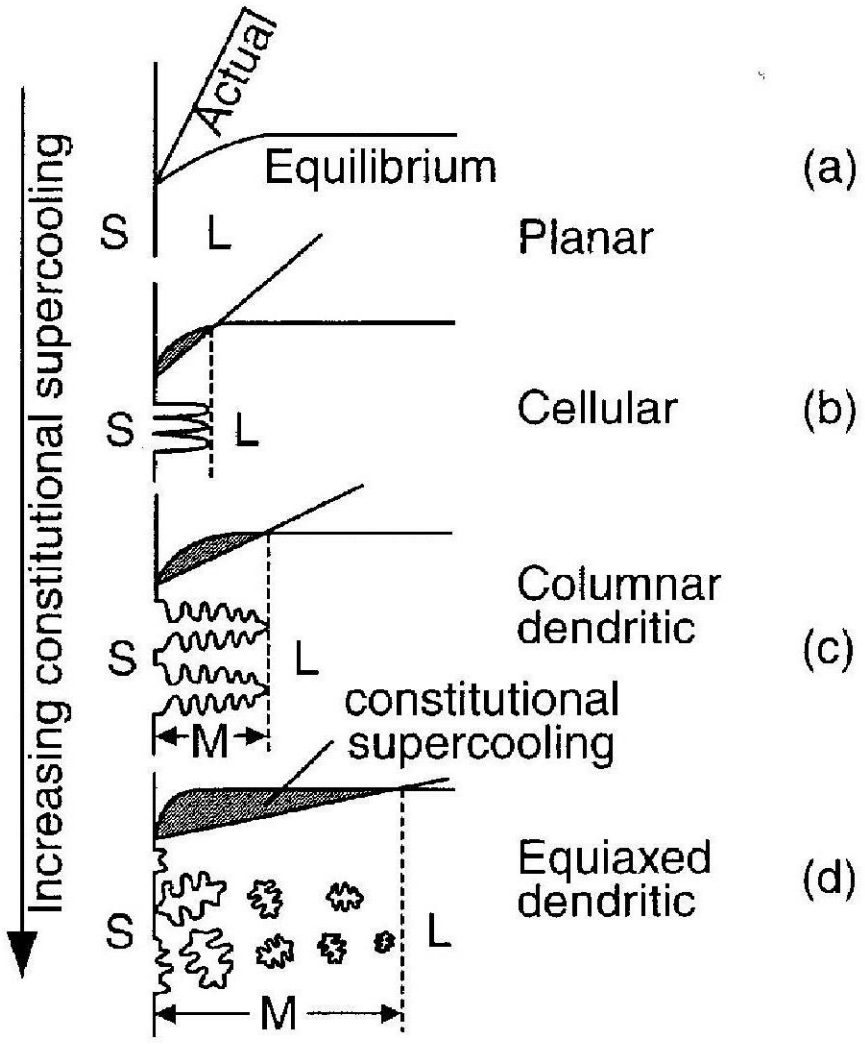

Figure 2-7: Effect of constitutional supercooling: (a) Planar; (b) Cellular; (c) Columnar dendritic; (d) Equiaxed dendritic (M denotes mushy zone) [16]

As the degree of constitutional supercooling increases, the solidification mode at the solid/liquid interface changes from planar to cellular, cellular to columnar dendritic, and finally, from columnar dendritic to equiaxed dendrite; this effect of constitutional supercooling is schematically described in Figure 2-7 [16]. The region where the liquid phase and dendrites coexists is termed as the mushy zone. With increasing degree of supercooling, the area of the mushy zone increases which makes it easier for equiaxed dendrites to nucleate compared to columnar or cellular dendrites, as at this stage, the temperature gradient across the melt is low with little or no turbulence. High energy power density welding, like laser welding, produces a narrow FZ typically observed as a wine glass shape.

Solute redistribution

Solute redistribution occurs during the rapid solidification of alloys in advancing weld pools. This is a very important phenomenon that occurs during welding and which can explain the behaviour of the segregation of elements which drastically affect the weldability, microstructure and properties of the weld produced. Segregation on a fine scale with dendrite arm spacing in the range of 10 to 100 μm is called micro-segregation. When the scale is as large as several hundreds of micrometers, the segregation is known as macro-segregation [20,23,24]. Micro-segregation occurs during planar, cellular, cellular dendritic and equiaxed interface growth in the weld solidification process. The compositional effects on the solidification of an alloy can be divided into three cases [23,25,26]. These cases essentially assist in understanding the weld-pool solidification.

- Case 1: Equilibrium solidification with complete solid and liquid diffusion of the solute. This case applies to welding situations.

- Case 2: There is little or no diffusion in the solid and complete mixing in the liquid by convection and diffusion is presumed. This leads to micro-segregation effects in weld microstructures.
- Case 3: Lastly, no diffusion is assumed in the solid, and there is limited diffusion in the liquid with no convection.

For welds with dendritic growth conditions, solute redistribution at the dendrite tip and in interdendritic regions have to be considered. Solute redistribution at the dendrite tip is determined by the extent of dendrite tip undercooling. Moreover, solute redistribution in the interdendritic regions is the same as in Case 2 where micro-segregation in welds is considered, and the following assumptions are made:

- negligible undercooling before nucleation of solid phases,
- negligible increase of solute in advance of growing dendritic tips, and
- complete diffusion within the liquid.

The composition of the solid is given by the Scheil equation [27]:

$$C_S^* = kC_o(1 - f_S)^{k-1}$$

where,

C_S^* - is the composition of the solid

f_S - is the volume fraction solid

C_O - is the overall alloy composition

k - is the equilibrium partition coefficient

This equation accurately describes the solute redistribution between the dendrite arms for the solidification process considered, provided that diffusion in the solid is negligible.

2.4.2 Heat Affected Zone

The HAZ is the region that extends outward from the FZ which experiences a temperature peak, which can alter the microstructure of a material due to the heat of the welding process [16]. Within this region, rapid thermal cycles are experienced with a gradual and progressive change in temperature from the solidus to the initial plate temperature. As a result of such thermal cycles, the amount of change in the microstructure in the HAZ of the base metal depends on the amount of heat input, peak temperature reached, time at the elevated temperature, and the rate of cooling [28]. Corollary to the marked changes in the microstructure of the HAZ, the mechanical properties are also subjected to changes in the HAZ. As a function of distance from the fusion line, there exists a well-defined gradient in the HAZ which can be further divided into two sub zones: a partially melted and a true HAZ. The PMZ is a region at the fusion boundary where the peak temperature falls between the liquidus and solidus so that melting is incomplete. The true HAZ is the region beyond the fusion boundary that exhibits a heat treated structure where all the microstructural changes induced occur in the solid state which involves phase transformation, recrystallisation and grain growth [29]. The HAZ region is usually the weakest section in a weldment and has detrimental effects on the material properties as this region is prone to cracking. In high energy density beam welding, like laser welding, the HAZ region is very narrow.

2.5 Weld Defects

Weld defects [30] are interruptions which occur in the typical microstructure of a weld. Imperfections that occur in a weld are related to either the metallurgy of the material process implemented or the design of the weld. Imperfections can occur in welds and these welding flaws are potentially disastrous as they account for high stress intensities which may result in sudden unexpected failure. Common weld defects include: porosities, inclusions, cracking, undercutting, lack of fusion and penetration, underfilling, craters, and lamellar tearing. A few of the welding defects that are formed in a weldment during welding are shown in Figure 2-8 [31].

Porosity

Porosities are fine holes or pores within the weld metal that are formed when gases are trapped in the solidifying weld metal. It is usually a sub-surface defect that is formed when the weld material absorbs large quantity of gases during welding (molten weld pool) and later during solidification. These gases are rejected and are trapped in the solidifying weld metal. The sources of porosity are oils, paints, rust, mill scale, oxygen and hydrogen in the air. Shrinkage voids that occur due to high volumetric shrinkage upon solidification near the center of the weld metal in between the dendrites are characterised as porosities with irregular outlines. The best way to avoid porosities, voids or blow holes in a weld joint is to use a perfectly clean base material.

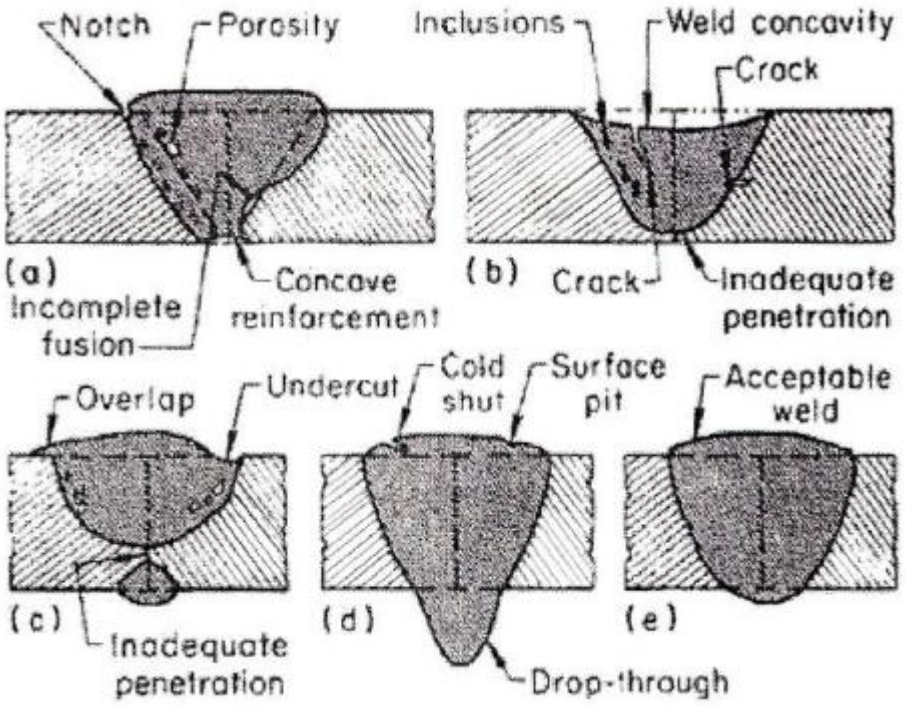

Figure 2-8: A few examples of welding defects formed in the weldment [31]

Inclusions

The entrapment of slag, which comprise oxides or other non-metallic solids that include phosphorous compounds and nitrides which are formed during welding, results in inclusions. They are formed in the weld metal or between the weld and base metals. Inclusions can be continuous, intermittent or very randomly placed. Due to slag inclusions, the mechanical strength, that is, the ductility of the weld is reduced.

Lack of fusion and penetration

The lack of fusion and penetration are flaws that are process related and caused by improper welding procedure. These types of imperfection are most likely to occur when access to the joint is restricted. In weld, these defects persist due to incomplete fusion with the base metals or previous layer as a result of insufficient melting occurred during welding. This is located on the side walls of a joint. Lack of penetration results from incomplete penetration of weld metal to the bottom of the weld joint, and located near the root and also develops into a built-in crack, which can run through weld metal or heat affected zone during service. These flaws are a resultant of improper joint preparation and as well as too low heat input and high welding speeds increase the risk of the occurrence of this imperfection in the weld.

Undercutting

Undercutting is a kind of a flaw that appears in the form of grooves in the base metal that are left unfilled by the weld metal and are located at the weld root or the toe of the weld metal. This type of weld defect is incurred by improper welding parameters i.e. the travel speed and heat input.

Underfilling

Underfilling is the occurrence of a depression (such as a contour) on the surface or at the bottom of the weld (root). It is generally a visible weld defect and can be addressed by proper design and fabrication.

Weld Cracking

A crack is defined as a localised discontinuity caused in the weldment due to the stresses generated during solidification or those that are acting on a structure. It is a type of imperfection found in a weld that not only reduces the strength of the weld, but acts as a medium for stress concentration at the tip which assists in crack propagation, especially during service. Depending on the position, that is, the location of cracks, they can be categorised as longitudinal, transverse, crater, underbead, or toe cracks. These cracks are visible and hence, referred to as surface defects in weld beads. Cracks occur in the FZ and HAZ of weldment during weld solidification or reheating of a weldment. Some of the common types of cracking include HAZ liquation cracking, cold cracking, solidification cracking, lamellar tearing, and post-weld heat treatment (PWHT) cracking. The following sections describe solidification, liquation, and PWHT cracking in more detail as they are more relevant to the present study.

2.6 Solidification Cracking

Solidification cracking is a weld defect that develops in the FZ of a weld metal during the fabrication process. This cracking occurs in the terminal stages of solidification (temperatures slightly above the solidus), where the dendrites are fully grown into grains and these grains are separated by a thin liquid film that exists in interdendritic and the intergranular regions [32,33]. Solidification cracking is intergranular in nature [34]. During rapid solidification and cooling

conditions, the rate of strain accumulation is rapid in the weld metal (FZ and HAZ) and limited time is available to accommodate the stresses/strains. The formation of cracks could be prohibited if semisolid weld could sustain the stresses such as the following: solidification shrinkage, thermal contraction stresses/strains and mechanical stresses. These stresses/strains are induced in the weld zone of the material during the weld thermal cycle (cooling and solidification). Thus, cracking occurs in the crack susceptible microstructure of weld metal, when stresses/strains present in the weldment surpasses the materials internal resistance to cracking i.e. cohesive strength of the grains. Solidification cracking is affected by both mechanical and metallurgical factors. The mechanical factors include stresses/strains developed in the weld metal during solidification (caused by dynamic expansion and contraction of the weld and HAZ due to non-uniform temperature changes), the thickness and size of the weld, weld joint design, and weld size and shape, thermo-mechanical properties of the alloy. The metallurgical factors include the conditions of solidification (presence of liquid phase both at the interdendrites and grain boundaries during specific temperatures), grain size, presence of low melting secondary constituents, etc [35]. Some of the factors will be discussed in more detail in the following paragraphs.

Weld pool solidification: The range of temperature over which the weld pool solidifies is a significant factor as it determines the stability of the liquid film that is present in the interdendritic and intergranular regions. Such a liquid film imparts very low strength and ductility during the last stages of solidification. This is caused by segregation elements with $k < 1$, which eventually would increase the solidification temperature range of an alloy. This widens the solid + liquid region which persists at lower temperatures, often below the solidus

temperature of the alloy and indirectly increases the region of low strength and hence, solidification cracking susceptibility.

Amount and distribution of liquid [16]: The cracking susceptibility of an alloy is influenced by the amount of microsegregation of low melting point solute elements that determines amount and distribution of liquid during the last stages of solidification. It is been reported that when the composition of the material lies somewhere between that of the pure metal and heavily alloyed material, it is highly susceptible to cracking. A pure metal is not susceptible to cracking because there is no low-melting-point eutectic formation at the grain boundary to cause solidification cracking. In highly alloyed materials, the eutectic liquid present between the grains would be just enough to heal the cracks. In between these two scenarios, the volume of eutectic liquid in-between grains could be just adequate enough to form a thin continuous grain boundary film that makes the metal highly susceptible to cracking, without having any adequate liquid present to heal the cracks. If the liquid is distributed over a smaller grain boundary area, it would result in increase in the susceptibility to solidification cracking. Conversely, if there is more grain boundary area, the liquid will not be localised creating more liquid-solid contact and weaken the the bridges of solid - solid contact area, drastically reducing the cracking resistance.

Grain structure of weld metal: A weld metal with a fine equiaxed dendritic structure can effectively accommodate contraction strains. Where as a coarse dendritic structure with columnar grains would be difficult to deform under stress and would readily crack. Hence, a coarse structure would enhance the susceptibility to cracking whereas, the susceptible to cracking is significantly less for fine equiaxed grains. In addition to this, a fine equiaxed microstructure improves ductility.

Magnitude of contraction stresses: Metallurgical factors influence the solidification of an alloy and provide the necessary conditions for cracking to occur during solidification. However, the occurrence of solidification cracking can only be determined by the severity of imposed strains on an alloy. The thermal cycle experienced during a welding process induce residual stresses into the weldment of the material. The stresses incurred can be due to thermal contractions, solidification shrinkage or both [36].

Thus, the combined effect of mechanical and metallurgical factors results in the occurrence of solidification cracking in welds. The presence of crack susceptible microstructures in alloys is not a sufficient enough factor that provokes materials to crack during welding. No cracking could occur without stresses that act on the adjacent grains. These conditions are equally important for cracks to occur in a material during welding [37,38].

Degree of restraint: The degree of restraint is another factor that influences solidification cracking. A higher degree of restraint in an alloy means that it is more susceptible to solidification cracking. These restraints could be minimised through proper joint design and appropriate welding parameters.

There are many theories that explain the mechanism of solidification cracking, which includes the shrinkage brittleness theory, strain theory of hot cracking, and generalised theory.

Shrinkage Brittleness Theory

According to the shrinkage brittleness theory [39-41], cracking occurs at a temperature which is near the solidus temperature, above the coherent temperature where the alloy is essentially brittle. This temperature range between coherent and solidus temperature is called the brittle temperature range (BTR). The strains generated during cooling are contraction strains that are

concentrated in the narrow liquid regions. If these imposed strains exceed the critical rupture stress cracking would occur while cooling through the solidus. These fissures persist in the alloy if there is no sufficient liquid present to heal the cracks. Therefore, solidification cracking occurs when the solidifying interface is imposed with enough shrinkage strain in the BTR.

Strain Theory

Pellini proposed the strain theory of hot tearing [42] that suggests that cracking occur in the material due to localised strains generated by thermal gradients that tend to separate the solidifying grains that are surrounded by a continuous thin liquid film. The cracking occurs when the film stage is reached (passing through the solidus temperature range) and localised strains are exceedingly high. The low melting segregates that are present in the molten state below equilibrium solidus temperatures are considered to be the most dangerous.

Generalised Theory

The generalised theory from Borland [36] explains how liquid quantity and its distribution during freezing affect cracking tendencies. This theory includes ideas from both the shrinkage brittleness theory and strain theory of hot cracking. Cracks are most likely to be formed when liquid present over a wide freezing range cannot sustain the high stresses built up between grains during cooling. The distribution of this liquid during solidification is influenced by the ratio of the interfacial energies of the solid/liquid interfaces and grain boundary energy. When this ratio is lower, the liquid phase covers the grain faces and the edges as well. Conversely, a higher ratio confines liquid to the edges and corners, which is beneficial because the grain faces can unite, thus preventing high stresses from being built up and enabling the weld to accommodate the thermal stresses generated during cooling.

2.7 Liquation Cracking

The cracks that are formed and are confined to the HAZ, i.e. adjacent to the FZ, (also known as the PMZ) of the weld metal during weld thermal cycle is termed liquation cracking. This type of cracking occurs at grain boundaries which get exposed to a variety of very high temperatures i.e. between the solidus and liquidus temperatures in and around the weld. The prevention of HAZ liquation cracking is a challenge as the major factors contributing to its occurrence are metallurgical factors such as the composition and microstructure of the material [28]. The inability of the thin liquid film formed on the grain boundaries during the weld thermal cycle to accommodate the thermally and mechanically induced tensile stresses during cooling causes liquation cracking. A combination of welding stresses and the reduced ductility of the alloy due to melting of the grain boundaries (grain boundary liquation) results in intergranular cracking in the HAZ. These intergranular cracks are also termed micro-fissures [16].

The occurrence of HAZ grain boundary liquation can either be by a non-equilibrium sub-solidus phase change or by super-solidus equilibrium melting. The non-equilibrium sub-solidus melting is predominantly insidious as the consequence of which is persistence of liquid film on the grain boundaries for a more wider temperature range (increasing the temperature range), and thereby increases its propensity to cracking [43,44].

Two underlying mechanisms that have been proposed to explain the grain boundary liquation are being discussed in the following sections [43,44]:

1. Constitutional liquation of second phase particles, and

2. Grain boundary segregation of melting point depressants, such as boron and phosphorus, during thermo-mechanical or thermal treatment of an alloy prior to welding.

Constitutional Liquation Theory

The theory of constitutional liquation was first proposed by Pepe and Savage [45] with experimental evidence, in which they observed the liquation of Ti sulphide particles in 18 Ni maraging steel. This phenomenon has been used to explain the sub-solidus liquation of secondary constituents during welding at the grain boundaries in the HAZ region of the weldment in various alloys, for example, superalloys, aluminium alloys and fully austenitic stainless steels and are being listed here; such as for TiS in 18-Ni maraging steel [45], TiC in austenitic alloys, A286 [46] M_3B_2 in Udimet 700 [47], Cr_7C_3 and Ti(CN) in Inconel 600 [48], M_6C in Hasteloy X [47], MC and MNP phosphides in Incoloy 903 [49], NbC and the Laves phase in Inconel 718 [50], MCs in Allvac 718PlusR [51], and the MC, γ', M_3B_2, and M_2SC phases in IN738 [52]. The formation of intergranular liquid films is made possible through a eutectic-type reaction taking place between the second phase particles and the surrounding matrix above eutectic temperatures (sub-solidus temperatures).

The phenomenon of "constitutional liquation" can be well understood by using a binary alloy phase diagram, as illustrated in Figure 2-9 [45]. The alloy of a nominal composition C_0 consists of a solid solution matrix,α which is finely dispersed with an A_xB_y intermetallic compound, a high temperature phase. The behavior of this alloy when heated from temperature T_1 to T_4 is different in extremely slow (at equilibrium) and rapid heating rates. On considering equilibrium solidification conditions, the solubility of B in the α matrix increases with increase in temperature which is very slow due to exceptionally slow heating rate.

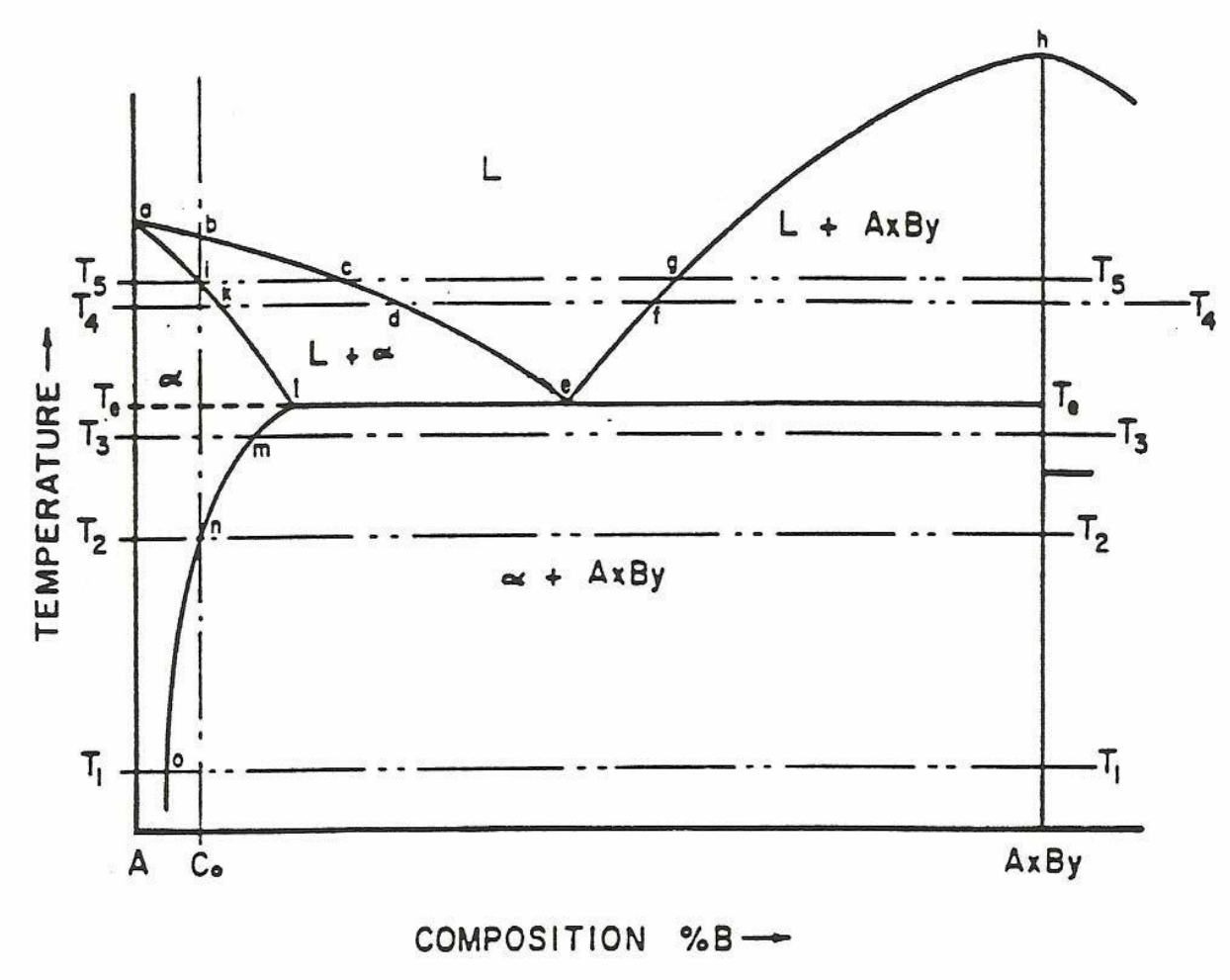

Figure 2-9: Schematic diagram exhibiting the phenomenon of constitutional liquation behavior for a hypothetical binary alloy [45]

Source: Welding Journal.

The A_xB_y, intermetallic second phase is uniformly diffused in the α matrix phase at a constant slow diffusion rate, thus resulting in a homogeneous single phase solid solution of composition C_0 for temperatures from T_2 to T_4. The solid solution phase persists as a single phase until it approaches the equilibrium solidus of the alloy where the first melting takes place. The amount of first infinitesimal liquid formed has a composition that corresponds to point c at temperature T_5.

The solidification behaviour of an alloy under non-equilibrium condition is drastically different from that in equilibrium condition and this intern is due to involvement of an extremely rapid heating rate. During welding, extreme heating rates are experienced in the HAZ of most the alloys and this does not provide sufficient time for the particles to completely dissolve into the matrix before reaching a temperature where, a eutectic reaction between A_xB_y and the surrounding matrix occurs. The intermetallic compound A_xB_y can be made to disappear on rapid heating and this takes place by dissolution of A_xB_y and subsequent accommodation of the excess B into the surrounding matrix. Generally, dissolution and accommodation processes limit the rate of dissolution of A_xB_y which occurs at a finite rate. As the heating rate is increased until a critical heating rate is reached, where, incomplete dissolution of the second phase particles takes place.

The A_xB_y second phase is assumed to have spherical particles to understand the dissolution process. Figure 2-10a-c [45] schematically shows the transformations taking place in the near vicinity of the particles during rapid heating to temperatures of T_3, T_e and T_4, respectively. The vertical line that is denoted by C_0 represents the equilibrium structure for an alloy of that composition with respect to temperature. Therefore, any deviation from the equilibrium structure via rapid heating causes redistribution of the solute. During heating to temperature T_3, the intermetallic phase A_xB_y starts to dissolve into the matrix as it being unstable with compared to

the α matrix of the alloy composition, C_0. Therefore, A_xB_y particles reduce from their original size (represented by the dashed circle in Figure 2-10a) to a smaller size. During this dissolution of A_xB_y particles, solute B atoms are released and diffused into the adjacent α matrix. However, as shown in Figure 2-10, for the two phases the A_xB_y phase and α phase (of composition 'm') to co-exists, they must be in good contact. Thus, around the intermetallic phase, a concentration gradient is built up in the surrounding matrix with a maximum of 'm' at the A_xB_y interface and this gradually reduces further away into the matrix towards the original matrix composition 'o'. Thus, this leads to formation of localized liquids at elevated temperatures along the particle matrix interface. The factors that determine the quantity of liquid formed are heating rate, size of the liquating particles, and their dissolution kinetics at elevated temperatures.

During heating from T_3 to T_e (the eutectic temperature), there exists continual dissociation and particle sized reduction taking place as shown in Figure 2-10b where the dashed and solid circles represents the A_xB_y particle at T_3 and T_e temperatures respectively. The changes in the solute distribution around the particle matrix interface at temperatures T_3 (represented by dashed line) and Te (represented by solid line) are shown in Figure 2-10 [45]. At the eutectic temperature, Te, the formation of a single phase liquid at the A_xB_y interface, which intern is surrounded by the α matrix in the alloy of composition 'e' and the solute distribution corresponding to the three phases that co-exists at temperature T_e is shown in Figure 2-10b. Further increasing the temperature to T_4, additional time is provided for the dissociation of A_xB_y and the expected solute distribution while reaching to T_4 is represented by solid lines in Figure 2-10c. when heating above T_e, there exists a reduction in equilibrium solubility of the B atoms in the α phase long the solidus line "akl".

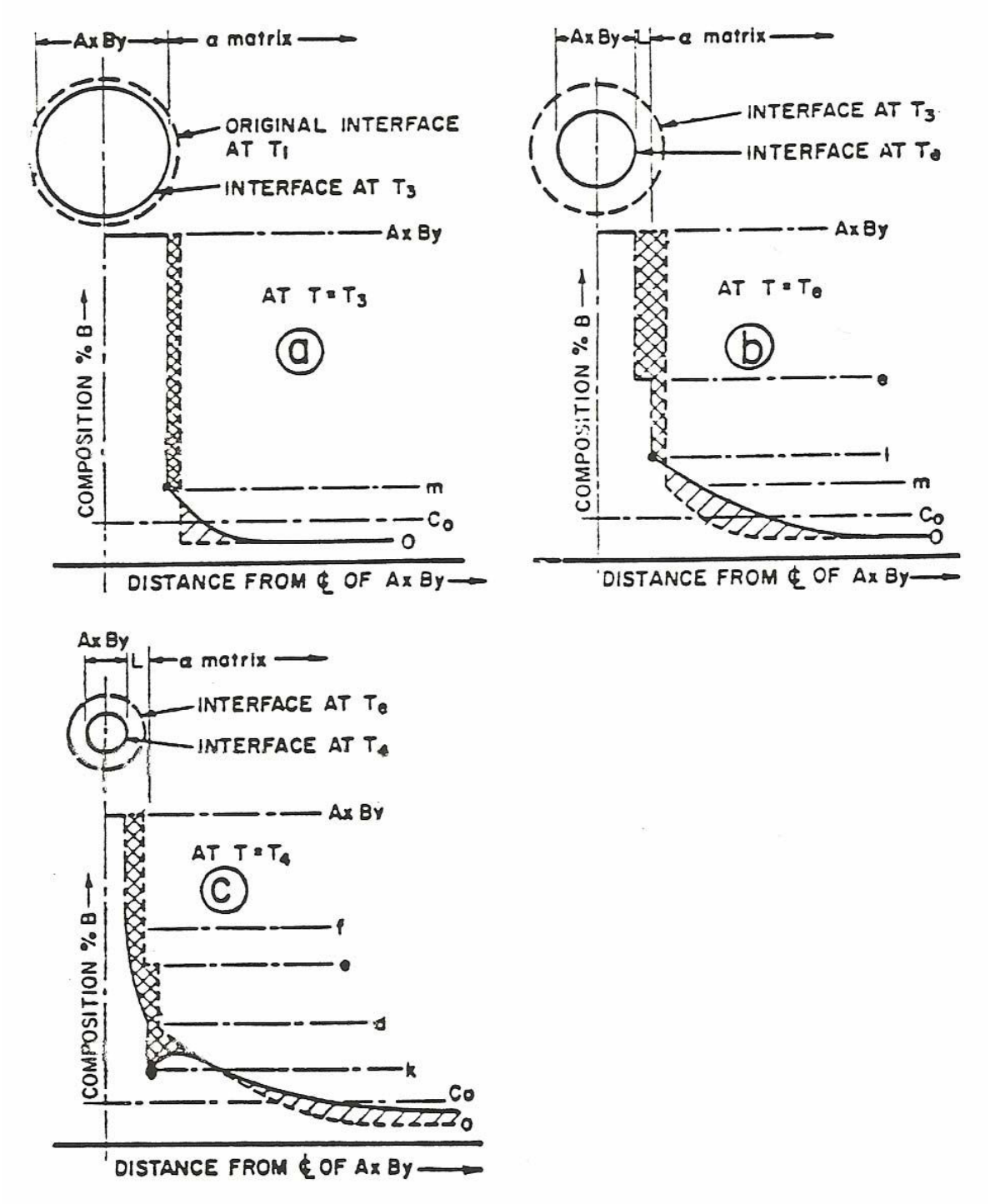

Figure 2-10: A schematic representation of formation of constitutional liquation at various temperatures also showing their respective concentration gradients [45]

Source: welding journal

Therefore k and d corresponds to the concentration of solid solution and the liquid film in contact with one another above temperature T_e, respectively.

This modification in the composition creates an inverted region in the concentration gradient as shown in Figure 2-10c. The presence of excess solute in the α matrix leads α-solid solution/liquid interface to epitaxially move into the α matrix until the excess solute is consumed by formation of liquid of composition 'd'. Upon reaching to temperature T_4, a formation of liquid film with variable composition ranging from 'f' at the A_xB_y interface to 'd' at the α matrix exists which surrounds each of the un-dissolved A_xB_y particle. Therefore, localised melting of these particles would take place when subjected to non-equilibrium heating rates to temperatures significantly below the equilibrium solidus temperature, T_5 and this is characterised as constitutional liquation. Accordingly, the phenomenon of constitutional liquation occurs at temperatures above eutectic temperature under rapid heating rates and results in the formation of low melting solute-rich liquid phases below the equilibrium solidus of the alloy.

Grain Boundary Segregation Mechanism

Liquation along the grain boundaries can also occur from segregation of alloying elements having lower solubility in the matrix to grain boundaries. These elements like boron, phosphorous, sulphur, etc act as melting point depressants, and thus lower the melting temperature of the grain boundary regions relative to their surrounding matrix. During welding, liquation of segregated grain boundaries take place as a result of non-equilibrium sub-solidus melting in contrast to constitutional liquation of the particles that does not, or cannot occur [44,53]. The segregation of elements to the grain boundaries prior to welding can occur during different thermal processes, such as casting, hot deformation and pre-weld heat treatments. It is diffusion controlled process and occurs as an equilibrium or non-equilibrium mechanism.

Equilibrium segregation [54-57] is when an alloy is isothermally held at a sufficiently high temperature which allows the diffusion of solute atoms or impurities within the grain of a polycrystalline to the disordered regions (loosely packed interfaces), such as the grain boundaries, precipitate/ matrix interfaces and stacking faults in order to achieve lower interfacial free energy of the system. Equilibrium segregation is a thermodynamic process, i.e. it is time and temperature dependent. This is usually restricted to a few mono layers and its effect decreases with a reduction in solute content of the alloy. Thus, slow heating conditions allow the solute to diffuse into the matrix when held at a sufficiently high temperature. The mechanism of equilibrium segregation is likely to occur during isothermal pre-weld heat treatment. Hence, the driving force for the occurrence of equilibrium segregation of the elements to the interface in a material is for acquiring a state of minimum free energy.

The non-equilibrium segregation phenomenon for grain boundary liquation was proposed by the authors [58-62] when the grain boundary embrittlement could not be explained by equilibrium segregation mechanism. This type of segregation occurs during cooling from elevated temperatures in a thermal cycle of a process. Non-equilibrium segregation is incurred as a result of the formation of atom-vacancy complexes and the presence of a gradient in the concentration of the complexes between the grain interiors and grain boundaries. These grain boundaries act as a sink for the vacancies; thus, under a concentration gradient, vacancies diffuse towards the grain boundaries. This results in vacancy complexes being absorbed by the grain boundaries and subsequent solute accumulation in the near vicinity of the grain boundaries. Non-equilibrium segregation is a reversible process, and its extent is dependent on the binding energy present between the solute atoms and the vacancies. It also depends on other important factors, such as starting temperature, cooling rate, bulk concentration of the solute.

2.8 Post-Weld Heat Treatment Cracking

PWHT cracking is also known as strain age or reheat cracking [63-70]. This heat treatment is designed to relax residual stresses that have incurred in an alloy during welding, and restore an optimum microstructure and associated mechanical properties in the weldment. Cracking occurs during PWHT and is usually intergranular in nature. The cracks are initiated in the HAZ and propagate into the base metal (which is unaffected by the weld thermal cycle). The stress contributing factors to cracking during PWHT include residual welding, localised thermal expansions and aging contraction. Strain age cracking is commonly observed in age hardenable superalloys [63-70].

The metallurgical reactions that take place in alloys (especially in the HAZ) during welding lead to brittle microstructures. Often, PWHT is performed for two reasons: first, to relieve stresses and secondly, to develop maximum strength. In order to develop maximum strength, the weldment is solution annealed and then subjected to aging. When the weldment is solutionized, the residual stresses are relieved. During aging, the weldment is held for a period of time at a temperature which is lower than that of the solutionizing temperature. At this temperature, contraction stresses are generated by the precipitation of the strengthening phases. Thus, due to an aging temperature that is below the solutionizing temperature, the aging action occurs before the residual stresses are relieved. This results in cracking during PWHT.

The various metallurgical factors that affect PWHT cracking are chemical composition, grain size, grain boundary precipitates and the pre-weld condition of the base metal [64,71]. For instance, superalloys that contain higher Al + Ti contents ((Al + Ti) > 6%) are exceptionally susceptible to cracking. With an increase in the Al + Ti content (primary γ' formers), the rate of precipitation and volume fraction of this strengthening phase also increase. As a result of

increased strength, the matrix is brittle and formation of aging contraction stresses makes it more susceptible to cracking during PWHT. Similarly, coarse grain size, brittle grain boundary phase and pre-weld heat treatments which lower the ductility of the alloy during welding have been observed to make the alloy highly susceptible to PWHT cracking.

2.9 Improvement of Weldability of IN-738 LC

It is a known fact that high temperature performance of the materials is considerably improved by eliminating or reducing the number of grain boundaries. The number of grain boundaries in a material is significantly reduced by directional solidification processing. Directional solidification is an improved special processing technique that brings about significant changes in the microstructural variables that are grain size, shape and orientation. Figure 2-11 shows a diagram representing the typical grain structure formed and its orientation in conventionally solidified (CS) and directionally solidified (DS) polycrystalline and single crystal (SC) processed alloys. CS cast form comprises of randomly oriented equiaxed grains (where each grain acts as a single crystal). DS cast form also consists of many grains (columnar grains) in such a way that each grain is elongated in preferred solidification direction there by eliminating the transverse grain boundaries. SC cast forms is a mono crystal in which all the grain boundaries are removed.

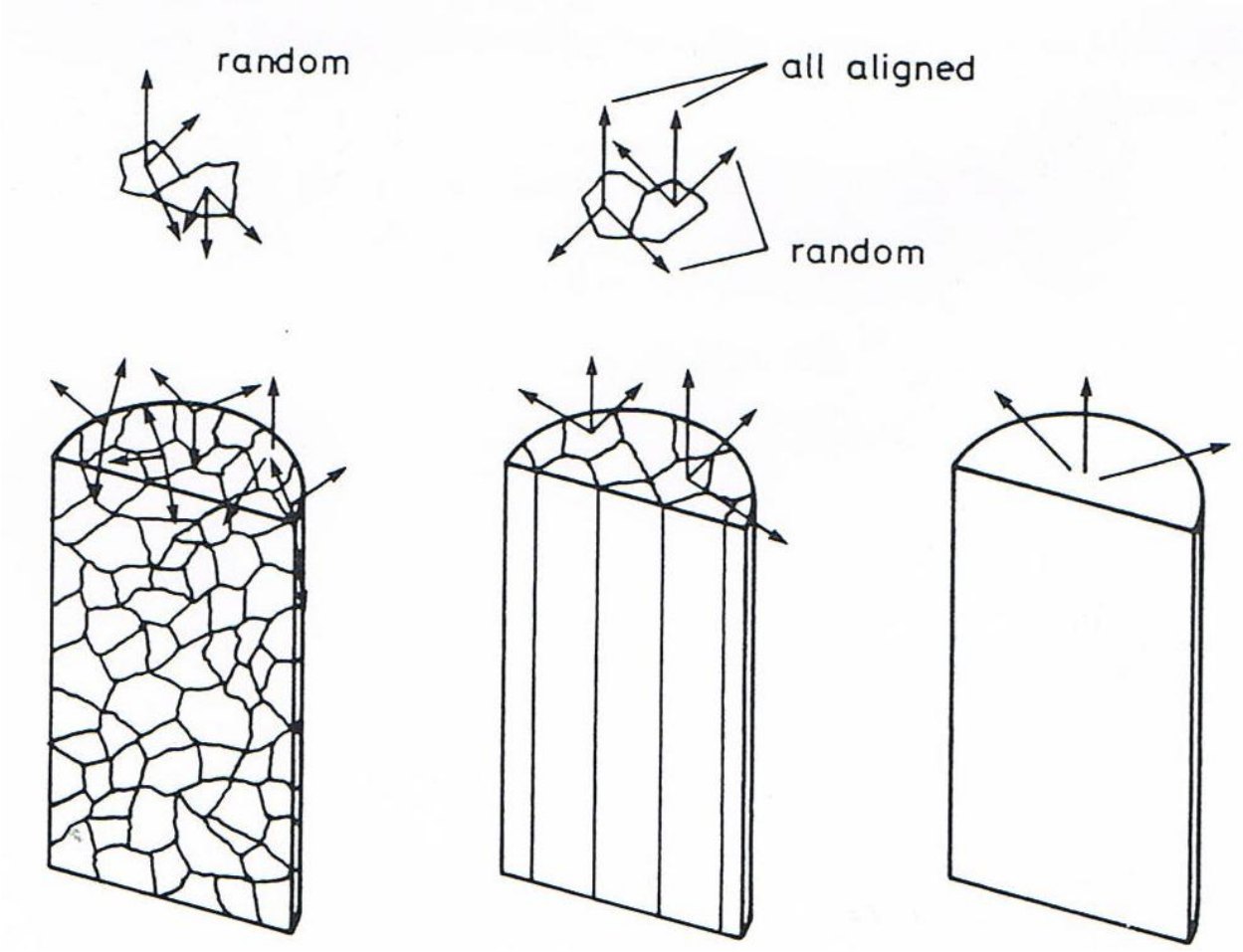

Figure 2-11: A diagrammatic representation of grain structure formation and their orientation in cast alloys [72]

Another way to improve the weldability that has been reported in the literature is via microstructural modifications i.e. pre-weld heat treatment. The strength of precipitation hardened alloy is dependent on the size, coherency and lattice parameter mismatch between the precipitate and the matrix. These can be optimised by using a suitable heat treatment which homogenizes the as-cast microstructure and impart the required properties. These modifications are caused by atomic movement and redistribution which could result in reduction or elimination of deleterious phase that are formed during thermal processing via segregation. Thus the microstructural changes produced through processing technique coupled with an optimised heat treatment would be helpful in enhancing the weldability of IN-738 LC superalloy.

2.10 Scope and Objective of the Present Study

IN 738, a precipitation hardened nickel based superalloy is very difficult to weld due to its high susceptibility to HAZ cracking during welding and subsequent PWHT. The cracking in IN 738 is mainly intergranular in nature and associated with liquation of secondary solidification products (such as MC carbides, γ - γ' eutectic phases), and solid state reaction products (γ' precipitate particles) that are present along the grain boundaries in the pre-weld material. It has been recognised that the weldability of an alloy could be improved by reducing the number of crack susceptible areas i.e. grain boundaries and also by subjecting the alloy to microstructural modifications processes. The current research was designed to combine the effect of heat treatments and the effect of grain boundaries by comparing three different cast forms of IN 738 subjected to two different pre-weld heat treatments. Also limited information exists on the effect of the new pre-weld heat treatment NHT that has been observed to reduce cracking in CS IN-738 LC on other CAST forms like DS IN-738 LC and SC IN-738 LC. Therefore, the main objectives of this research are:

1. A comparative study on the effect of grain boundaries on the weldability, by taking three different cast forms with different number of grain boundaries.
2. To further investigate the HAZ cracking behaviour in DS and CS IN-738 LC by using NHT and UMT pre-weld heat treatments.

Chapter 3.Experimental Procedure

3.1 Materials

The IN 738 material used in the present study was procured in three different cast conditions, which were conventionally and directionally solidified polycrystalline and single crystal cast forms. Conventionally cast polycrystalline IN 738 was supplied by Hitchiner Manufacturing Company in the form of plate that measured 238 mm in length by 58 mm in width by 14 mm in thickness, Directionally solidified IN 738 was procured in the form of a slab, and single crystal IN 738 was supplied in a form of a cylindrical billet with a diameter of 16mm. The nominal composition of the alloy is given in Table 3-1.

3.2 Welding

Welding test coupons with a dimension 50mm X 10mm X 5mm were cut from the bulk material by using a numerically controlled wire electro discharge machine (EDM). These coupons were subjected to two pre-weld heat treatments that are listed in Table 3-2. The heat treatments were performed in a Marshall tube furnace in argon atmosphere. After the heat treatment, the weld coupons were subjected to surface grinding to remove the oxide layer formed on the surface. In order to study the effect of the heat treatments and grain structure on HAZ cracking, the prepared coupons were subjected to bead-on-plate autogenous welding performed in a CO2 laser welding facility at StandardAero Ltd., in Winnipeg. Welding parameters that were used for welding have been tabulated in Table 3-3. After welding, 10 sections were cut perpendicular to the weld direction from the welded coupons by using a wire EDM, and they were used for the crack measurements.

Table 3-1: Composition of IN-738 LC used in the present study

Elements	*wt%*
Carbon	0.11
Cobalt	8.50
Chromium	15.84
Molybdenum	1.88
Tungsten	2.48
Tantallum	1.69
Niobium	0.92
Aluminium	3.46
Titanium	3.47
Boron	0.012
Zirconium	0.04
Iron	0.07
Manganese	0.01
Silicon	0.01
Sulphur	0.001
Nickel	Bal

3.3 Post-Weld Heat Treatment

To study and understand the cracking behaviour in IN-738 LC, conventional post weld heat treatment (PWHT) was carried out. The PWHT consisted of solution treatment at 1120^0C for 2 h followed by air cooling and subsequently aging at 845^0C for 24 h followed by air-cooling.

3.4 Hardness Test

The bulk hardness of the as received and pre-weld heat treated material was measured with a Vickers hardness machine by using a load of 10kg. All of the specimens were polished using standard metallographic methods prior to measuring the hardness. Ten hardness measurements were recorded for each specimen and the average value was calculated based on these ten measurements.

3.5 Gleeble Thermo-Mechanical Simulation

Gleeble thermo-mechanical simulation was used to simulate the HAZ microstructure in order to understand the liquation behaviour of different micro-constituent particles in the IN-738 LC alloy during welding. This simulation was carried out by using a Gleeble 1500 thermomechanical system at the University of Manitoba. It is a computerised testing device that precisely and independently controls thermal and mechanical operations on a specimen. The specimen is heated by its resistance to the flow of an electrical current and mechanical loading is carried out by using a servo-hydraulic loop. The test specimen is mounted onto water cooled copper wedged jaws.

Table 3-2: A list of pre-weld heat treatment

1120^0C / 2hr / AC + 1025^0C / 16hr / WQ	(UMT)
1120^0C / 2hr / AC + 1120^0C / 24hr / FC	(NHT)

AC - Air Cool

WQ -Water Quench

FC - Furnace Cool

Table 3-3: Laser welding parameters

Power, KW	*Welding Speed, mm/min*	*Focal Point, mm*	*Shielding Gas, l/min*	*Welding Gas, l/min*
1.5	1.5	-2.0	30	25

Rectangular rods with a dimension of 3mm X 2mm X 42mm were sectioned from the material that underwent UMT and NHT by using the EDM and later the surface was grounded to remove the oxide layer. The mid-section of these rods was spot welded with chromel-alumel thermocouples in order to monitor and control the temperature during simulation.

The simulations were performed by rapidly heating the specimen at a rate of 150°C/s to a temperature that ranged from 1120°C-1220°C, isothermally held for 1s at the peak temperature and then cool to room temperature by water quenching. Water quenching was performed in order to retain the microstructural changes that occur at peak temperatures. After the simulation, the specimens were sectioned at the location of thermocouples by using a wire EDM.

3.6 Metallography Sample Preparation

As-received, pre-weld heat treated, as-welded, post-weld heat treated and Gleeble simulated samples were metallographically prepared for microstructural examination and crack length measurement. These samples were mounted in a bakelite medium (black phenolic powder) by using a Buehler mounting press, followed by manual grinding and polishing. Silicon carbide papers of 240, 320, 400, 600, 1200 grit were successively used for the manual grinding. Subsequently, fine polishing was performed by using an emery cloth embedded with 6 micron diamond suspension on a rotating wheel and a final polish on a 1 micron diamond suspension wheel until a mirror-like surface was achieved. Ultrasonic cleaning of the specimens in methanol was performed before the fine polishing was carried out. The prepared samples were then electrolytically etched by using a gamma prime etchant i.e. 12ml H_3PO_4 + 40ml HNO_3 + 48ml H_2SO_4 for 4 sec at 4 volts.

3.7 Microstructural Examination

The microstructure of the as-received, pre-weld heat treated, as-welded, post weld heat treated and Gleeble simulated samples was examined by using an optical microscope and a scanning electron microscope (SEM).

A Zeiss Axiovert 25 inverted reflected-light microscope, equipped with a CLEMEX Vision 3.0 image analyzer was primarily used to study all the metallographically prepared samples. A Nikon EPIPHOT-TME microscope was also used to obtain an overall view of the weld cross-section.

A detailed microstructural study was undertaken by using a JOEL 5900 LV SEM equipped with JSM 5000 software. Both the secondary emission (SE) and the back scattered (BSE) modes were used for the analysis. The extent of microfissuring in the as-welded as well as PWHT condition was determined by measuring the crack lengths in ten sections of each weld and the total crack length (TCL) in the HAZ and FZ was calculated. An ultra thin window energy-dispersive spectrometer (EDS; Oxford Instruments, Oxford, United Kingdom) and Inca analyzing software for the SEM were used for a semi-quantitative chemical compositional analysis of the different micro-constituents present in the alloy.

Chapter 4.Results and Discussion

The results of the analysis are categorized as follows:

4.1Microstructure of pre-weld material.

4.2Microstructure of As-welded material.

4.3Effect of grain boundary on weldability of IN-738 LC.

4.4Effect of pre-weld heat treatment on HAZ microfissuring.

4.5Post -weld heat treatment microfissuring.

4.1 Microstructure of Pre-Weld Material

In this section, the as-received and pre-weld heat treated microstructure of the nickel based superalloy IN-738 LC will be discussed. IN-738 LC, in three different castings, conventionally solidified, CS IN-738 LC, directionally solidified, DS IN-738 LC, and single crystal, SC IN-738 LC were used in this study. The pre-weld heat treatments used were new heat treatment (NHT), also known as (NUMT), and the University of Manitoba heat treatment (UMT). Since, the initial microstructure plays an important role in determining the weldability of the material, microstructures of as-received and pre-weld heat treated (UMT, NHT) materials were examined to identify the various microstructural - constituents that might be present within the alloy.

4.1.1 Microstructure of As-Received Materials

An optical low magnification image, given in Figure 4-1 illustrates the different grain structures formed within the three different castings, CS IN-738 LC, DS IN-738 LC, and SC IN-738 LC.

a)Conventionally Solidifiedb)Directionally Solidified

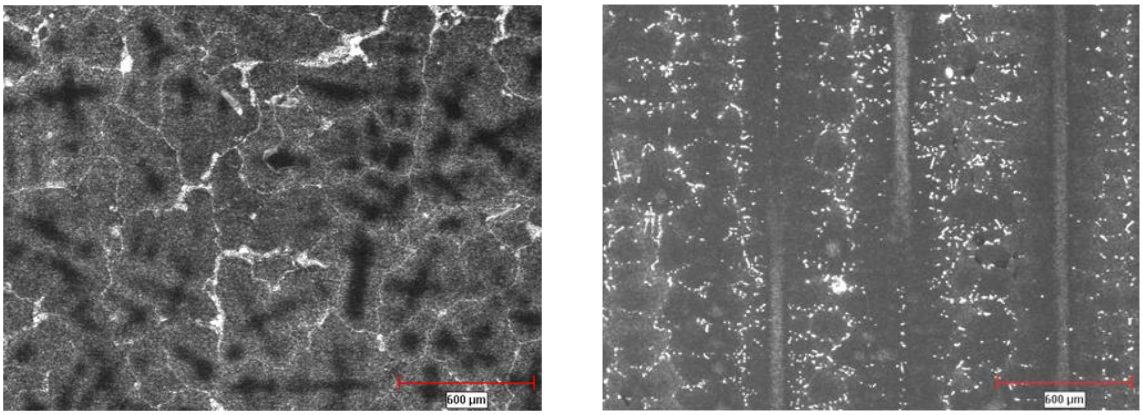

c)Single Crystal

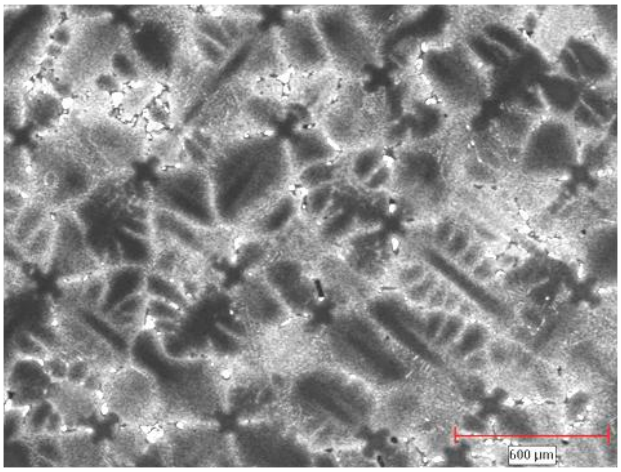

Figure 4-1: Optical image illustrating the different grain structure formation in three different cast forms

In CS cast form the nucleation and growth takes place in all directions forming equiaxed grains and is uniform throughout the volume (Figure 4-1a). On the other hand, in DS cast form the nucleation and growth of a crystal is controlled i.e. the growth of a grain is restricted to the direction of solidification thus forming large columnar grains with parallel grain boundaries to the direction of solidification (seen in Figure 4-1b). In SC cast form one grain survives and grows into a mono-crystal. It is also produced by directional solidification in combination with grain selector. Figure 4-1c shows a dendritic microstructure present in single crystal and its crystal orientation.

Microstructural examination of the as-cast CS IN-738 LC alloy, by using a scanning electron microscope (SEM), revealed a core dendritic structure with extensive precipitation of ordered FCC intermetallic γ' in γ matrix that was uniformly distributed both in the dendrite core and interdendritic regions, as shown in Figure 4-2 and Figure 4-3. During ingot solidification, there exists a compositional variation in interdendritic and dendrite core regions due to dendritic microsegregation. This phenomenon of elemental partitioning which occurs during solidification causes enrichment of negatively segregating elements ($k > 1$) like Co, Al, W, Cr, and Ni within the dendrite core region. Meanwhile, the positively segregating elements like ($k < 1$) like Ti, Nb, Ta, Zr, and Mo are enriched in the interdendritic regions [73,74]. It has been reported previously [75-77], that for CS and DS IN 738 alloy, similarities exist in the partitioning behaviour of alloying elements, thus exhibiting a similar micro-segregation in the dendritic and interdendritic regions. Thus, the microstructural analysis of CS IN-738 LC will be discussed in detail, to avoid repetition and for the sake of brevity. The microstructure of this alloy consists of the γ matrix, γ' precipitates and many secondary solidification constituents, that include MC carbides, M_2SC sulpho-carbides and γ-γ' eutectics.

Occasionally, the region in front of some γ-γ′ eutectics, other last to solidify products such as Cr-Mo borides, intermetallic compounds rich in Ni-Zr, and Ni- Ti were observed [2,6].

γ′ precipitates

IN-738 LC is a very complex casting alloy, with extensive dispersion of discrete γ′particles which are formed due to precipitation reactions, involving nucleation and growth of these coherent precipitates. SEM analysis of γ′ precipitated particles revealed significant variation in their morphology and size is presented next.

In Figure 4-2, the uniform distribution of ordered γ′ precipitate particles having ogdoadically diced cube morphology (also represented by cluster of cube particles) were observed in the dendrite core regions, while in Figure 4-3, an irregular shaped and relatively coarse γ′ particles can be seen in the interdendritic and intergranular regions. Also, arrow head shaped γ′ precipitates were occasionally seen in the interdendritic regions, as shown in Figure 4-4. This suggests that the different shaped and sized γ′ particles nucleate at different temperature regimes at different times during solidification [78].

There also exists a considerable difference in the solvus temperature of the γ′ particles within the dendrite core and of those that form in the interdendritic regions. This is attributed to the partitioning of solute atoms i.e. micro-segregation induced enrichment of negatively segregating atoms in the dendrite core γ′ whose solvus temperature lies in between 1120^0C-1130^0C and conversely, the enrichment of positively segregating atoms in the interdendritic γ′ particles where higher solvus temperatures is in the range of 1160^0C to 1170^0C [76,79].

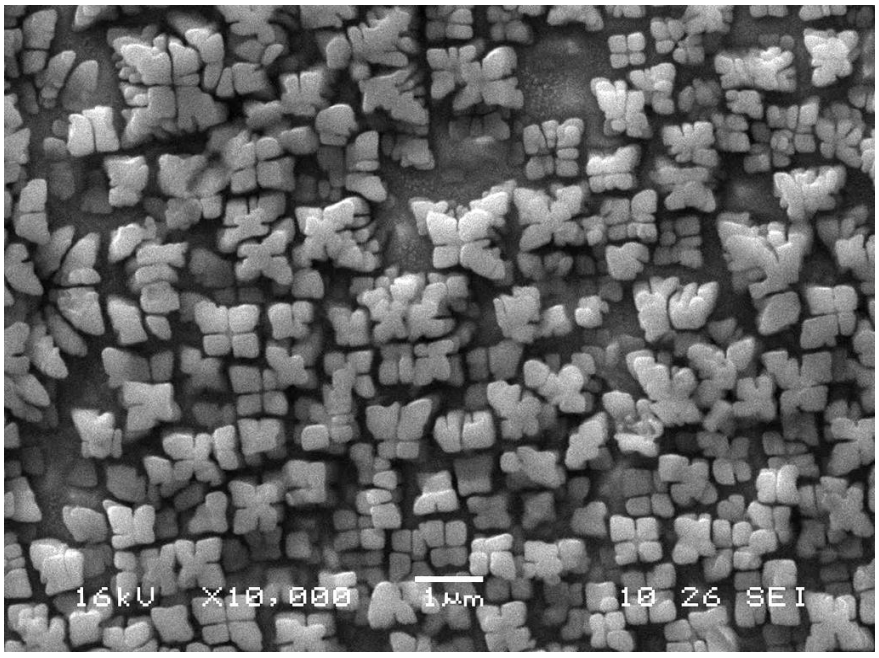

Figure 4-2: SEI micrograph of γ′ particles in dendrite core of as received IN-738 LC

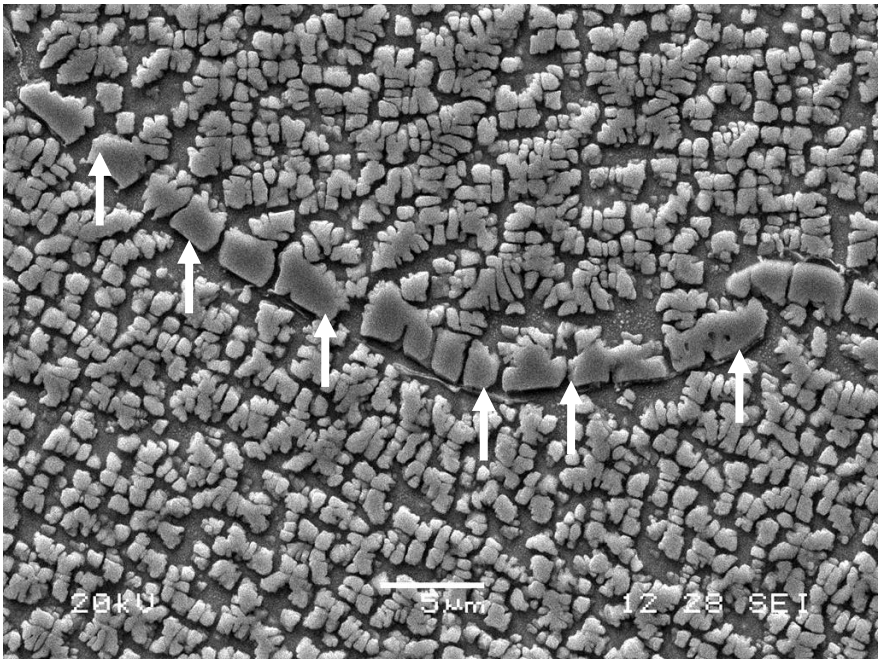

Figure 4-3: SEI micrograph showing γ′ precipitates at the grain boundaries (as indicated by arrows)

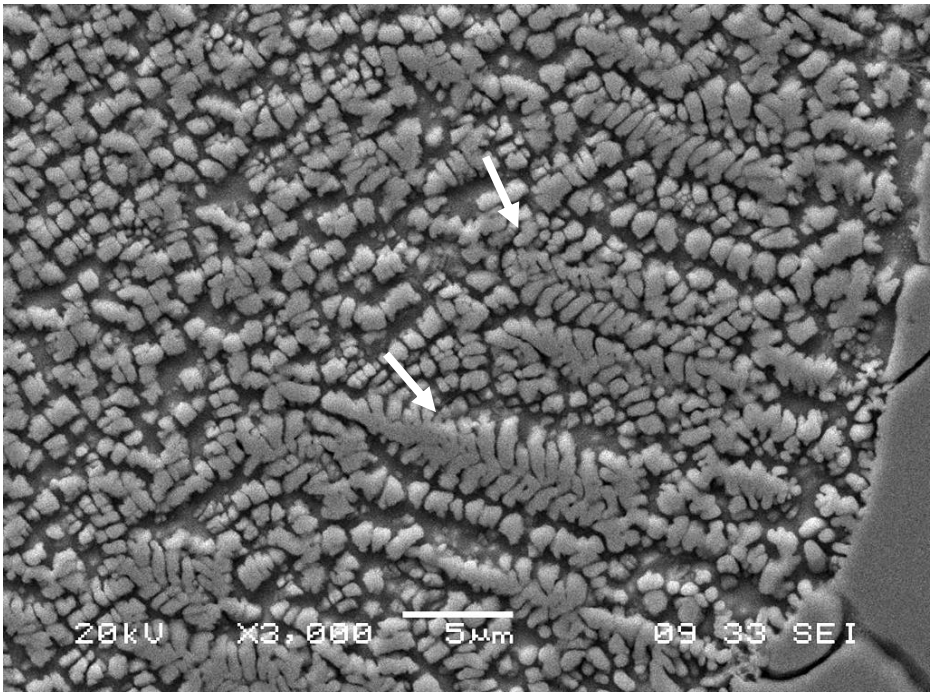

Figure 4-4: SEI micrograph showing arrow head γ′ precipitates in the interdendritic region (as indicated by arrows)

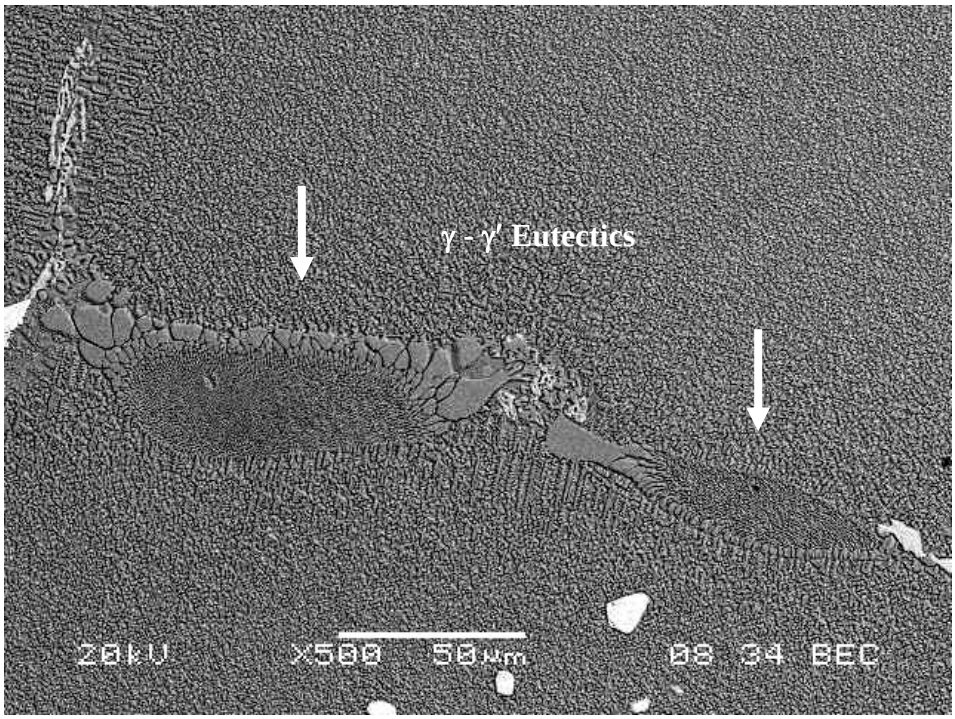

Figure 4-5: BSE micrograph showing γ - γ′ eutectics formed in the interdendritic region

γ - γ′ Eutectics

γ - γ′ eutectics were seen in the interdendritic regions as shown in Figure 4-5.These are formed from the last to solidify liquid that is present in the interdendritic regions during alloy solidification due to microsegregation. These eutectics are formed as a product of non-equilibrium solidification and consist of γ′ particles separated by thin γ matrix regions, and moreover, they are considered undesirable.

Elements like Al and Ti with k < 1 are rejected into the liquid ahead of the growing dendrite arm, thus resulting in continual enrichment of γ′ forming elements within the liquid present in the interdendritic regions until the temperatures reach equilibrium solidus temperature. According to Rosenthal and West [76], γ - γ′ eutectics in IN-738 LC form over a range of temperatures that could be as low as 1180^0C. In addition to this, based on DTA analysis from other researcher, γ - γ′ eutectic forms around 1198^0C and 1230^0C [80-82].

MC Carbides

MC type carbides are primary carbides that form at high temperatures in different shapes that include blocky, irregular and Chinese script like morphologies. Most of the MC carbide particles exist as discrete particles (Figure 4-6) both intragranularly as well as intergranularly, with some along the grain boundaries (Figure 4-7) and some of which are closely associated with γ - γ′ eutectics (Figure 4-5). Table 4-1 shows that there is significant variation in the composition of the carbide particles as determined by semi-quantitative SEM/ EDS analysis. This was initially reported by Ojo [83]. Thus based on the variation in morphology, location and composition, it is concluded that different types of carbides form over a range of temperatures which could vary from 1300^0C to temperatures close to eutectic transformations [81,82].

The metallic content represented by 'M' in MC carbides represents Ti, Ta, Nb, W, and Zr in IN-738 LC. Most of the interdendritic carbides were enriched in Ta, Ti, and Nb, except those that were closely associated with γ - γ' eutectics.

BSE micrograph in Figure 4-8 shows carbides that formed in close association with the γ - γ' eutectics. These carbides are reported to form at lower temperatures compared to other primary carbides and are enriched in Zr, and Nb as determined by semi-quantitative compositional analysis performed by EDS. This suggests that micro-segregation plays a major role in carbide formation. During ingot solidification, enrichment of carbide forming elements, which includes Ta, Ti, Nb, Zr, and C, takes place. These elements are positively segregating in the interdendritic region. When the concentration of these elements in the residual interdendritic liquid reaches a maximum, then the formation of these carbides begins by a eutectic type transformation reaction. Ti, Ta, and Nb rich carbides can be categorised into two main types [83]: TYPE 1 and TYPE 2, based on the atomic ratio of Nb/Ta. If the atomic ratio of Nb/ Ta is less than 1, then these carbides are categorised as TYPE 1 whereas, if the atomic ratio of Nb/Ta is greater than 2, then these carbides are categorised as TYPE 2. TYPE 1 carbides are high temperature carbides and TYPE 2 carbides are low temperature carbides. The elemental composition variation of TYPE 1, TYPE 2 and Zr, and Nb rich carbides is shown in Table 4-1

Sulphocarbide

Interdendritic regions also comprised of some sulphur rich particles either along the grain boundaries or in the near vicinity of eutectics, with the carbide particles. A back scattered electron (BSE) micrograph, shown in Figure 4-9, illustrates a sulphocarbide particle. X-ray mapping performed by using the energy dispersive spectroscopy (EDS) revealed that these

particles mainly constituted of S, Ti, Zr, Nb, and Ta. These particles are also terminal solidification products that are formed in the cast during cooling.

Sulphur, like many trace impurities, have been known to intensely segregate in nickel and its alloys even though present in parts per million (PPM) levels [84,85]. Sulphur traces mainly partition into last to solidify liquid in conventionally cast alloys. Its severe segregation onto the grain boundaries has been reported to increase shear strength thus causing grain boundary embrittlement and deterioration of the performance of superalloys at higher temperatures [86,87]. Various studies have shown that, alloying elements such as Ti, Zr, and Hf have very strong affinity towards sulphur [88,89]. The elements such as Ti, Zr, Nb, and Ta, are present in last to solidify liquids with rejected S and C forms M_2SC type sulphocarbides.

Other Terminal Solidification Products

A microstructural examination revealed other phases in the as-received IN-738 LC that solidifies close to some of the γ-γ′ eutectics and are also a part of secondary solidification products.

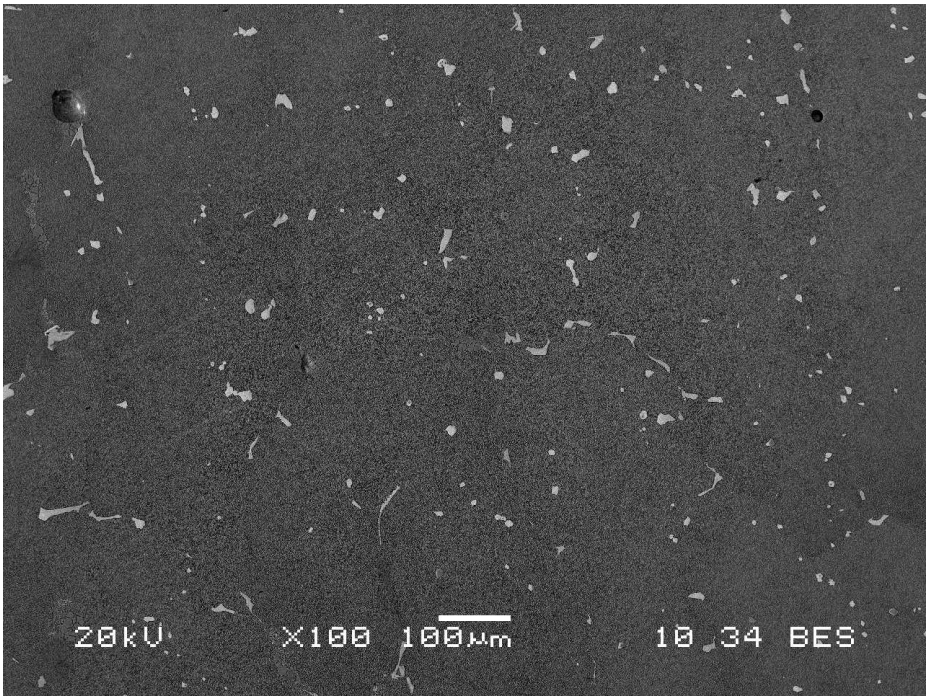

Figure 4-6: SEI low magnification micrograph of discrete MC carbide particles in as-received IN-738 LC

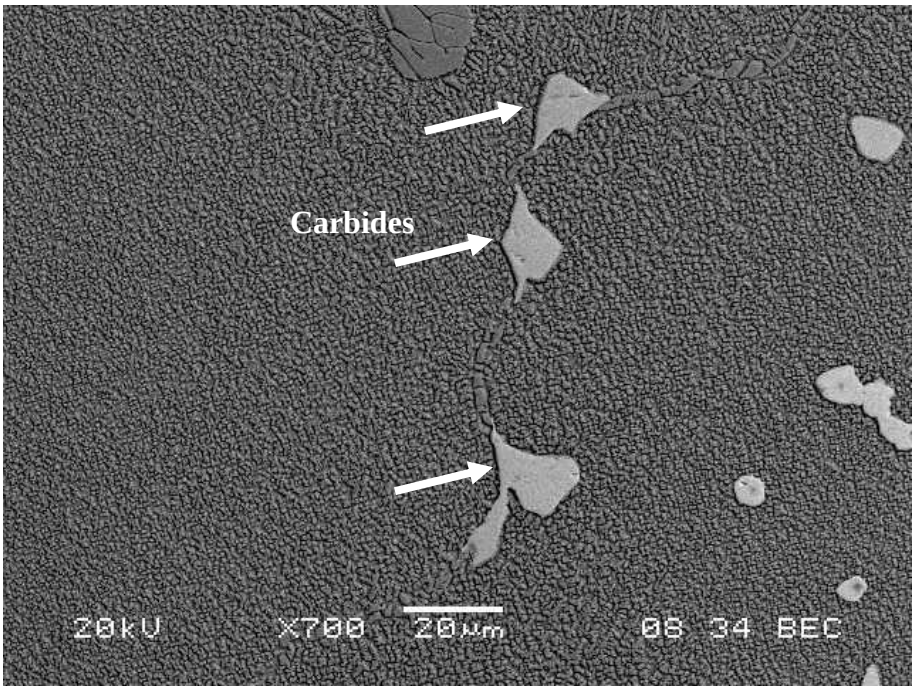

Figure 4-7: SEI micrograph showing carbide particles along the grain boundaries

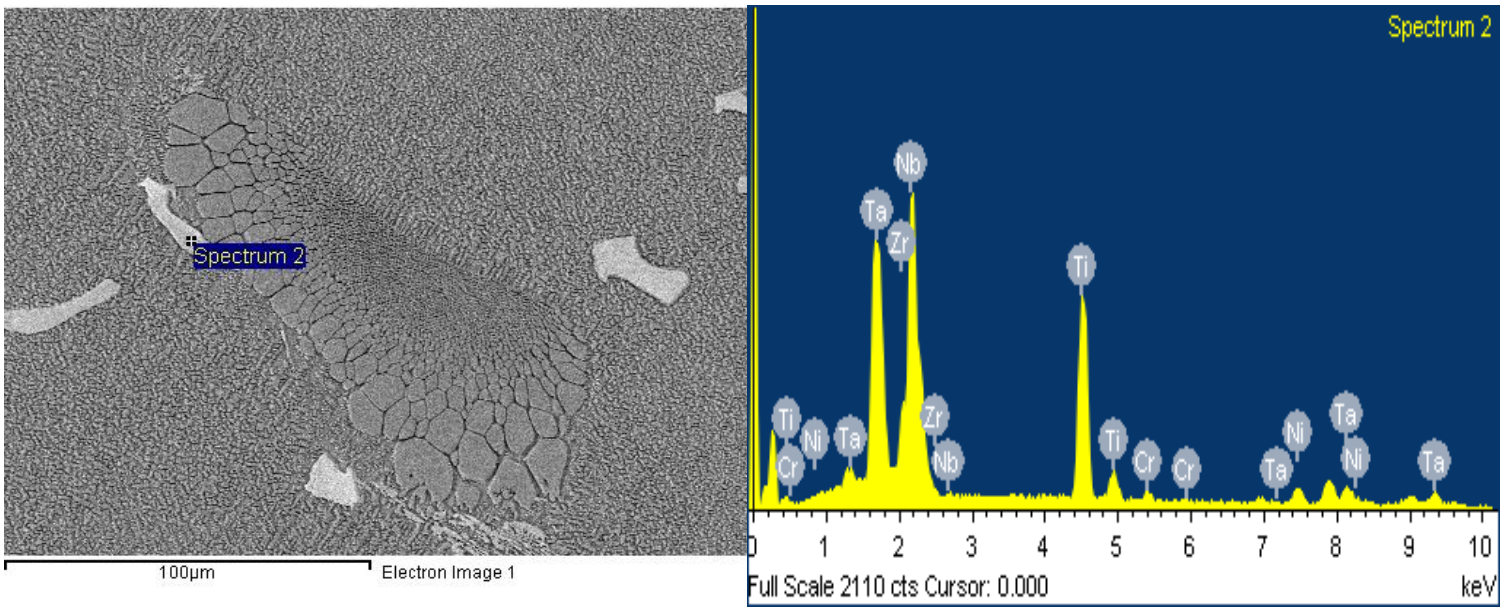

Elements	Atomic %
Ti	42.03
Cr	1.83
Ni	6.40
Zr	8.85
Nb	34.39
Ta	6.48

Figure 4-8: a) SEI micrograph of carbides associated with the γ -γ′ eutectics with EDS compositional analysis profile and b) elemental composition of the Zr- Nb rich carbide phase

Table 4-1: Elemental composition of MC carbides in as-cast IN-738 LC

Elements, at%	Type 1	Type 2	Zr-rich
Ti	52.9	51.7	42.0
Cr	1.4	1.5	1.8
Ni	2.9	4.9	6.4
Zr	-	-	8.8
Nb	11.7	30.6	34.4
Ta	27.4	11.2	6.5
W	3.7	-	-
Nb/Ta Ratio	~0.427	~2.732	~5.292

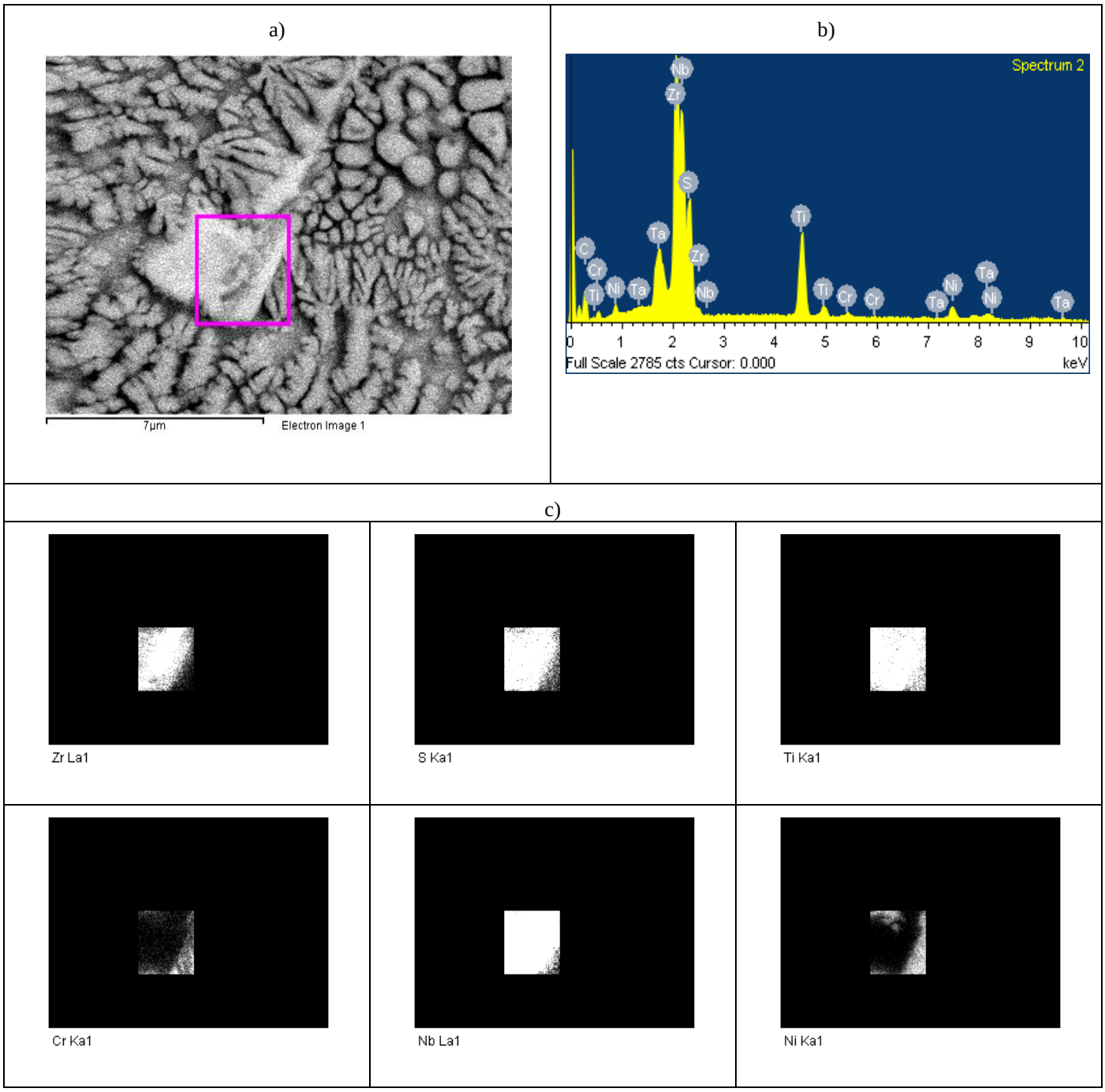

Figure 4-9: EDS area analysis of M_2SC sulphocarbide particle

Figure 4-10 is a BSE micrograph that illustrates different terminal solidification products that form at low temperatures in the alloy. These phases were characterised as Cr-Mo rich boride phase and intermetallic Ni-Zr and Ni-Ti phases, which are reportedly the terminal solidification products that form via ternary or quaternary eutectic type transformation in the present alloy [74].

Boron rich phases are generally formed along the grain boundaries or anti-phase boundaries during casting [90]. Although boron and Zr are added in very small quantities for their beneficial effects, such as improving high temperature strength and properties of the alloy. However, at the same time, these elements are observed to form complex phases that are hard and brittle, along the grain boundaries, which are detrimental to the alloy's performance because these phases act as melting point depressants.

Figure 4-11 is a SE micrograph that shows a boride phase and the associated EDS spectrum. The Cr- Mo peaks in the spectrum are considered to be a characteristic feature of M_3B_2 boride particles that form in nickel-base superalloys [91].

Ni-Ti and Ni-Zr rich phases also form as terminal solidification products based on intermetallic Ni_3Ti and Ni_5Zr, respectively. The remaining last to solidify liquid present in the interdendritic regions ahead of the γ - γ' eutectics is enriched with Zr, Ta, and Ti due to dendritic microsegregation. These elements have low solubility in γ and γ' phases and in other terminal solidification products. Thus saturation of the liquid by these elements results in the formation of products by eutectic transformation reactions.

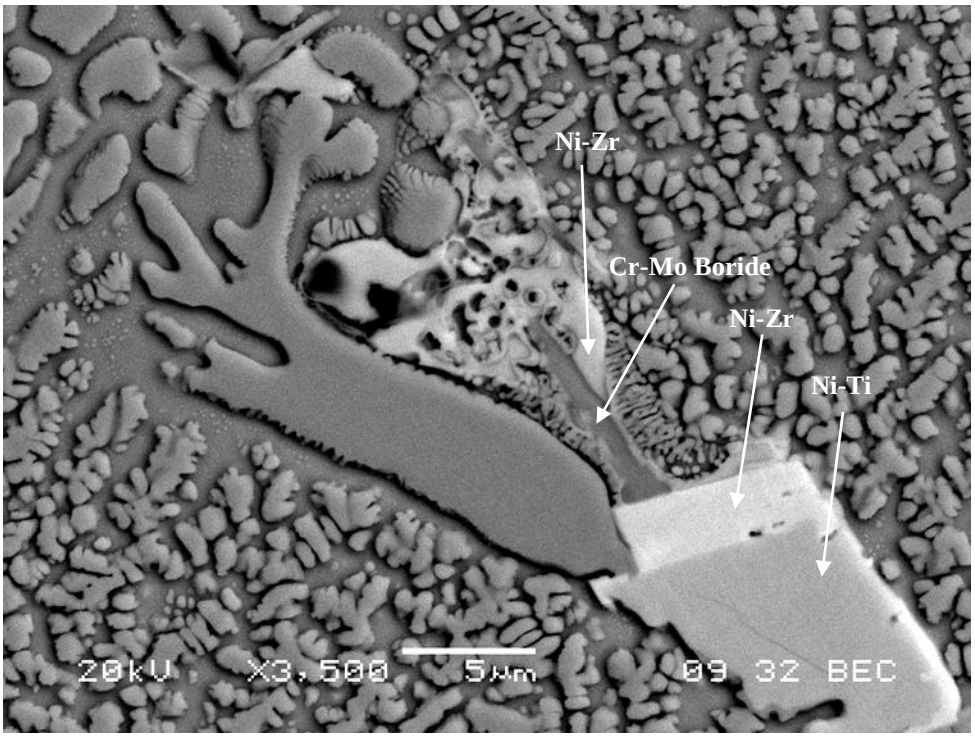

Figure 4-10: BSE micrograph showing the different terminal solidification products of IN-738 LC

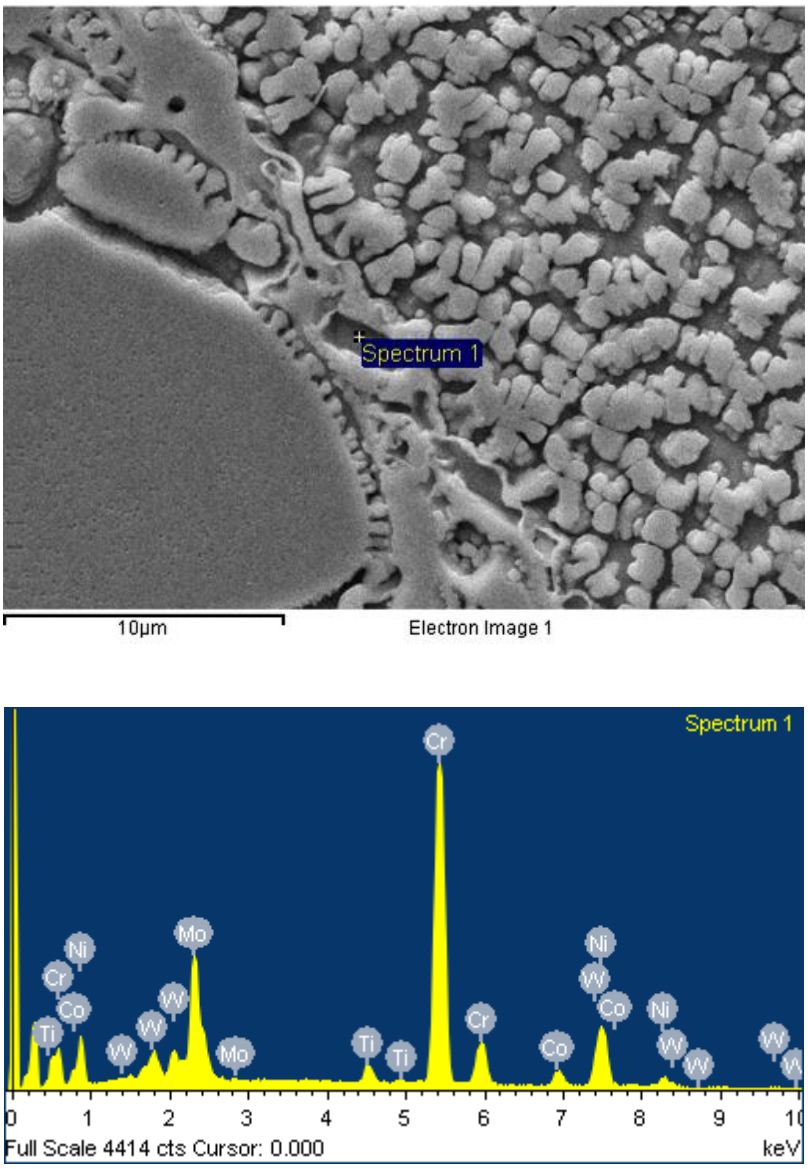

Figure 4-11: Secondary electron micrograph of Cr - Mo boride phase with associated EDS spectrum

4.1.2 Microstructure of pre-weld heat treated IN-738 LC

In the present work, all the three different castings of the IN-738 LC materials were given UMT and NHT pre-weld heat treatments, details of which are shown in Table 3-2. Like those in the as-received condition, the phases present in CS, DS, and SC are similar, and hence the microstructure of CS is discussed here for brevity. The UMT involves first, solutionizing at 1120^0C for two hours followed by air cooling that results in complete dissolution of γ′particles present in the dendrite core and a partial dissolution of γ′ particles present in the interdendritic region. After solutionizing, aging is performed at 1025^0C for 16hrs followed by water quenching. This mainly results in a predominant dispersion of spherical γ′ precipitates in γ matrix, as shown in Figure 4-12. The irregular shaped γ′ precipitates present along the grain boundaries in the as-received material still remained after UMT. The other micro-constituents including γ - γ′ eutectics, MC carbides and terminal solidification products were consistently present in the matrix (Figure 4-13). Zhang et al [92] carried out a comprehensive analysis on this alloy by using UMT and identified intergranular formation of M_5B_3 borides.

NHT heat treatment consisted of solutionizing at 1120^0C for 2hr and air cooling, followed by aging at 1120^0C for 24 hours and then furnace cooling. This heat treatment resulted in coarse and coagulated irregular shaped morphology of γ′ particles, as shown in Figure 4-14a, and secondary solidification products are seen to be still present within the γ matrix. A needle like phase is observed to be present with the carbide and is shown in Figure 4-15. From semi-quantitative EDS x-ray spectrum analysis showed that the particle is Zr-Ti rich sulphocarbide microconstituent. However, the grain boundaries after this heat treatment constituted of coarse and irregular shaped γ′ particles (Figure 4-14c).

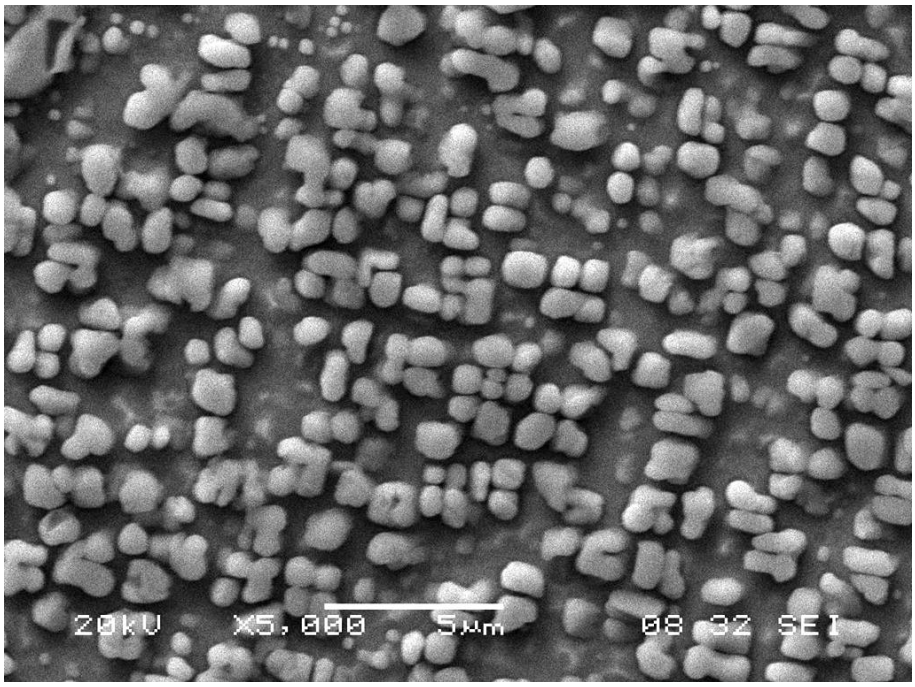

Figure 4-12: SEI micrograph showing γ′ precipitate formed in UMT pre-weld heat treated IN-738 LC

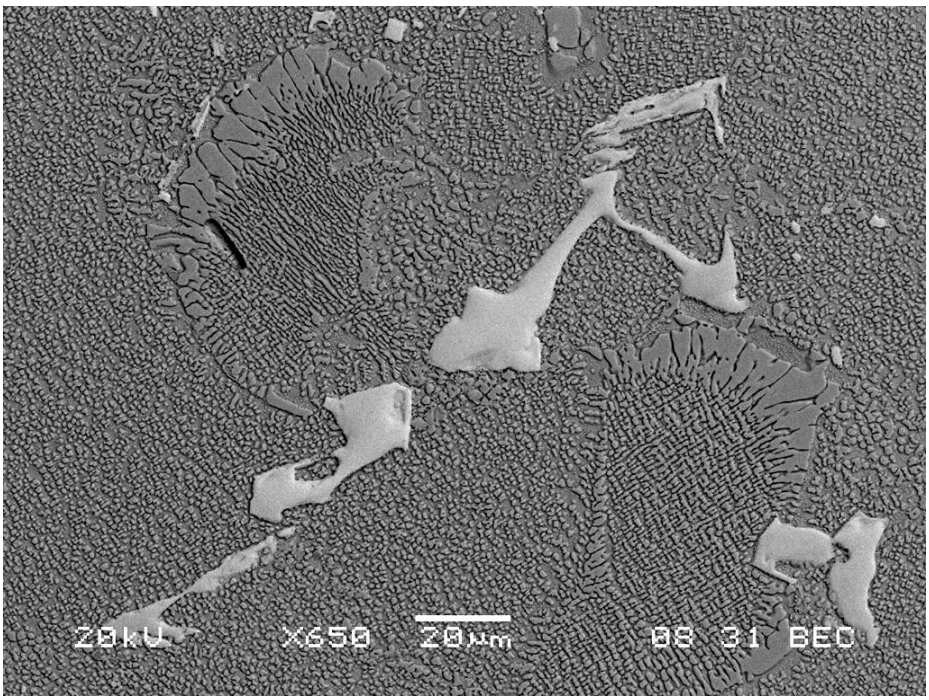

Figure 4-13: BSE Micrograph showing secondary solidification microconstituents

a)

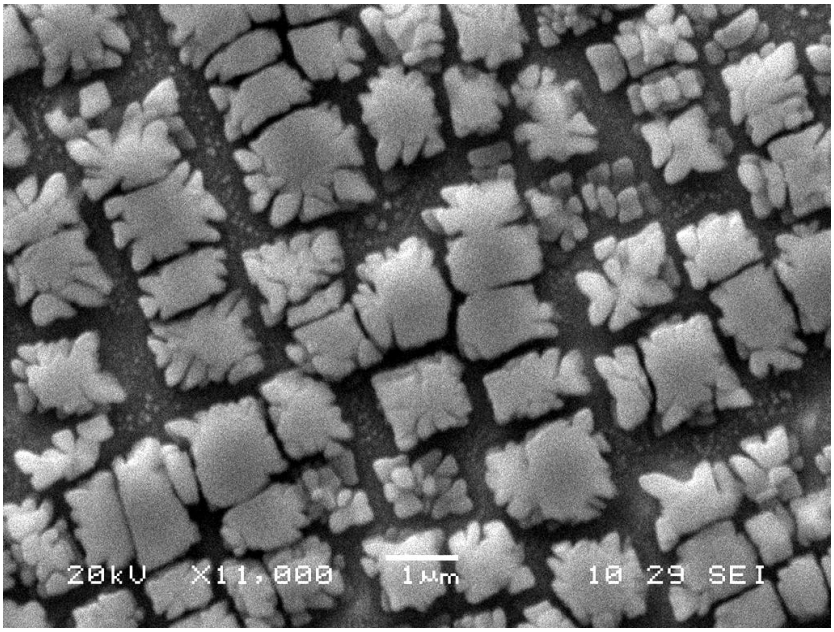

b)c)

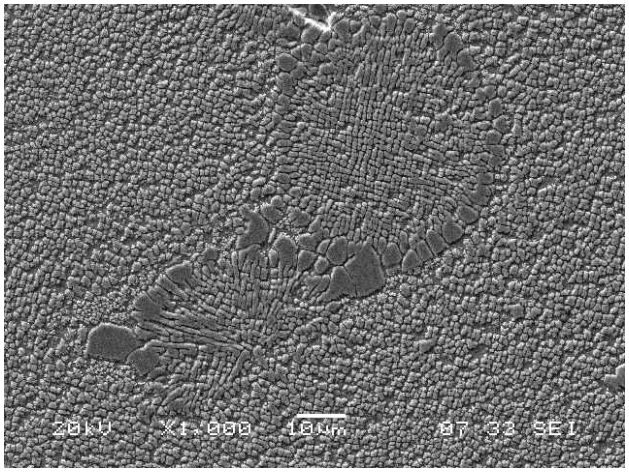

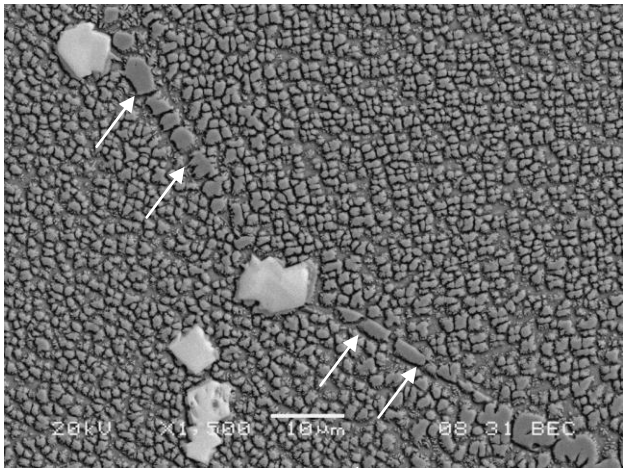

Figure 4-14: a) SEI micrograph of γ′ morphology b) γ - γ′ eutectics c) γ′ along the grain boundary formed in NHT pre-weld heat treated IN-738 LC

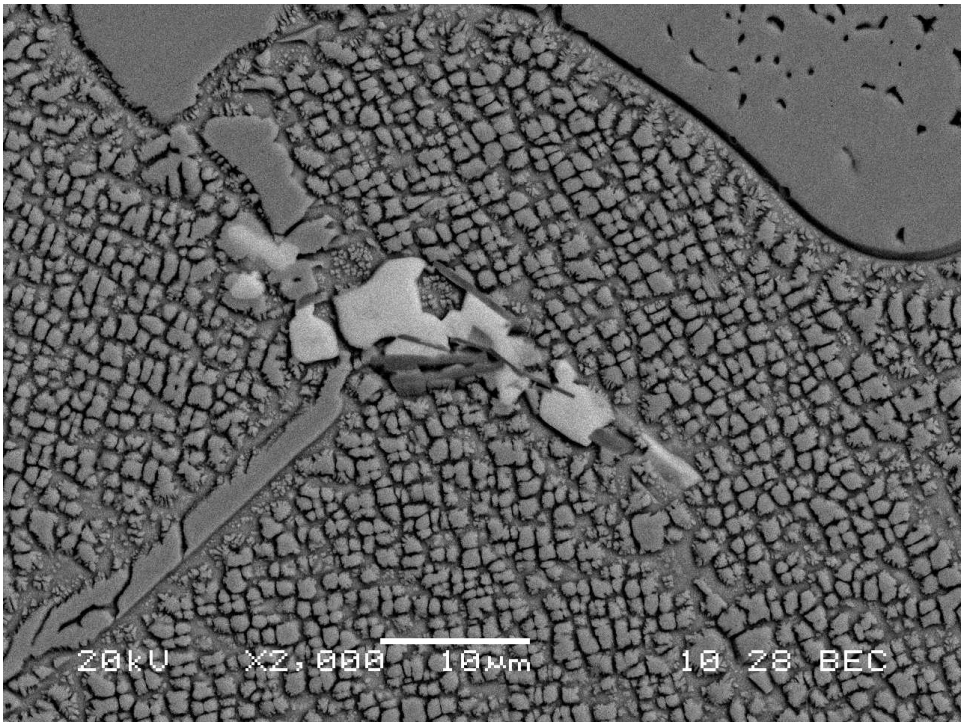

Figure 4-15: BSE micrograph of M_2SC sulphocarbide formed in NHT pre-weld heat treated IN-738 LC

4.2 Microstructure of As-welded Material

Similar features were observed in the microstructure of as-welded CS, DS, and SC IN-738 LC, and for the sake of brevity the microstructure of CS IN-738 LC that was treated by using UMT and NHT are discussed in detail here.

4.2.1 Microstructure of Fusion Zone

Figure 4-16, shows an optical micrograph of a weld cross-section of IN-738 LC that was subjected to UMT heat treatment, which shows a nail head type of weld profile obtained by autogeneous CO_2 laser welding. A typical cellular dendritic microstructure is shown in Figure 4-17 as a higher magnification optical image. There is no evidence of exclusive FZ cracking i.e. centerline cracking in all the welds except in DS IN-738 LC, however, there are some microfissures observed in the HAZ regions that intersect the fusion boundary and extends into the FZ. Besides these, other cracks were observed to generally occur towards the bottom of the weld. The centerline cracking in the DS alloy was found to be related to the welding parameters used, and could be considerably controlled by using optimised welding parameters and also by the addition of the filler alloy. Since, FZ cracking is not a major weldability problem for IN 738, this work only focuses on HAZ cracking.

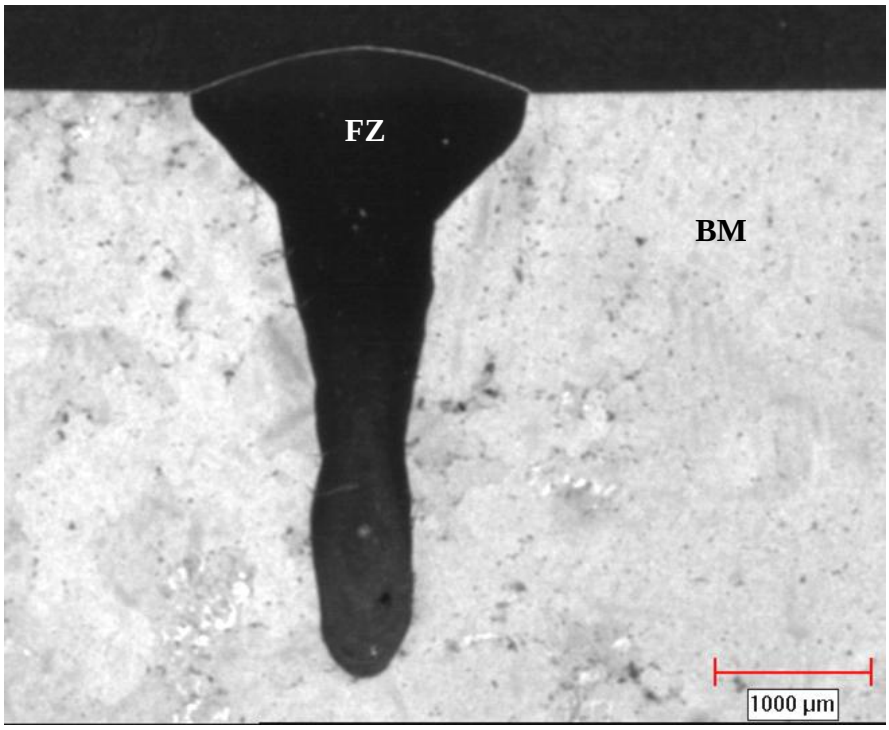

Figure 4-16: Optical image illustrating the weld profile

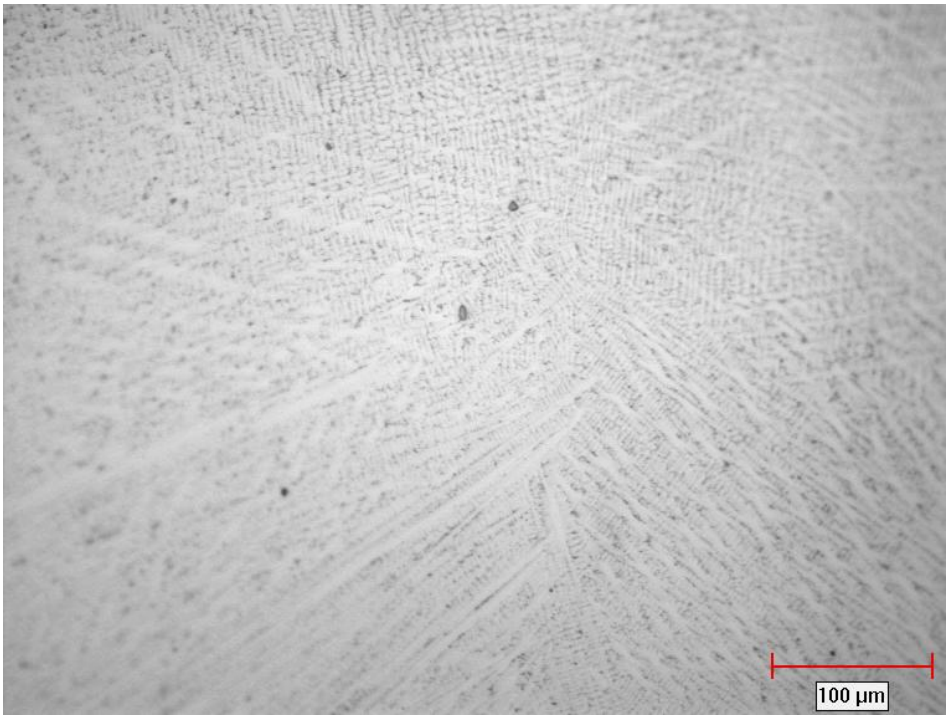

Figure 4-17: An optical image of fusion zone showing cellular dendritic morphology.

The FZ is an area where complete melting occurs followed by solidification of a stirred liquid pool of high temperature gradients, and rapid growth rates [93,94]. The weld solidification is initiated by the formation of γ dendrites from the fusion boundary and continues to the fusion centerline. The direction and extent of micro-segregation can be described by a fundamental solidification parameter, that is, the elemental distribution partition coefficient k, of the alloying elements. Under equilibrium conditions, and by neglecting undercooling at the dendrite tip, the solute redistribution can be described by using Scheil's equation:[27]

$$C_S = kC_0\,[1 - f_s]^{(k-1)}$$

where C_S is the solute concentration in the solid at the solid - liquid interface, k is the equilibrium distribution coefficient, C_0 is the nominal solute concentration, and f_s is the fraction of the solid. The first solid to form from the melt is the dendrite core, with a composition of kC_0. Thus, at the beginning of solidification, $f_s = 0$, the ratio between the composition at the dendrite core and nominal composition will give the value of k partitioning coefficient. An assumption taken in this approach is that, there exists no diffusion of solute elements in the solid during solidification. The initial partitioning coefficients of various alloying elements present in IN-738 LC have been previously determined and reported by Ojo [83], where the k values indicate that the dendrite core is enriched with the elements Ni, Cr, Co, W, which have k values greater than unity. On the other hand, the interdendritic regions are enriched with elements with k values less than unity which includes Ti, Zr, Nb, Ta, Mo, and Al. The interstitial elements carbon and boron extensively segregate into the interdendritic regions.

The extent of the solid - state diffusion during solidification is a factor which is dependent on the cooling rate and interdendritic arm spacing. The average value of secondary dendrite arm

spacing along the centerline of FZ was measured to be about 3.5μm. The cooling rate was calculated from the following equation [95]:

$$\lambda s = k_s \theta^n$$

where, θ is the cooling rate, λs is the secondary dendrite arm spacing, and k_s, n are the constants. Experimentally, the values of the constants are $k_s = 4.7 \times 10^{-2}$mmK$^{1/3}$s$^{-1/3}$ and $n = -0.4$, respectively, as determined by Quested and Mclean [95]. The cooling rate in the FZ was calculated to be around 660^0C/s. This cooling rate in the FZ is extensively rapid when compared to solidification rates observed in conventional welding and casting techniques. This extremely fast cooling rate drastically reduces any diffusion of solute during weld metal solidification. Thus, the use of Scheil's equation is validated. Similar elemental segregation behaviour (partitioning coefficient) has been observed in IN-738 LC and other superalloys by various researchers [96-98].

An investigation of FZ showed that the interdendritic region mainly consisted of secondary solidification microconstituents with a blocky, irregular, rod-like, or Chinese-script like morphology (Figure 4-18). Most of these irregular shaped particles were MC carbides rich in Ti, Ta and Nb that formed by the following eutectic transformation reaction, $L \rightarrow MC + \gamma$

Some MC carbides were observed in the FZ with sizes similar to those of the MC type carbides present in the base metal. Such coarse primary MC carbides shown in Figure 4-18, which survived through the heating cycle during welding has been commonly observed in the FZ of other superalloys as well. Liu et al [99] reported that such primary carbides can sustain up to temperatures above 1550^0C in the weld pool for 5 - 10 minutes.

The other secondary micro-constituents present in the interdendritic region included γ - γ′ eutectics and very fine nano sized γ′ precipitate particles, which are reportedly difficult to be observed with SEM.

In IN-738 LC, many secondary solidification products are possible which include carbides, borides, eutectics and intermetallics that are rich in Ti, Nb, Mo, Ta, and Zr. Auger electron microscopy confirmed the presence of carbon partitioning into the solidifying liquid [100]. Furthermore, the k values for carbon and boron, as indicated by a binary Ni-X phase diagram are less than unity [101], which plays a significant role in the formation of secondary solidification products.

This positive dendrite micro-segregation of carbon into liquid with the presence of strong carbide formers like Ti, Nb, and Ta, gradually results into precipitation of carbides by a monovariant eutectic reaction, $L \rightarrow \gamma + MC$. Upon further cooling, the super saturation of the remaining interdendritic liquid with γ′ forming elements Ti, Al, Ta takes place. The eutectic transformation reaction that forms the γ - γ′ eutectic phase would then continue to occur until the solidification is completed.

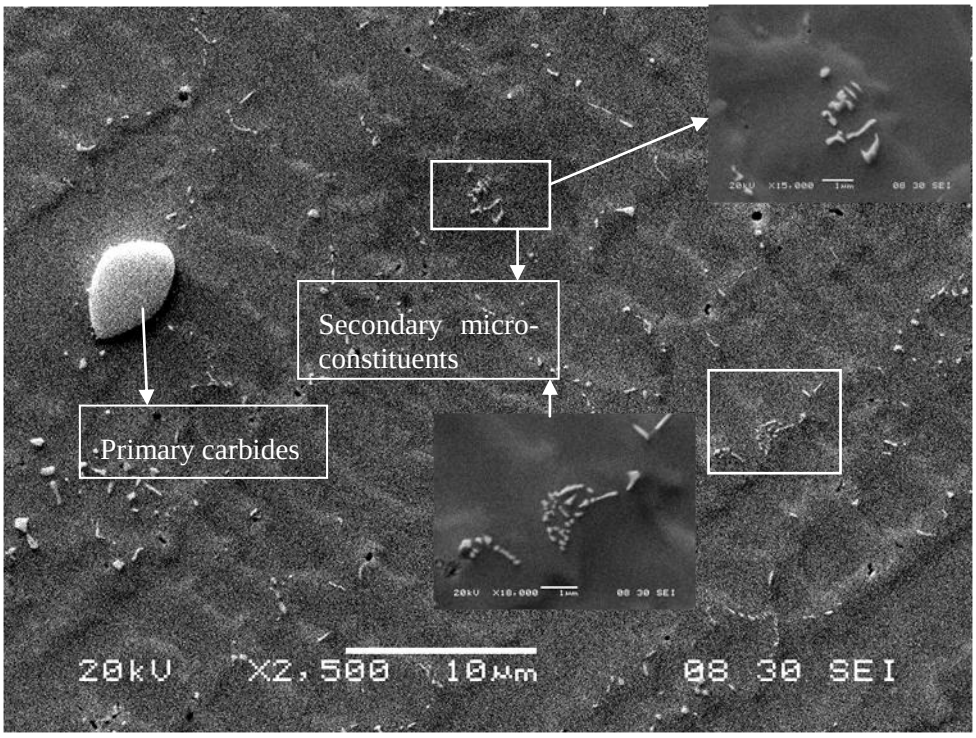

Figure 4-18: SEI micrograph of solidification microconstituents formed in fusion zone

4.2.2 HAZ Microstructure

The HAZ regions in the weld revealed the occurrence of micro-fissures around the fusion boundary in the CS and DS IN-738 LC alloy, irrespective of the heat treatment, although single crystal IN-738 LC did not show any evidence of cracking. The cracks that formed were intergranular in nature and intersected the fusion boundary, of which some extended into the FZ and some into the base material. The intergranular microcracks had an irregular and zig-zag morphology with irregular crack paths with smooth edges, which is a distinctive feature of liquation cracking. A SE micrograph representing liquation cracking in HAZ is shown in Figure 4-19. A careful examination of these cracks under high magnification in the SE and BSE modes revealed that the cracked surfaces were decorated with resolidified products. The resolidified microconstituents were characterised as γ - γ' eutectic, carbides, borides, intermetallic and also γ' precipitate particles.

The metallurgical factors that contribute to HAZ microfissuring have been attributed to the liquation of grain boundaries in the HAZ region, as previously discussed in the literature review (Chapter 2). During welding, liquation of the grain boundaries present in HAZ region results in replacement of strong solid-solid interface with weak solid-liquid interface which consequently reduces the inherent resistance to cracking. Thus, HAZ intergranular liquation cracking mainly occurs by decohesion across the solid -liquid interface when on -cooling welding tensile stresses exceed the local strength of the interface.

HAZ intergranular liquation can occur via equilibrium super-solidus melting or non-equilibrium sub-solidus melting [43,44]. The former generally occurs in all the weldments as temperatures during the weld thermal cycle reaches above the equilibrium solidus temperature.

However, non-equilibrium sub-solidus melting is considered to be the most detrimental. The liquation due to sub-solidus melting is mainly driven by constitutional liquation of secondary microconstituents present along the grain boundaries in the pre-weld alloy. This reaction takes place by a eutectic type transformation. The presence and persistence of low melting liquid phases on HAZ grain boundaries and its inability to accommodate the thermal-mechanical stresses during weld cooling, often results in cracking. This phenomenon was first observed by Pepe and Savage [45], where this mechanism was used to explain the melting of Ti sulphide particles in 18- Ni maraging steels. In the present alloy, constitutional liquation of γ′ precipitates, γ - γ′ eutectic, carbides, borides, and intermetallics has been observed and reported by Ojo et al [52].

A microstructural analysis of the HAZ region of the weldment shows constitutional liquation of γ′ precipitates, γ - γ′ eutectic, MC carbides, and other phases such as Cr-Mo borides and M_2SC sulphocarbides, (Figure 4-21). The extent of liquation is heavily influenced by the chemical composition and location, relative to the fusion boundary.

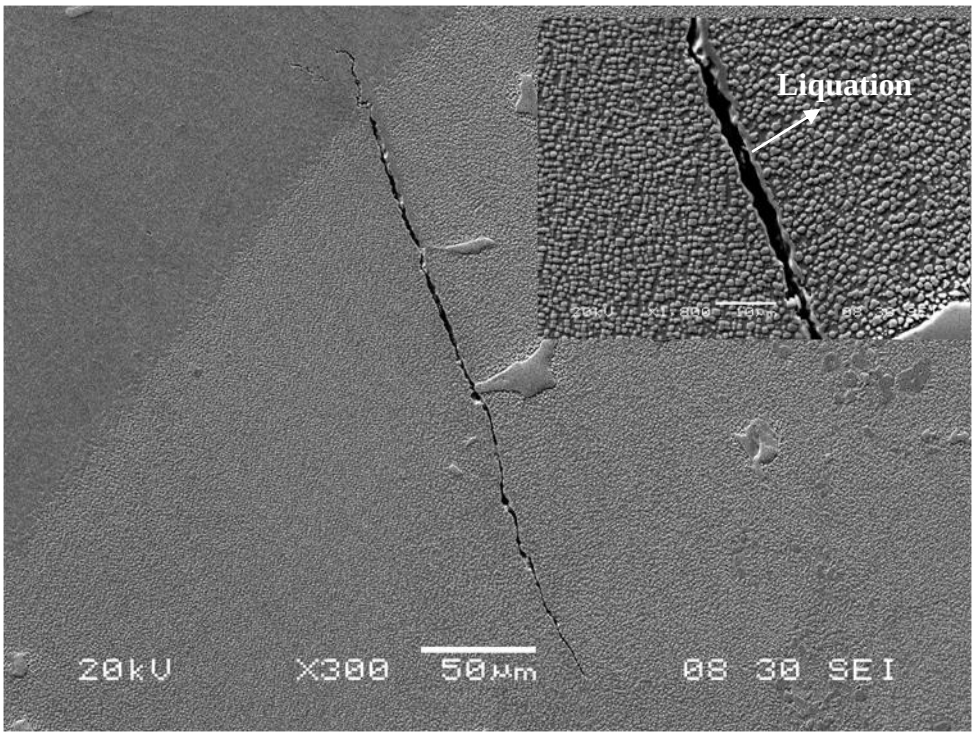

Figure 4-19: SEI micrograph of HAZ liquation cracking

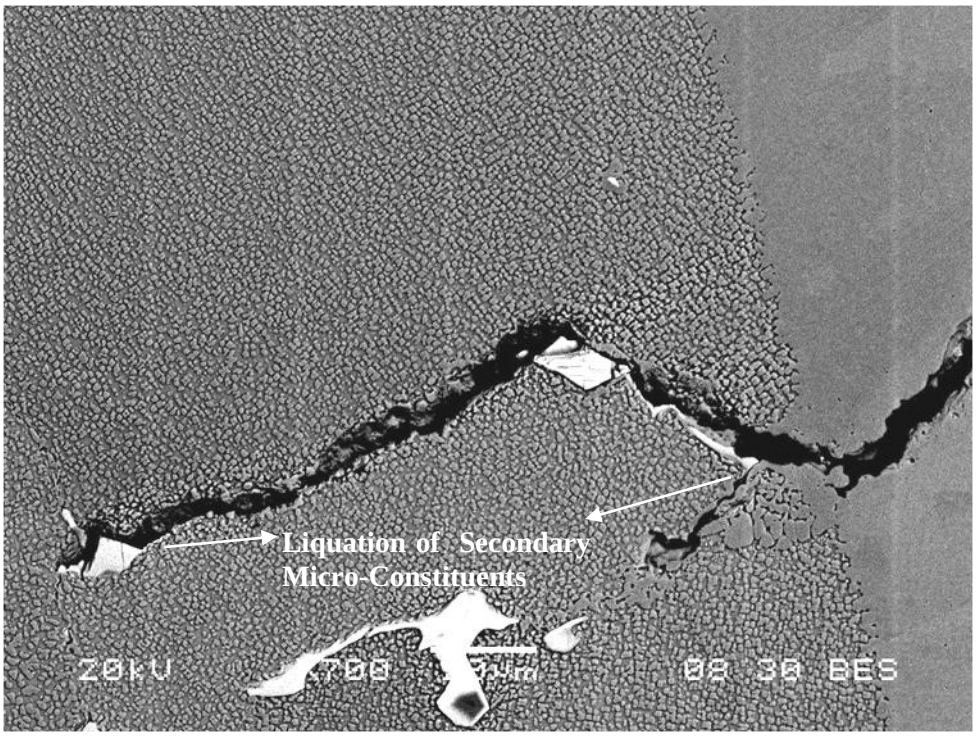

Figure 4-20: BSE micrograph of secondary micro-constituents present along the crack

One of the major contributors to constitutional liquation that has been reported in the literature is the carbides constituents which exacerbate the causes of intergranular liquation cracking [49,52,100,102]. An examination of the HAZ region by using the SEM revealed that MC type carbides present in the HAZ region have constitutionally liquated and contributed to liquation along the grain boundaries and subsequently to cracking. A Ta, Ti and Nb rich constitutionally liquated carbide particle is shown in Figure 4-21.

Cr- Mo borides phases have been observed to significantly contribute to intergranular liquation. Rapid heating during heating during welding may lead to decomposition of these particles releasing boron and sulphur atoms. The boron atoms form solute vacancy complexes and these complexes at high temperature sink into the grain boundaries. The boron particles which are enriched at the grain boundaries serves as melting point depressants in the nickel alloy, thereby lowering the local melting temperature of the areas that surround their respective particle matrix interfaces. Co-existence of M_3B_2, M_2SC or MC carbide particles with γ-γ' eutectic colony may lead to considerable liquation [52]. This sub-solidus melting of various phases in the alloy is a major contributing factor to HAZ intergranular liquation. However, the presence of liquid is not a sufficient determinant of the cracking susceptibility of an alloy, but its ability to sufficiently wet and effectively flow along the grain boundaries has more pronounced effect on HAZ intergranular liquation.

In order to overcome cracking in the IN-738 LC alloy, two different aspects were considered which included: (a) reduction in number of sites (grain boundaries) susceptible to cracking (b) optimization of microstructure by using a suitable pre-weld heat treatment. These will be discussed in the following sections.

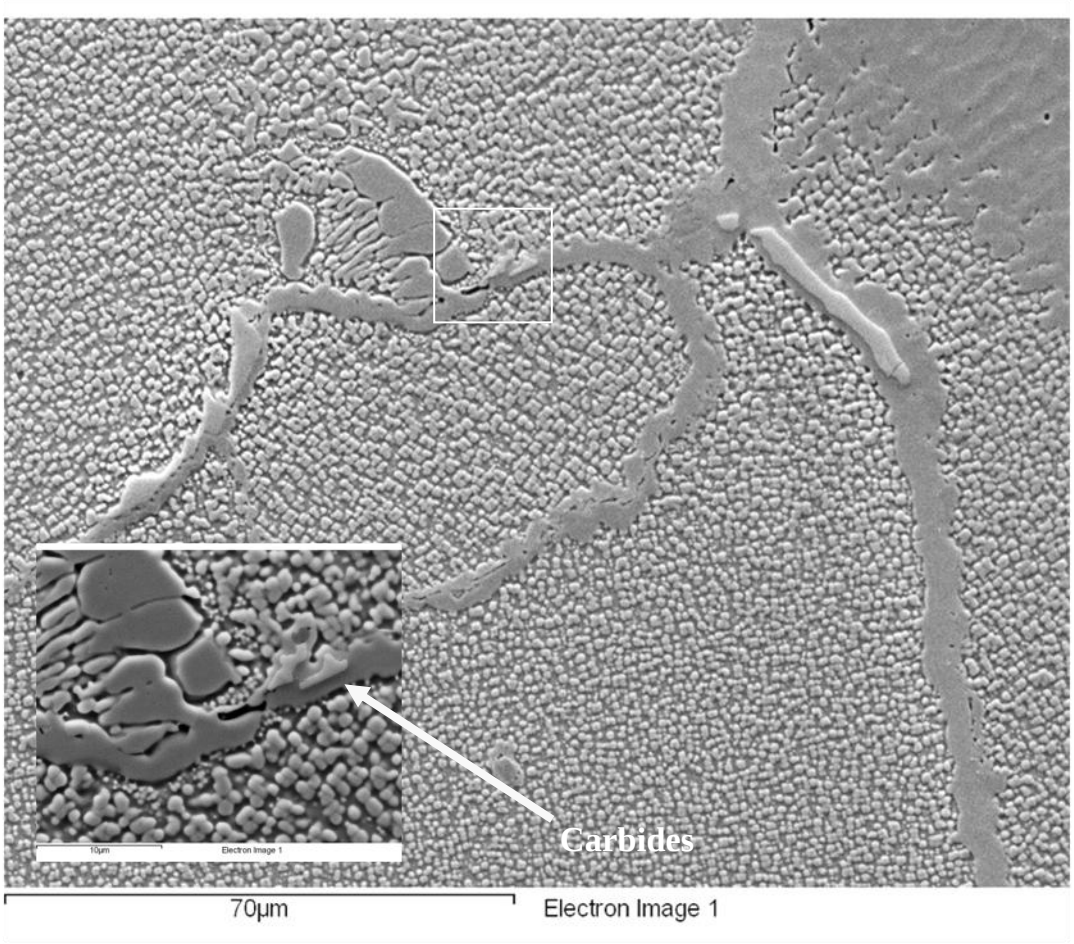

Figure 4-21: SEI micrograph of HAZ liquation and microconstituents associated with it.

4.3 Effect of grain boundaries on weldability of IN-738 LC

The weldability of IN-738 LC and its association with the grain structure of the alloy was studied and is presented in this section. Laser welding was performed on different castings, the CS, DS and SC IN-738 LC, which were subjected to a pre-weld heat treatment by using UMT. The total crack length (TCL) measured in the HAZ region from 10 sections of each welded sample is shown by a graph plotted in Figure 4-22, which illustrates the extent of microfissuring in the different cast forms. It is evident from the graph that, as the number of grain boundaries reduced, there was a significant reduction in HAZ cracking, following the trend of CS > DS > SC. This implies that, IN-738 LC in the CS cast form has a higher probability of crack development in the HAZ due to grain boundary liquation, whereas IN-738 LC in the DS cast form has a lower probability of cracking in the HAZ due to large grain size and consequently, fewer number of grain boundaries intersect the fusion boundary. Finally, due to the absence of grain boundaries in SC cast form of IN-738 LC, there is no evidence of HAZ liquation cracking, therefore SC IN-738 LC has the least probability of intergranular liquation cracking in the HAZ.

In the previous section, observations of the microstructure of various phases that contribute towards liquation reactions were discussed. These are important reactions that result in the formation of low melting phases on the HAZ grain boundaries in IN-738 LC. However, the existence of low temperature melting phases on the grain boundaries is not the factor that is solely responsible for the occurrence of HAZ liquation cracking.

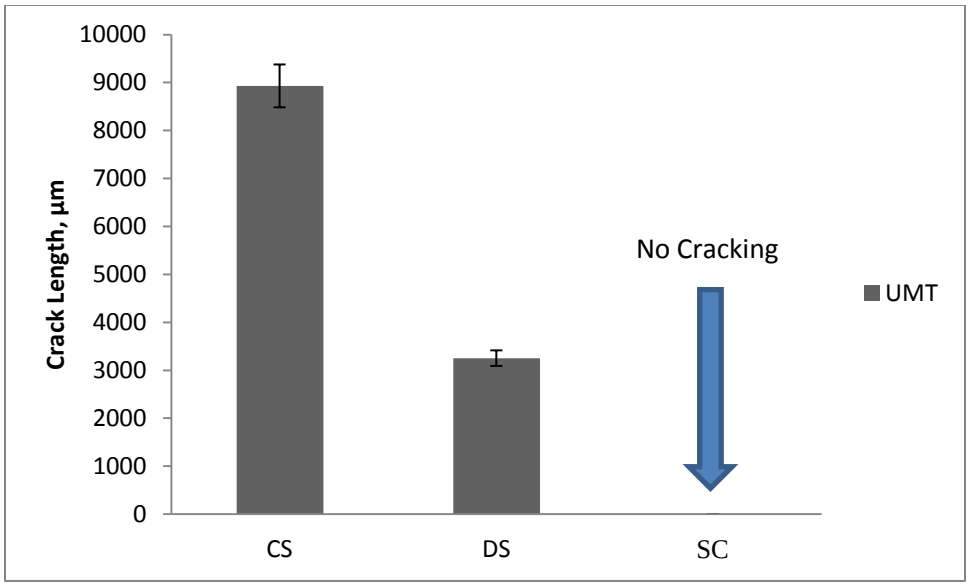

Figure 4-22: A graph comparing the extent of cracking in HAZ of IN-738 LC in as-welded condition

To create favourable conditions for cracking, the liquid formed on the HAZ grain boundaries should uniformly wet the grain boundaries and continuously spread along them. This would then, reduce the ductility of the alloy, as well as, its capability to accommodate and relax welding stresses. As proposed by Smith, the distribution of intergranular liquid along the grain boundaries is represented by the first approximation equation: [103]

$$\gamma_{gb} = 2\gamma_{SL} \cos\theta$$

where θ is the wetting angle, γ_{gb} is the grain boundary energy, and γ_{SL} is the solid - liquid surface energy. From this equation, it is deduced that for a given value of the solid - liquid interfacial energy, if the grain boundary energy is high, its tendency to be penetrated and wetted by the liquid phase is subsequently higher. It is known from the literature that the grain boundary energy is inherently high for random or high angle grain boundaries [104]. Similar observations were reported by Guo et al [105], where the grain boundary character distribution was correlated with intergranular liquation in IN 718. The results showed that liquation mostly occurs at random grain boundaries and extensively occurs at high angle grain boundaries when compared to low angle or special boundaries such as twin boundaries. Rappaz et al [106] proposed a coalescence model that principally described the coalescence of primary phase dendritic arms within a single grain or at the grain boundaries. The cause of cracking in a material was due to difficulty in bridging or coalescence of the dendritic arms during the last stages of solidification. According to this model, an increase in the grain boundary energy, changes the force on the solid-liquid interface from an attractive ($\gamma_{gb} < 2\,\gamma_{SL}$) to a repulsive one ($\gamma_{gb} > 2\,\gamma_{SL}$).

The liquid present between two repulsive grains could sustain up to temperatures below the melting point. It has been suggested that last to solidify liquids that are significantly apparent at

high angle grain boundaries which persist below the solidus temperatures, further widen the solidification temperature range. The consequence of which leads to an extended region of extremely low shear strength in which the strains are highly localised and can induce cracking. Thus reduction in cracking could be possibly achieved by reducing the number of high angle grain boundaries.

In the present study, observations made from comparisons of the grain boundary structure in CS, DS and SC cast forms of IN-738 LC are presented. The grains present in the CS cast form were randomly oriented, with a significant number of high angle grain boundaries that intersected the weld fusion boundary. This further assisted the liquid from the weld zone to wet and penetrate the grain boundaries in the HAZ region. In contrast, the grains in the DS cast form were multi-columnar with grain boundaries aligned in the direction of solidification (i.e. <001> direction for FCC nickel based superalloy) which reduced the possibilities of the perpendicularly oriented grain boundaries to intersect the FZ. Therefore, fewer crack susceptible grain boundaries intersected the weld fusion boundary. Finally, a single grain constitutes the SC cast form of the IN-738 LC alloy where there was no HAZ grain boundary liquation cracking as there were no grain boundaries that intersected the fusion boundary. This has been deduced from previously mentioned graph (Figure 4-22). Therefore, identical compositions of CS, DS, and SC IN-738 LC, laser welded under similar conditions, showed a reduction in extent of cracking with a reduction in the number of grain boundaries, in the following order: SC < DS < CS. A similar observation was made by Huang et al [107], wherein the effect of grain size was studied on cast alloy 718 that was electron beam welded.

The results showed that improved weldabilty is facilitated by coarsening of the grain, which reduces the probability of number of grain boundaries that intersected the fusion boundary. Sidhu

et al [108] also indicated similar observations in laser welded DS IN-738 LC alloy. Their results showed a reduction in the HAZ microfissuring with reduction of number of high angle grain boundaries that intersect the weld bead. The weld beads in the work of Sidhu et al [108] were produced in the transverse and longitudinal directions in order to obtain variation in the number of grain boundaries. Another approach by the same authors [109], showed a reduction in HAZ microfissuring with a decreasing number of grain boundaries which was demonstrated by comparing the extent of weld cracking in three different nickel based superalloys (CS IN-738 LC, DS RENE 80 and a Single crystal) welded with similar parameters.

Another aspect of the SC welding is its tendency to form new grains during the weld thermal cycle. These new grains are often formed near the weld centerline and destroy the integrity of the single crystal morphology. These grains have different orientation than those of the grains in the base metal, and are termed stray grains. The undesirable high angle grain boundaries are associated with the stray grains formed in the weld FZ which act as weak links in the microstructure and thus make it highly susceptible to exclusive FZ cracking [110-112]. Gaumann et al [113], proposed a theory of constitutional supercooling based on solidification processing in order to predict the columnar to equiaxed transition in the weld repair of SC alloys. According to their theory, the volume fractions of stray grains,Φ, depends on the temperature gradient, G, and the solidification velocity, V, and hence the equation:

$$\frac{G^n}{V} = K$$

where K is a factor that depends on nucleation rate (a supercooling factor) and n is a material constant. Columnar solidification is achieved by satisfying the above equation. These solidification parameters are significantly influenced by the welding parameters, which indirectly

influence the volume fraction of stray grains. Previous research has provided contradicting information on how these welding parameters affect stray grain formation.[110,113-115] Centerline cracking was not observed in the SC IN-738 LC weld metal even with the presence of stray grains, as shown in Figure 4-23. Therefore, the presence of stray grains is not the only factor responsible for solidification cracking in the FZ. The solidification behaviour also significantly influences the cracking tendency of the alloy.

Hot cracking usually occurs in a material at the last stage of solidification where there is uniform distribution of liquid film along solidifying grain boundaries and interdendritic regions. At this terminal stage of the solidification, shrinkage stresses are highly developed in the alloy and the presence of terminal liquid along the grain boundaries limits the accommodation of the stresses and strains produced.

The solidification cracking susceptibility of a material is extensively influenced by two material properties, viz. (a) solidification temperature range (ΔT) (b) distribution of terminal liquid that persists during the last stages of solidification. The propensity for solidification cracking is increased with the widening of the solidification temperature range and as well increase in the amount of distribution area of the interfacial liquid [116].

The composition of the liquid present in the terminal stages also significantly contributes to cracking. In the case of the IN-738 LC superalloy, very small amount of interfacial liquid is present during the terminal stages of solidification, and FZ cracking was observed to be reduced.

a)

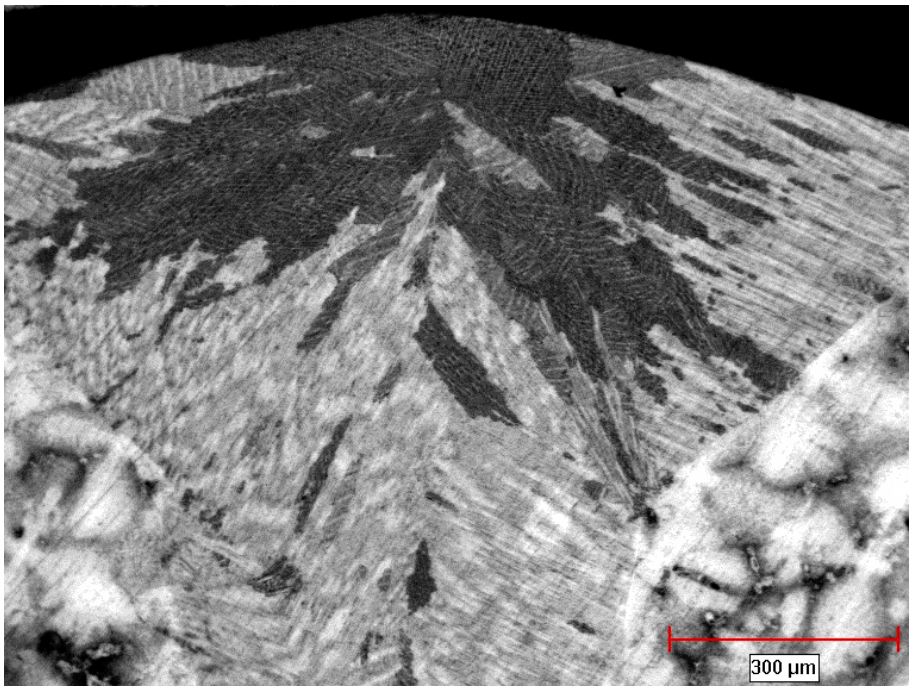

b)

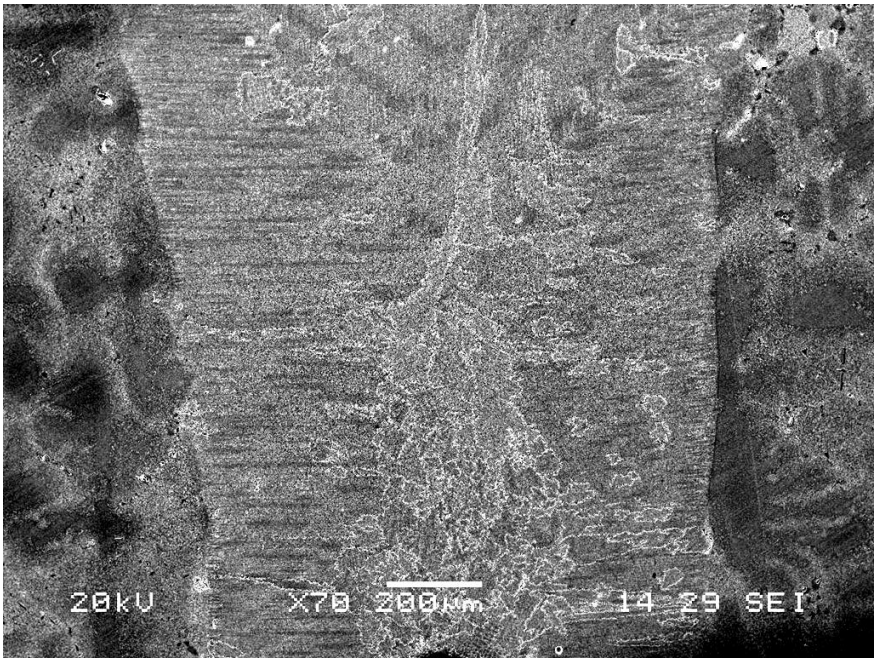

Figure 4-23: a) Optical image b) SEI micrograph showing stray grains formed in weld fusion zone of SC IN-738 LC

The susceptibility to cracking could be significantly reduced with the presence of carbon in the alloy. The addition of carbon significantly influences the nature of the micro constituents formed during terminal solidification. The carbides are formed by eutectic type reactions which takes place over a range of temperatures in a multi-component alloys. Liquidus projections of Ni-Nb-C ternary systems were used by Dupont and Robino [117] and Radhakrisnan and Thompson [43] to describe the solidification behaviour of Fe-Ni-Cr superalloys and IN718 alloy, respectively. In order to describe the solidification sequence of IN-738 LC superalloy, Ojo et al [83,118] developed a psuedo-ternary solidification diagram, which was based on Ni-Ti-C ternary diagram developed by Backerned [119]. This pseudo-ternary diagram, as adapted by Sidhu et al [120] is shown in Figure 4-24. In this diagram, γ_0, is a FCC solid solution of substitutional alloying elements, and γ' and MC carbide phases. D is an invariant peritectic isotherm. The twofold saturation between γ'- γ_0 is represented by a mono-variant line AD, similarly, the saturations between γ_0 - MC and γ'- MC are depicted by DB and DC respectively.

According to this diagram, the carbon content determines the point where primary solidification path (Path 1 or Path 2) and the mono-variant line γ_0-MC (DB) would meet. The primary solidification path 2: Figure 4-24, with lower carbon content would intersect the mono-variant line closer to the point D resulting in a relatively large amount of liquid remaining for the formation of eutectics γ - γ',. This eutectic reaction would occur over a temperature range until the end of solidification.

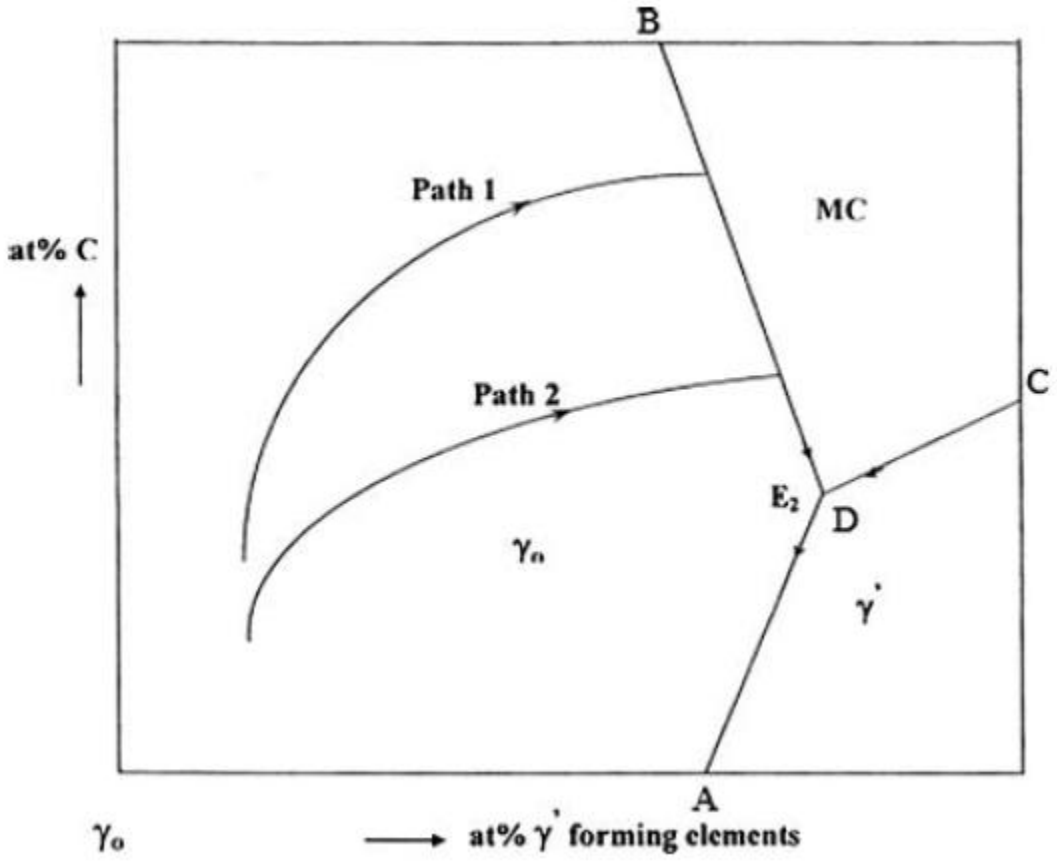

Figure 4-24: A pseudo-ternary diagram illustrating the carbon influence on solidification behaviour of an alloy [118]

However, with an increase in the amount of carbon, the primary solidification path is represented by Path 1 (Figure 4-24). γ and MC phases are formed by the following eutectic reaction: $L \rightarrow \gamma_0 + MC$ and represented by the two-fold saturation line BD. In this condition, the interdendritic liquid is enriched in γ′ forming elements (k > 1) which include Ti, Ta, Nb, Al. All of these are also carbide formers. Thus, γ and MC carbide phases form, as per the above equation, over a range of temperatures until it reaches a peritectic point D after which γ - γ′eutectic transformation takes place. A significant amount of the terminal liquid is consumed by the formation of γ and MC carbide phases, and hence, less liquid is available for the γ - γ′ eutectic transformation. In IN-738 LC, the MC carbides are formed at a much higher temperature which is almost near the liquidus temperature. Thus the formation of MC carbides also decreases the solidification temperature range, ΔT. Therefore for carbon bearing alloys such as IN 738, a small volume of interdendritic liquid is present in the terminal solidification stage such that little or no γ - γ′ eutectic form. Another scenario, which is when the carbon content is negligible or even carbon-free, the primary solidification path shifts very close to the peritectic point which results in comparatively significant amounts of liquid to be present at D, that forms γ - γ′ eutectics until it solidifies. Formation of eutectic further increases the solidification temperature range, ΔT. Thus, a greater solidification temperature range means a greater susceptibility to cracking. Solidification cracking in electron beam welded PWA1480, a carbon free single crystal superalloy, was related to the formation of γ - γ′ eutectic constituents during the last stages of solidification [110]. SC IN-738 LC contains 0.11 wt% carbon, which is relatively high when compared to other superalloys.

The presence of carbon would therefore produce small amounts of interdendritic liquid during the terminal stages of solidification and promote the formation of solid-solid bridges, which may lead to reduction in solidification cracking.

4.4 Effect of Pre-Weld Heat Treatment on HAZ Microfissuring

As discussed in the previous section, HAZ microfissuring in the IN-738 LC alloy was reduced to a large extent by decreasing or completely eliminating grain boundaries. However, the manufacturing of service components with single crystal materials is not readily feasible due to the high costs involved and most of the engine parts are still made by using conventional solidification process or directional solidification process. However, DS and CS IN-738 LC superalloys are highly susceptible to HAZ microfissuring. Thus, their weldability needs to be improved. This could be achieved by using appropriate pre-weld heat treatment thereby modify the microstructure, local composition and chemical distribution of the alloys, to increase their ductility, and thus, enhance their weldability by obtaining a microstructure capable of relieving welding tensile stresses.

It is known from the literature that NHT, a heat treatment also known as NUMT has the capability of reducing HAZ cracking in laser welded CS IN-738 LC [121]. In this research, further examination was carried out on the use of this heat treatment in reducing cracking in DS and CS IN-738 LC and compared with another heat treatment process, the UMT, which has shown significant reduction in HAZ cracking of GTA welded IN-738 LC [122].

CS and DS IN-738 LC, subjected to UMT and NHT were welded under similar conditions. The results of the TCL measurements from 10 sections of each weldment in the HAZ measured and presented in Figure 4-25.

The results show that cracking in HAZ cracking is significantly reduced in NHT sample opposed to UMT laser welded DS and CS IN-738 LC.

Based on prior studies, the liquation cracking in HAZ results from two main factors: mechanical and metallurgical factors. Mechanical factors corresponds on cooling tensile stresses generated during the weld thermal cycle due to the difference in thermal expansion and contraction coefficients between the different regions of the HAZ. The metallurgical factors corresponds to the susceptibly of this microstructure to crack under the above mentioned tensile stresses. The amount of intergranular liquid that formed extensively affected alloy resistance to microfissuring. Furthermore, the time taken for the grain boundary liquid to solidify can be expected to be influenced by the volume of liquid formed on the grain boundaries. This in turn influences the solid - liquid interface and its ability to resist the on cooling tensile stresses that are generated during a thermal cycle. According to Miller and Chadwick [123], the tensile stress required to overcome the surface tension (γ_{sl}), at the solid- liquid interface on grain boundary that contains a liquid film of thickness h, is given by the following equation:

$$\sigma = (2\gamma_{sl})/h$$

The inference from this equation is that an increase in the thickness of the intergranular liquid film reduces the amount of stress that would induce the initiation of cracks at a solid - liquid interface. The re-solidification of the liquid film could be possible with solute segregation that would further increase the range of solidification temperature. In addition, the accumulation of on-cooling tensile stresses takes place. Thus, the time required for the grain boundary liquid film to solidify is also very crucial as solidification of the solid- liquid interface should be completed before substantial amounts of on-cooling tensile stress are generated which could cause cracking.

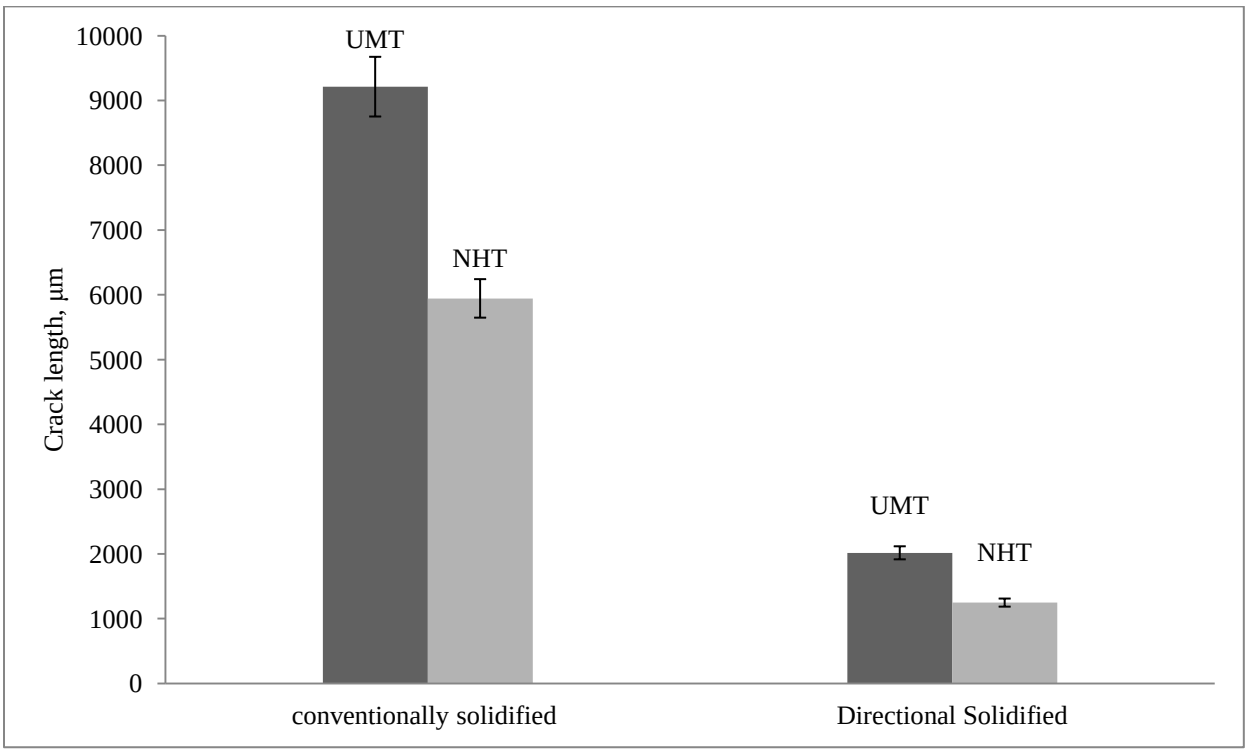

Figure 4-25: A graph illustrating HAZ cracking in UMT and NHT conditions for CS and DS IN-738 LC

Microfissuring occurs when tensile stresses developed during weld cooling exceed the available strength of the liquated grain boundaries. Therefore, any factor that increases intergranular liquid's thickness would increase susceptibility to cracking. Two major factors that contribute towards grain boundary liquation are segregation of low melting phases (particularly borides) and constitutional liquation of solidification microconstituents (including primary strengthening phase γ′ and MC carbides).

As mentioned above, the type of cracking and the composition of the resolidified microconstituents is similar in both NHT and UMT conditions, although NHT has significantly less cracking when compared to UMT. It is imperative to clearly understand resistance to microfissuring with the use of the NHT. Also, it is important to understand the onset of liquation and the nature of the intergranular liquid that forms in both NHT and UMT for CS IN-738 LC. Therefore, carefully planned simulations of the weld heating thermal cycle were performed by using a Gleeble thermo-mechanical simulator. The parameters used were discussed in Chapter 3.

The microstructural examination of the UMT simulated sample showed constitutional liquation of secondary solidification constituents at a simulation temperature of 1150^0C with a hold time of 1s, as seen in Figure 4-26. Cluster of boron rich phases were observed along the grain boundaries which are formed by the decomposition of boride particles due to rapid heating. At the same simulation temperature, the re-solidification of liquid was observed to occur in the vicinity of the carbide particles (adjacent surface of the carbide particles).There was also significant liquation of the γ’ precipitate particles in the interdendritic regions. Samples rapidly heated to 1180^0C and 1200^0C temperature showed complete dissolution of intergranular γ’ particles and considerable liquation of the intragranular γ’ precipitates.

a) At 1150^0C

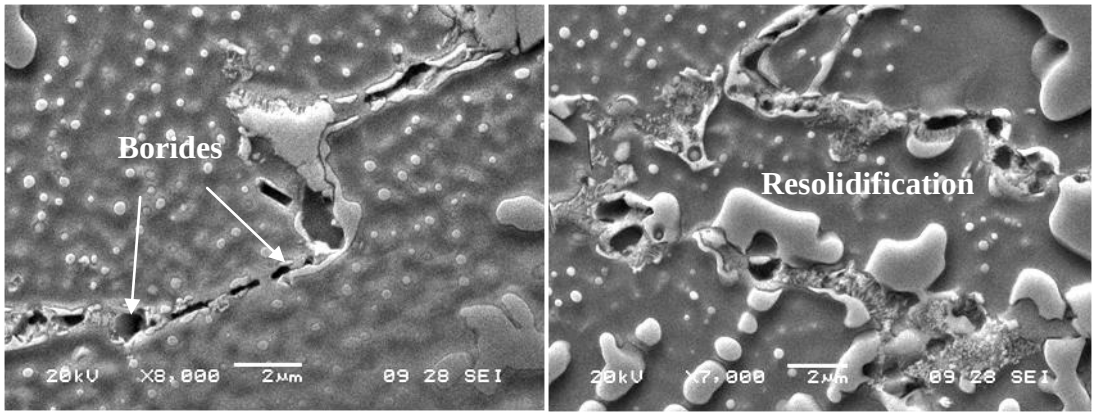

b) At 1180^0C

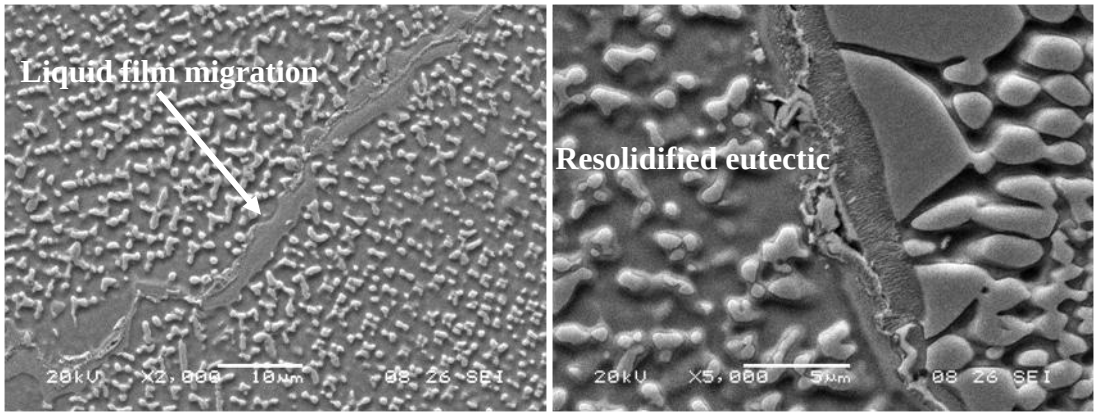

c) At 1200^0C

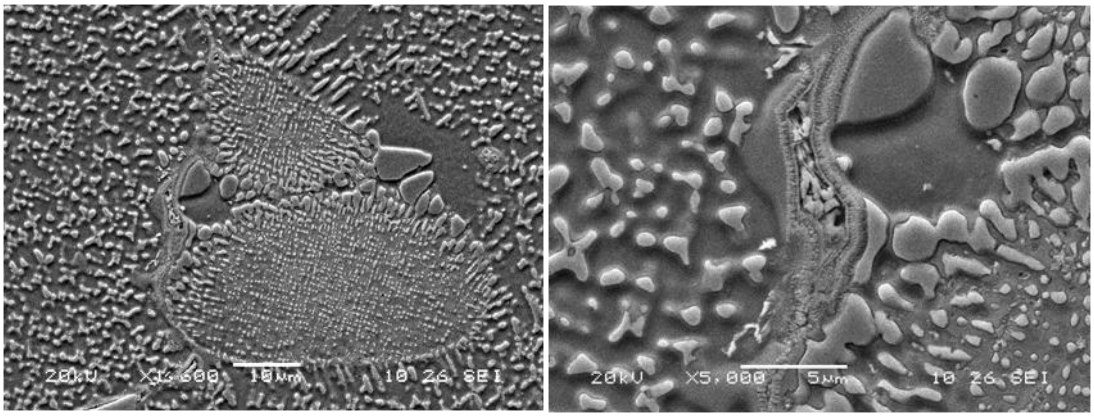

Figure 4-26: SEM micrograph of UMT samples simulated at various temperatures.

A microstructural analysis of the Gleeble simulated samples of NHT treated at peak temperatures are shown in Figure 4-27, the γ′ precipitates present in the matrix are dissolving into the solid solution and intergranular regions were not significantly liquated as the discrete coarse γ′ particles present along the grain boundaries did not appear to be affected by the thermal cycle. However, a thin film that is connected to the grain boundary can be observed. Upon increasing the peak temperature to 1180^0C, constitutional liquation of the γ′ particles was observed, but no significant intergranular liquation. Upon further increasing the peak temperature to 1200^0C, re-solidification was observed to occur near eutectics and carbides. However, in the NHT samples, boride phases were not observed to be present in the intergranular regions.

This microstructure is considerably different from that of the UMT treated sample. The total amount of liquation in the NHT sample was significantly less than that in the UMT sample. This is further evident upon a comparison of the micrographs, as shown in Figure 4-28.

The major factor that has been recognized to exacerbate the propensity for HAZ microfissuring in the UMT samples is the formation of boride particles along the grain boundary region. These phases formed along the grain boundary due to low solubility and size mismatch which favour their segregation into loosely packed regions. This non-equilibrium segregation of boron particles could occur during cooling. The extent of this type of segregation is significantly influenced by the thermal processing temperature (i.e. heat treatment temperature) and the incurred cooling rates [124]. As shown in Figure 4-28i, boron segregation is apparent at the grain boundaries in the UMT at a simulation temperature of 1150^0C, whereas no segregation was observed in the NHT sample at the same temperature. At a Gleeble simulation temperature of 1180^0C (Figure 4-28ii), a thick grain boundary film with presence of resolidified γ - γ′ eutectics was observed in the UMT sample.

During cooling from simulation temperature of 1200^0C (Figure 4-28iii) in UMT samples cracking occurred in the liquated region (i.e. freshly formed and alloyed zone). On the other hand, at the same simulation temperature of 1200^0C, the extent of intergranular liquation is substantially less in NHT samples.

Accordingly, the detrimental effects of the segregation of boride particles upon rapid heating include a reduction in the intergranular liquation temperature by sub-solidus reactions that involve the constitutional liquation of secondary phase particles. The segregation of boron particles lowers the melting point of the grain boundary with respect to the adjacent matrix and also enhances the liquation kinetics during thermal cycles, thereby significantly reducing the terminal solidification temperature during cooling. This increases the solidification temperature range which reduces the ductility and the resistance of the material to cracking. Thus, segregating grain boundaries have a very high tendency to liquate during welding, hence, resulting in HAZ microfissuring. Therefore, weldability is enhanced with the use of NHT by improving the material resistance to liquation.

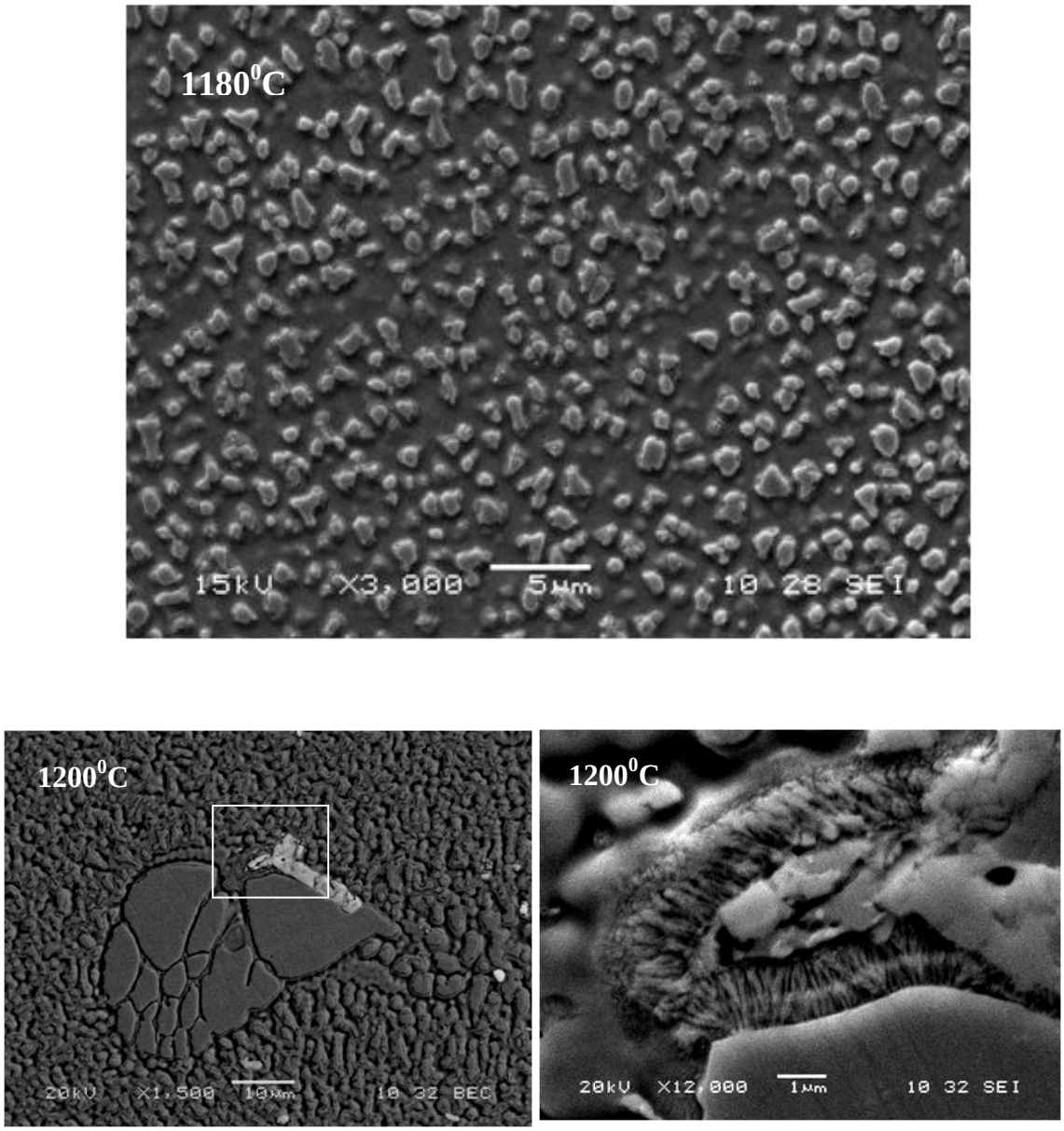

Figure 4-27: SEI micrographs of NHT sample simulated at various temperatures

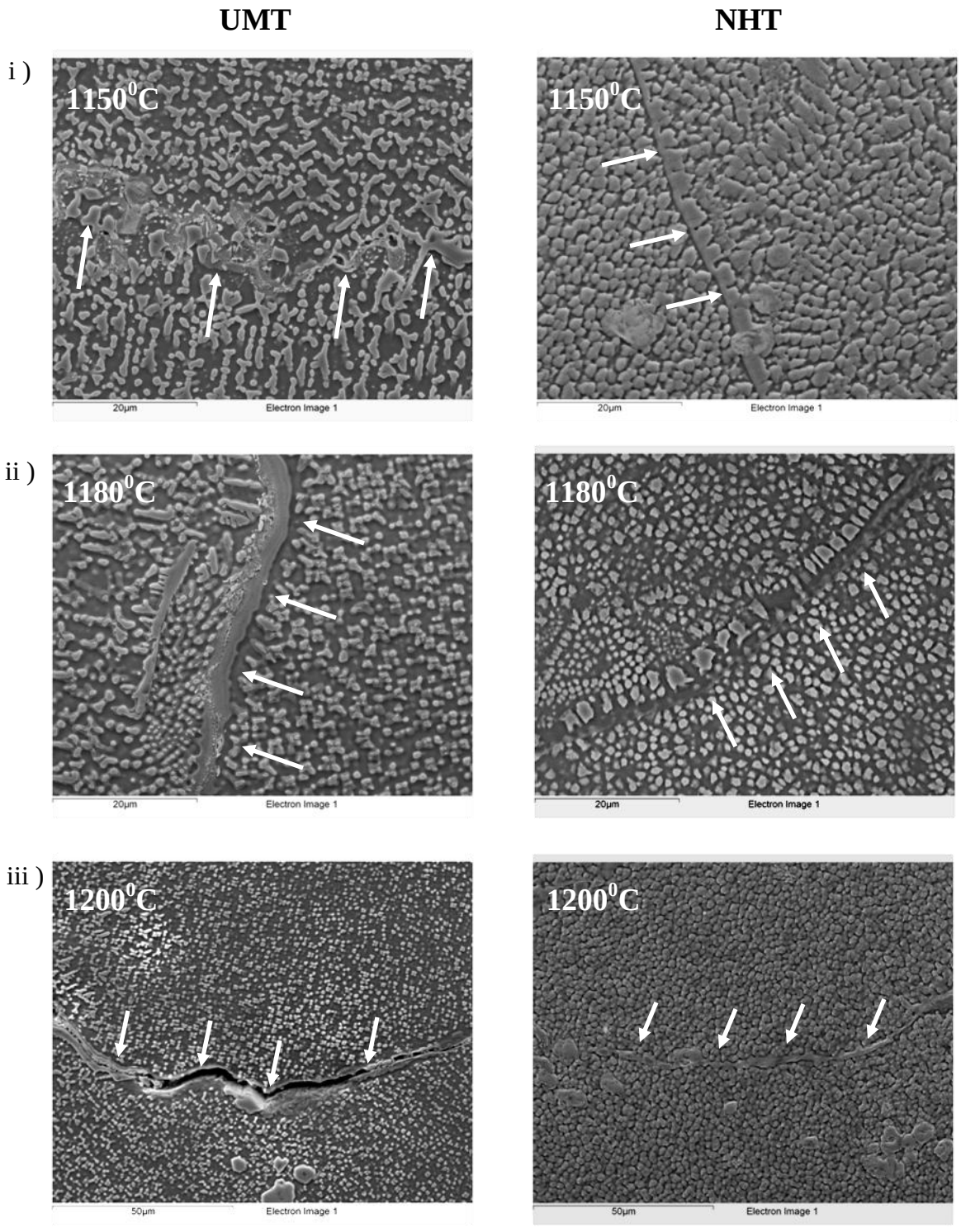

Figure 4-28: SEI micrograph showing grain boundary liquation in UMT and NHT sample simulated at i) 1150^{0}C ii) 1180^{0}C iii) 1200^{o}C

4.5 Post Weld Heat Treatment

IN-738 LC, experiences cracking during PWHT, also observed in similar high temperature superalloy strengthened by γ′ phase particles. It is a standard industrial practice that is usually applied before the welded components are taken into service to relieve residual welding stresses and homogenize the microstructure [65,125].

The PWHT of IN-738 LC involves its solutionizing at 1120^0C for 2 hours followed by air cooling and subsequently aging at 845^0C for 24 hours and then followed by air cooling. After welding, inhomogenity is incurred in the microstructure of the weldment, mainly due to γ′ precipitate particles. An inhomogenous microstructure is not capable of imparting reliable properties. Therefore, PWHT is significant because it can reinstate the microstructure and restore mechanical properties. To further understand the effect of different cast forms and different pre-weld heat treatment on PWHT behaviour of IN-738 LC, a comprehensive characterisation was carried out in the present study.

4.5.1 Post Weld Heat Treated Microstructure

An optical micrograph that shows the weld cross section of a PWHTed sample of SC IN-738 LC with the use of UMT is shown in Figure 4-29. The FZ after the PWHT contained extensive amounts of γ′ precipitated particles, MC carbides and $M_{23}C_6$ carbides. The SE micrograph of fusion boundary is shown in Figure 4-30. The fusion boundary is evident due to the presence of slight variations in the size of the γ′ particles present across the area. Also, a large number of smaller sized grains are present in the FZ with different orientations from those of the base metal grains. The primary γ′ particles are comparatively coarser in the HAZ base metal than in the FZ. A bi-modal size distribution of the coarse primary and fine spherical secondary γ′ particles was

observed in a higher magnification SE image shown in Figure 4-31. The interdendritic regions consist of the coarse γ′ particles, MC carbides and fine linked $M_{23}C_6$ carbide particles. Due to segregation during solidification, γ′ forming elements segregate into the interdendritic regions. There is an increase in the Al + Ti concentration in the interdendritic regions which inherently increases the γ′ solvus temperature. This consequently causes precipitation of the γ′ particles within the interdendritic regions at a much higher temperature. The precipitation of secondary γ′ particles occurs during the solutionizing treatment and subsequent aging treatment coarsens the primary and secondary γ′ particles. $M_{23}C_6$ carbide particles are formed during the aging treatment by the precipitation reaction from a carbon supersaturated γ matrix.

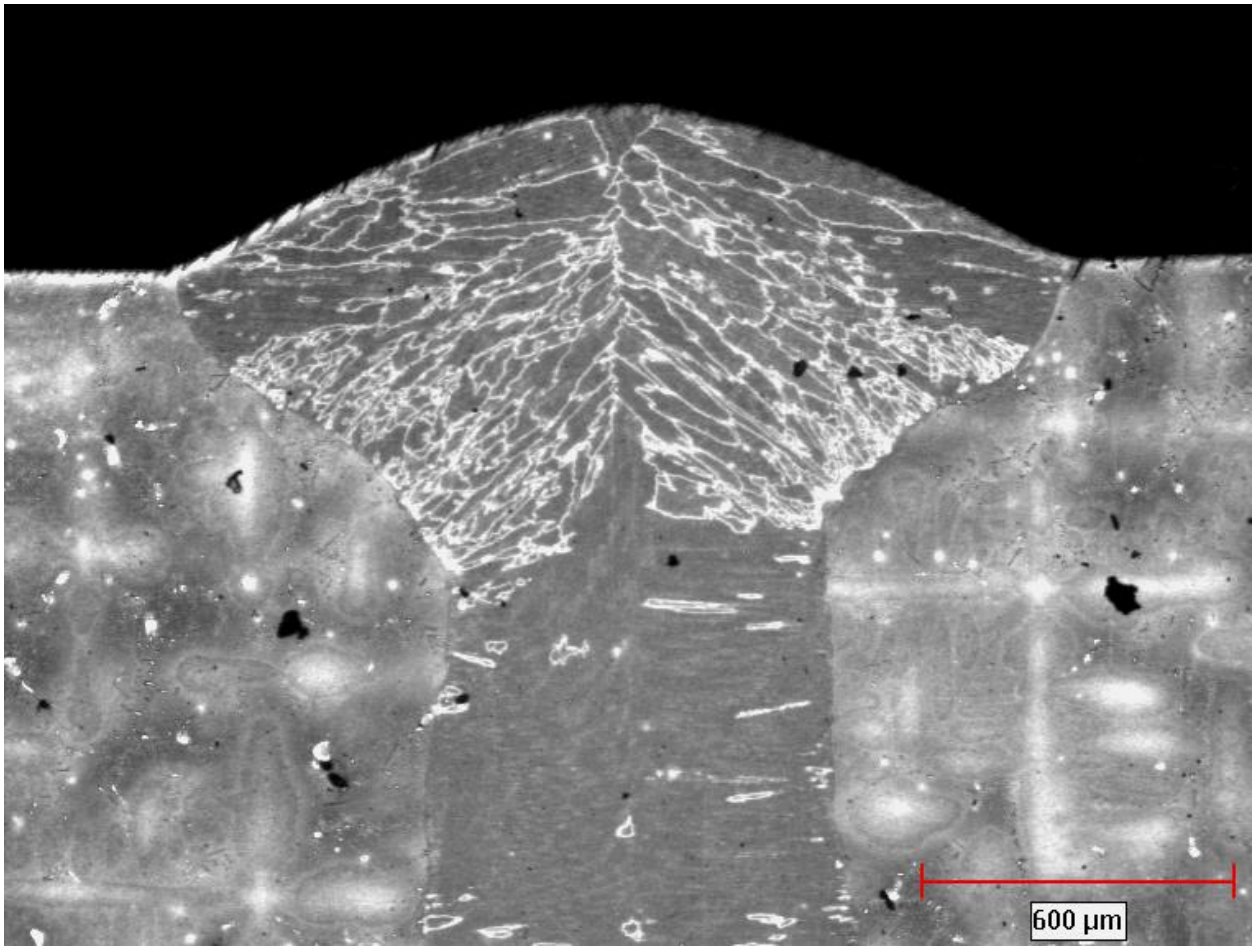

Figure 4-29: Weld profile of PWHTed SC IN-738 LC

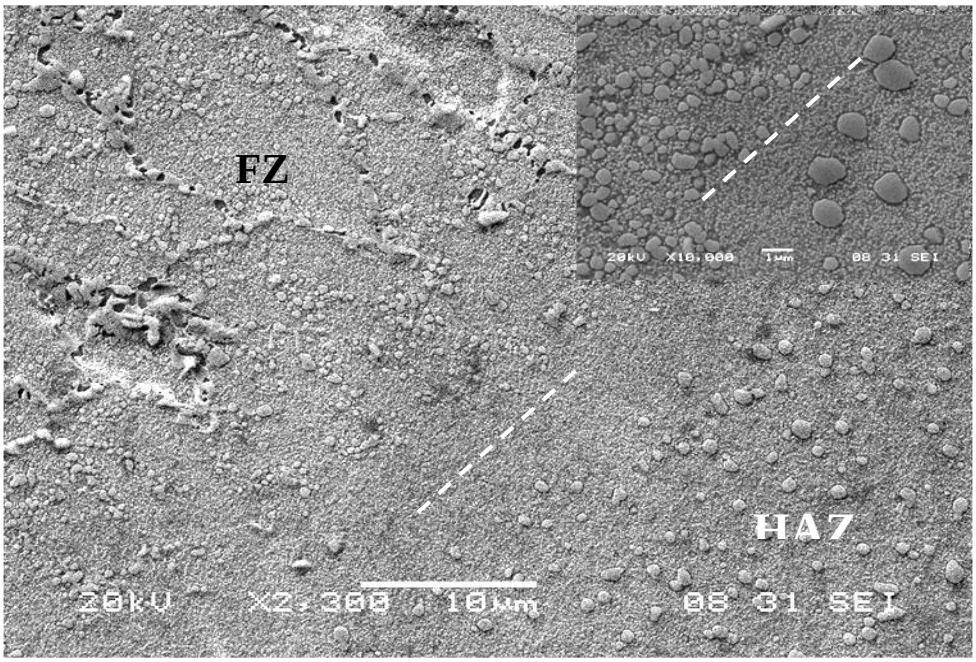

Figure 4-30: SEI micrograph showing the fusion boundary of a PWHTed CS IN-738 LC

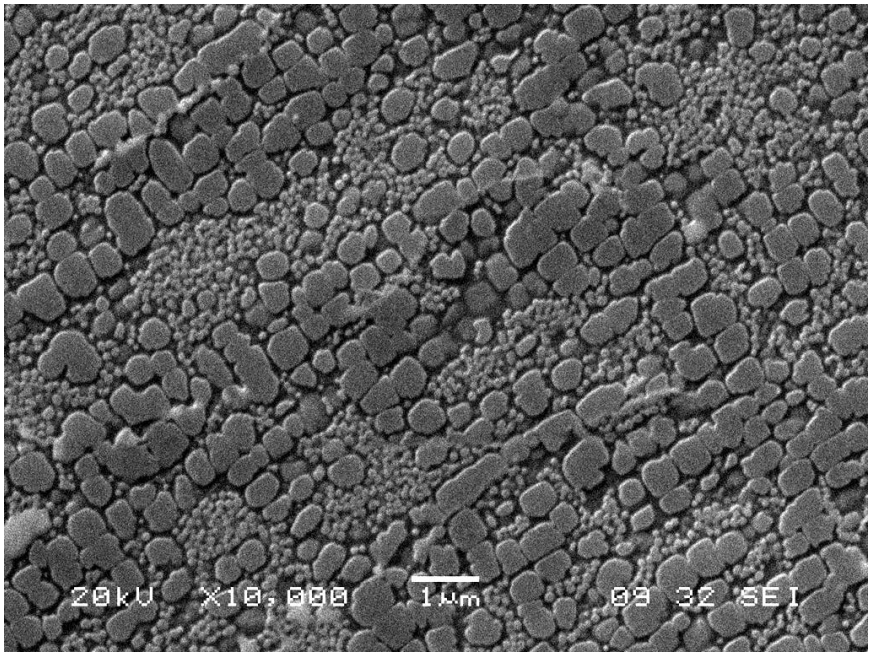

Figure 4-31: SEI micrograph showing the bi-modal distribution of γ′ in fusion zone

4.5.2 Post Weld Heat Treatment Cracking

Table 4-2 lists the TCLs measured in HAZ after PWHT. There was no significant increase in TCL observed in the as-welded and after PWHT. The major factors that contributed to cracking are the different stresses developed during the PWHT cycle. These different stresses include: thermal, residual, and aging-contraction stresses [71]. These stresses are preferentially concentrated in the HAZ region. The magnitude of the stresses developed is significantly influenced by mechanical and metallurgical factors. The metallurgical factors include: grain size, properties of the grain boundary and the pre-weld condition of the base metal. These factors will be discussed in the following section.

The cracks observed in the samples after PWHT were intergranular, with irregular, zig-zag morphology and also observed to be associated with various phases (Figure 4-32). The various phases present in the vicinity of the crack include MC carbides, fine γ' precipitate particles and $M_{23}C_6$ carbides. Only a few cracks were observed to be formed in the fusion zone, and most of the cracks were observed to be formed along the grain boundaries in the HAZ base metal region. The cracks observed were present in the weldment prior to PWHT i.e. they were formed during welding. The cracking during PWHT in the IN-738 LC superalloy, as mentioned in the literature is due to the occurrence of melting during the solutionizing treatment which increases susceptibility to cracking during the subsequent PWHT cycle [97].

Table 4-2: Total crack length measurements in HAZ of PWHTed CS, DS, and SC IN-738 LC

HAZ Micro-fissuring				
	UMT		NHT	
	As-Welded	PWHT	As-Welded	PWHT
DS IN-738 LC	2771	3253	1348	1248
CS IN-738 LC	9214	8930	5945	6023
SC IN-738 LC	0	0	0	0

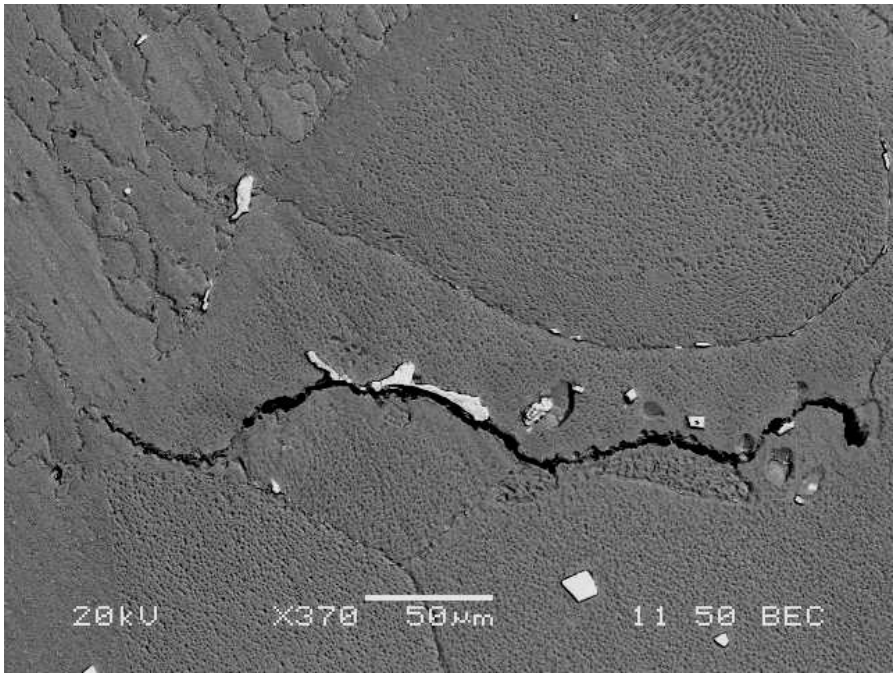

Figure 4-32: SEI micrograph illustrating the HAZ microfissuring in PWHTed IN-738 LC

4.5.2.1 Effect of Grain Boundaries on PWHT Cracking

Figure 4-33 is a graph that plots the comparison of the TCLs measured in the HAZ after PWHT for CS and DS IN-738 LC. It can be observed that the extent of cracking after PWHT is reduced with a reduction in the number of grain boundaries. The PWHT of SC IN-738 LC after UMT shows no cracking. The least amount of HAZ cracking can be observed in DS IN-738 LC in comparison to CS IN-738 LC for both UMT and NHT after PWHT. The HAZ intergranular regions are the most heterogeneous which show non-uniform deformation during stress relaxation and result in cracking during PWHT due to localised concentrations of strain. Therefore, a reduction in the grain boundary area also reduces the extent of cracking during PWHT. Moreover, as mentioned in Section 4.3, decrease in the number of grain boundaries that intersecting the FZ reduces cracking for the as welded condition also holds true for PWHT.

4.5.2.2 Effect of Heat Treatment on PWHT Cracking

Figure 4-34 compares the TCLs measured in the HAZ after PWHT for CS and DS IN-738 LC subjected to UMT and NHT. It can be seen from the graphs that HAZ cracking after PWHT is comparatively lower for the IN 738 superalloy that underwent NHT as opposed to the superalloy that underwent UMT for both the CS and DS cast forms. The pre-weld heat treatment condition of the base metal plays an important role in PWHT cracking susceptibility [71]. The reduced cracking phenomenon in the as-welded condition of DS IN-738 LC continued after PWHT. The as-welded CS IN-738 LC was already compromised before the PWHT, and resulted in more cracking. Extensive cracking in CS can also be due to more liquation observed in the as- welded condition, which could have made the microstructure more susceptible to cracking.

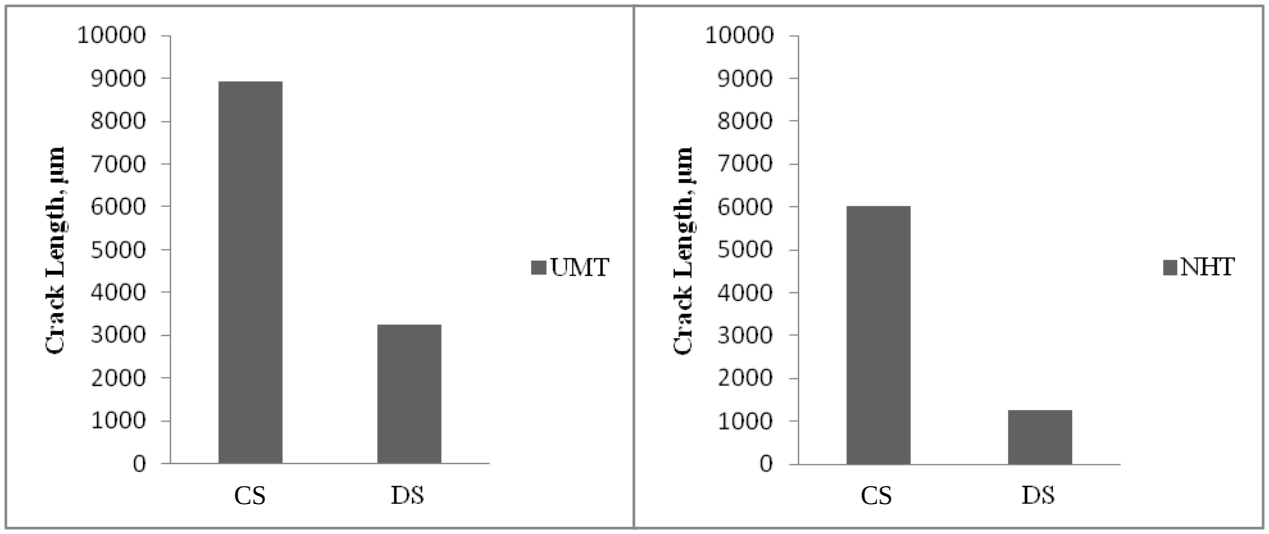

Figure 4-33: Graphs illustrating the effect of grain boundaries on HAZ cracking after PWHT.

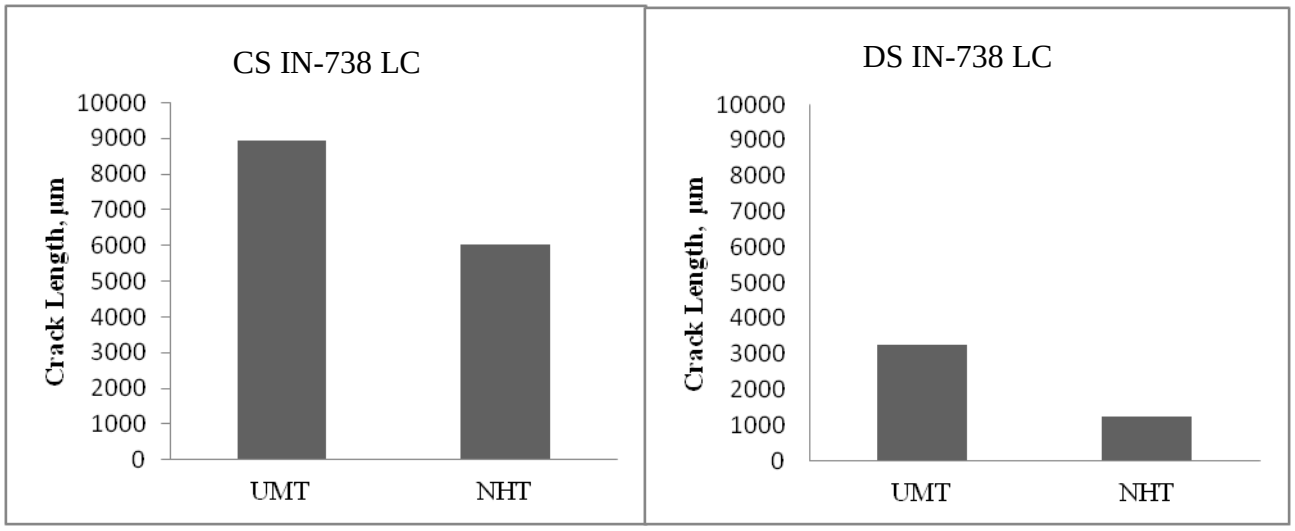

Figure 4-34: Graphs illustrating the effect of heat treatment on HAZ cracking after PWHT

By optimizing the pre-weld heat treatment, optimum ductility was imparted onto a material, thus improving its inherent resistance to cracking during welding and after PWHT. Therefore, reduction in cracking in the as welded condition further reduced the number of sites that are susceptible to cracking during PWHT.

Chapter 5.Conclusions

The following are the major conclusions of the present research:

1) HAZ intergranular liquation cracking was caused by constitutional liquation of secondary solidification microconstituents (MC carbides and γ - γ′ eutectics) and phases with low melting point (which include borides and sulphocarbides), as determined by the microstructural analysis of laser welded samples.
2) The HAZ cracking was observed to be reduced as the number of grain boundaries reduced in the following sequence, CS > DS > SC, as determined by quantitative evaluation of HAZ microfissuring in CS, DS, SC IN-738 LC alloy. This implies that as the number of grain boundaries intersecting the fusion boundary decreased, the susceptibility to HAZ microfissuring also reduced. Due to the absence of grain boundaries in SC IN-738 LC, there was no evidence of HAZ liquation cracking. Therefore, an increase in grain size obtained by directional solidification processing can lead to a reduction in the susceptibility of an alloy to intergranular liquation cracking.
3) The centerline cracking was not observed in FZ in the welds of SC IN-738 LC despite the presence of stray grains. Thus, the formation of stray grains is not the only factor that contributes to the formation of FZ cracks in the welds. The absence of centerline cracking is attributed to relatively high concentrations of carbon and rapid solidification rates experienced during laser welding, which suppress the formation of γ -γ′ eutectic micro-constituents and thereby, reduce susceptibility to cracking.
4) NHT further decreased the susceptibility to the HAZ microfissuring of IN-738 LC, as opposed to the use of UMT. An important factor that influenced microfissuring was the

formation of boride phases during UMT, which liquate at lower temperatures than at the equilibrium solidus temperature and thus increase the solidification temperature range which then increased the propensity for microfissuring.

5) Gleeble simulations on UMT samples showed formation of boride phases at the grain boundaries and non-equilibrium sub-solidus liquation, which occurs at much lower temperature (1150^0C), whereas the presence of boride particles along the grain boundaries was not observed in Gleeble simulated NHT samples, and thus, the extent of liquation was much lower even at higher temperatures.
6) The most effective combination of heat treatment and number of grain boundaries for reduction in the extent of HAZ cracking in laser welded IN-738 LC material was found to be DS IN-738 LC subjected to a pre-weld heat treatment by using NHT.
7) After PWHT, the propensity for HAZ microfissuring was not observed to significantly increase, and a similar pattern was observed during welding (i.e. CS > DS > SC, and NHT < UMT).
8) IN-738 LC is more susceptible to cracking during welding than PWHT as there was only a marginal change in the TCLs in the as welded and PWHTed material.

Chapter 6.Recommendations and Future Work

1) As observed in this research, the susceptibility for HAZ microfissuring during welding of IN-738 LC was reduced with the use of an optimized pre-weld heat treatment in CS and DS alloys. Further research should be done to evaluate the high temperature performance of the alloy in as-welded, including PWHTed samples to determine the mechanical properties of the material, and low-cycle, and high cycle fatigue, as well as, high temperature creep.
2) Further investigation to study the weldability improvement of the alloy with the use of filler alloy in combination with the NHT pre-weld heat treatment needs to be undertaken.

Chapter 7.REFERENCES

[1] M.B. Henderson, D. Arrell, R. Larsson, M. Heobel, G. Marchant, Nickel based superalloy welding practices for industrial gas turbine applications, Science and Technology of Welding and Joining. 9 (2004) 13-21.

[2] G.C. Bieber, R.J. Mihalisin, 2nd International Conference on the Strength of Metals and Alloys, Asilomer, ASM. 4 (1970) 1031.

[3] Alloy IN 738: A Technical Data, INCO, New York, 1 – 11,.

[4] M.J. Donachie, S.J. Donachie, Superalloys - A Technical Guide (2nd Edition), (2002).

[5] R.F. Decker, Strengthening mechanisms in nickel -base superalloys, Paper from steel - strengthening mechnisms, Climax Molybdenum Co., Greenwich, Conn., 1970, 147-171, 180. (1970).

[6] W. Hoffelner, E. Kny, R. Stickler, W.J. McCall, Effects of Aging Treatments on the Microstructure of the Ni-Base Superalloy IN-738, Z.Werkstofftech. 10 (1979) 84-92.

[7] C.T. Sims, N.S. Stoloff, W.C. Hagel, Superalloys II, Wiley, New York, 1987.

[8] W.F. Smith, Structure and properties of engineering alloys, New York : McGraw-Hill. (1981).

[9] R.C. Reed, The superalloys, (2006) 372.

[10] T.J. Garosshen, G.P. McCarthy, Low Temperature Carbide Precipitation in a Nickel Base Superalloy, Metall.Trans.A. 16A (1985) 1213-1223.

[11] W. Hagel, H. Beattie, Special Report No. 64, Iron and Steel Institute, London. (1959) 98-107.

[12] J.M. Larson, Carbide Morphology in P/M IN-792, Metall.Trans.A. 7A (1976) 1497-1502.

[13] R.C. Reed, The superalloys, (2006) 372.

[14] R.F. Decker, C.T. Sims, The Metallurgy of Nickel-Base Superalloys, Paul D. Merica Research Laboratory, 1972.

[15] C.H. Lund, Physical metallurgy of Nickel-base superalloys, (1961) 39.

[16] S. Kou, Welding Metallurgy, 2nd ed., Wiley-Interscience, Hoboken, N.J., 2003.

[17] ASM handbook. Volume 6, Welding, brazing, and soldering, Welding, brazing, and soldering.

[18] ASM Handbook, Volume 06A - Welding Fundamentals and Processes,.

[19] S.A. David, S.S. Babu, J.M. Vitek, Welding: Solidification and Microstructure, JOM. 55 (2003) 14-20.

[20] T. Koseki, Solidification and solidification structure control of weld metals, Welding International (UK). 16 (2002) 347-365.

[21] K. Easterling, Solidification Features of Weld Metal, Metallography and Interpretation of Weld Microstructures; Denver, Colorado; USA; 21-22 July 1985. (1985) 1-22.

[22] M.C. Flemings, Solidification processing, Metallurgical Transactions. 5 (1974) 2121-2134.

[23] T. DebRoy, S.A. David, Physical processes in fusion welding, Reviews of Modern Physics. 67 (1995) 85-112.

[24] W.F. Savage, Solidification, Segregation and Weld Defects, Weldments: Physical Metallurgy and Failure Phenomena; Bolton Landing, Lake George; N.Y.; 27-30 Aug.1978. (1978) 1-18.

[25] S. Katayama, Solidification phenomena of weld metals. II. Solidification theory, solute redistribution and microsegregation, Kei Kinzoku Yosetsu (Journal of Light Metal Welding and Construction) (Japan). 38 (2000) 12-24.

[26] S.A. David, J.M. Vitek, Correlation between solidification parameters and weld microstructures, International Materials Reviews. 34 (1989) 213-245.

[27] E. Scheil, Z. MetallK, 34 (1942) 70.

[28] W.F. Savage, B.M. Krantz, AN INVESTIGATION OF HOT CRACKING IN HASTELLOY X, WELD J. 45 (1966) 13S-25S.

[29] K.E. Easterling, Predicting Heat-Affected Zone Microstructures and Properties in Fusion Welds, Advances in Welding Science and Technology; Gatlinburg, Tennessee; USA; 18-22 May 1986. (1986) 177-185.

[30] Overview of Weld Discontinuities, ASM International, Materials Park, Ohio 44073, 1993, pp. 1073-1080.

[31] E.F. Bradley, Superalloys: A Technical Guide, ASM International, Metals Park, Ohio 44073, USA, 1988.

[32] S. Kou, Solidification and Liquation Cracking Issues in Welding, JOM. 55 (2003) 37-42.

[33] J.N. DuPont, Phase Diagrams and Microstructural Development in Welding Alloys, (1996) 11-11.

[34] S. Katayama, Solidification phenomena of weld metals. III. Mechanism and susceptibility of solidification cracking, Kei Kinzoku Yosetsu (Journal of Light Metal Welding and Construction) (Japan). 38 (2000) 13-23.

[35] Z. Feng, T. Zacharia, S.A. David, Thermal stress development in a nickel based superalloy during weldability test, Welding Journal (USA). 76 (1997) 470s-483s.

[36] J.C. Borland, Generalized theory of super-solidus cracking in welds (and castings), British Welding Journal. 7 (1960) 508-512.

[37] J.C. Borland, Fundamentals of Solidification Cracking In Welds.--I, Welding and Metal Fabrication. 47 (1979) 19-21.

[38] W.R. Apblett, W.S. Pellini, Factors which influence weld hot cracking, Welding Research Supplement. 33 (1954) 83s.

[39] A.R.E. Singer, P.H. Jennings, Hot-shortness of aluminum silicon alloys of commercial purity, Institute of Metals -- Papers. (1946) 16.

[40] P.H. Jennings, A.R.E. Singer, W.I. Pumphrey, Hot-shortness of some high-purity alloys in systems aluminium-copper-silicon and aluminium-magnesium-silicon, Institute of Metals -- Papers. (1948) 22.

[41] A.R.E. Singer, S.A. Cottrell, Properties of aluminium-silicon alloys at temperatures in region of solidus, (1946) 22.

[42] W.S. Pellini, Strain Theory of hot tearing, Foundry. 80 (1952) 125.

[43] B. Radhakrishnan, R.G. Thompson, Phase diagram approach to study liquation cracking in alloy 718, Metallurgical transactions. A, Physical metallurgy and materials science. 22 A (1991) 887-902.

[44] M.C. Chaturvedi, Liquation Cracking in Heat Affected Zone in Ni Superalloy Welds, Mater. Sci. Forum. 546-549 (2007) 1163-1170.

[45] J.J. Pepe, W.F. Savage, Effect of Constitutional Liquation in 18-Ni Maraging Steel Weldments, Welding Research Supplement. 46 (1967) 411-422.

[46] J.A. Brooks, Effect of alloy modifications on HAZ cracking of A-286 stainless steel, Weld J (Miami Fla). 53 (1974) 517s-523s.

[47] D.S. Duvall, W.A. Owczarski, Further heat affected zone studies in heat resistant nickel alloys, Weld J. 46 (1967) 423S-432S.

[48] B. Weiss, G.E. Grotke, R. Stickler, Physical metallurgy of hot ductility testing, 49 (1970) 471-s -487-s.

[49] R. Nakkalil, N.L. Richards, M.C. Chaturvedi, Microstructural characterization of INCOLOY 903 weldments, Metallurgical Transactions A (Physical Metallurgy and Materials Science). 24A (1993) 1169-79.

[50] B. Radhakrishnan, R.G. Thompson, The Effect of Weld Heat-Affected Zone (HAZ) Liquation Kinetis on the Hot Cracking Susceptibility of Alloy 718, Metallurgical Transactions B (USA). 24A (1993) 1409-1422.

[51] K.R. Vishwakarma, N.L. Richards, M.C. Chaturvedi, HAZ microfissuring in EB welded Allvac 718 Plus alloy, (2006) 637-47.

[52] O.A. Ojo, M.C. Chaturvedi, N.L. Richards, Liquation of various phases in HAZ during welding of cast Inconel*738LC, Materials Science and Technology. 20 (2004) 1027-1034.

[53] R.G. Thompson, Intergranular Liquation Effects on Weldability, Weldability of Materials; Detroit, Michigan; USA; 8-12 Oct.1990. (1990) 57-63.

[54] D. McLean, Grain Boundaries in Metals, 346 pp, Clarendon Press, Oxford, 1957.

[55] M. McLean, A. Strang, Effects of Trace Elements on Mechanical Properties of Superalloys, Met.Technol. 11 (1984) 454-464.

[56] E.D. Hondros, M.P. Seah,
Physical Metallurgy (Ed. R.W. Cahn) , 3rd edn ed., North Holland, Amsterdam, 1984.

[57] M.P. Seah, E.D. Hondros, Grain boundary segregation, Proceedings of the Royal Society of London, Series A (Mathematical and Physical Sciences). 335 (1973) 191-212.

[58] J.H. Westbrook, K.T. Aust, Solute hardening at interfaces in high-purity Lead -- 1, Acta Metallurgica. 11 (1963) 1151-1163.

[59] K.T. Aust, R.E. Hanneman, P. Niessen, J.H. Westbrook, Solute induced hardening near grain boundaries in zone refined metals, Acta Metallurgica. 16 (1968) 291-302.

[60] D.C. Paine, G.C. Weatherly, K.T. Aust, A STEM study of grain-boundary segregation in Al-6.5 wt.% Mg alloy, J. Mater. Sci. 21 (1986) 4257-61.

[61] K.T. Aust, Selective segregation at grain boundaries, Can. Metall. Q. 13 (1974) 133-143.

[62] R.L. Eadie, K.T. Aust, Solute induced grain boundary hardening in aluminum, Scripta Metallurgica. 4 (1970) 641-4.

[63] W.P. Hughes, T.F. Berry, A Study of the Strain-Age Cracking Characteristics in Welded RENE 41--Phase 1, Weld J. 46 (1967) 361S-370S.

[64] A.W. Dix, W.F. Savage, Factors influencing strain-age cracking in INCONEL X-750, WELD J. 50 (1971) 247S-252S.

[65] L.C. Lim, J. Yi, N. Liu, Q. Ma, Mechanism of post-weld heat treatment cracking in Rene 80 nickel based superalloy, Materials Science and Technology (UK). 18 (2002) 407-412.

[66] C.D. Lundin, R. Menon, Z. Chen, Post Weld Heat Treatment Cracking in a 710 HSLA Precipitation Strengthened Steel, Advances in Welding Science and Technology; Gatlinburg, Tennessee; USA; 18-22 May 1986. (1986) 559-569.

[67] J.E. Franklin, W.F. Savage, Stress Relaxation and Strain-Age Cracking in Rene 41 Weldments, AWS 55th Annual Meeting, Houston, Tex.American Welding Society, 2501 NW 7th St., Miami, Fla.33125.7-9 May 1974, 4 p. (1974).

[68] R. Thamburaj, J.A. Goldak, W. Wallace, The Influence of Chemical Composition on Post-Weld Heat Treatment Cracking in Rene 41, SAMPE Q. 10 (1979) 6-12.

[69] J.B. Carlton, M. Prager, Variables infuencing the strain-age cracking and mechanical properties of RENE 41 and related alloys, Weld Res Counc Bull. (1970) 13-23.

[70] T.J. Kelly, Welding Metallurgy of Investment Cast Nickel-Based Superalloys, Weldability of Materials; Detroit, Michigan; USA; 8-12 Oct.1990. (1990) 151-157.

[71] R. Thamburaj, J.A. Goldak, W. Wallace, Post-Weld Heat-Treatment Cracking in Superalloys, Int.Met.Rev. 28 (1983) 1-22.

[72] P.N. Quested, S. Osgerby, Mechanical Properties of Conventionally Cast, Directionally Solidified and Single-Crystal Superalloys, Mater.Sci.Technol. 2 (1986) 461-475.

[73] M.A. Taha, W. Kurz, Microsegregation of Nickel Base Superalloys, Zeitschrift fur Metallkunde. 72 (1981) 546-549.

[74] O.A. Ojo, N.L. Richards, M.C. Chaturvedi, On incipient melting during high temperature heat treatment of cast Inconel 738 superalloy, J. Mater. Sci. 39 (2004) 7401-7404.

[75] R. Rosenthal, D.R.F. West, Discontinuous gamma '-Precipitation in Directionally Solidified IN738LC Alloy, Mater.Sci.Technol. 2 (1986) 169-174.

[76] R. Rosenthal, D.R.F. West, Continuous gamma ' precipitation in directionally solidified IN738 LC alloy, Materials Science and Technology (UK). 15 (1999) 1387-1394.

[77] H.Q. Zhu, Z.Q. Hu, Y.X. Zhu, S.R. Guo, H.R. Guan, C.X. Shi, M. Morinaga, Y. Murata, Effect of phosphorus on solidification process and segregation of directionally solidified IN738 superalloy, Metall.Mater.Trans.B (USA). 26B (1995) 831-837.

[78] G.M. McColvin, Effects of Thermal Treatments on the Gamma-Prime Precipitate Morphology and Creep-Rupture Properties of Nimocast Alloy 738, Met.Sci. 11 (1977) 447-452.

[79] R.A. Steven, P.E.J. Flewitt, Microstructural Changes Which Occur During Isochronal Heat Treatment of the Ni-Base Superalloy IN-738, J. Mater. Sci. 13 (1978) 367-376.

[80] S.N. Tewari, M. Vijaykumar, J.E. Lee, P.A. Curreri, Solutal Partition Coefficients in Nickel--Based Superalloy PWA-1480, Materials Science and Engineering A. A141 (1991) 97-102.

[81] J.S. Zhang, Z.Q. Hu, Y. Murata, M. Morinaga, N. Yukawa, Design and Development of Hot Corrosion-Resistant Nickel-Base Single Crystal Superalloys by the d-Electrons Alloy Design Theory. I. Characterization of the Phase Stability, Metallurgical Transactions A (USA). 24A (1993) 2443-2450.

[82] R. Sallemark, Progress Report 2 Cost 50 Programme Sweden, (1975).

[83] O.A. Ojo, On liquation cracking of cast Inconel 738LC superalloy welds, ProQuest Dissertations and Theses. (2005).

[84] S.M. Bruemmer, R.H. Jones, M.T. Thomas, D.R. Baer, Sulphur induced fracture mode transition of nickel at cathodic potentials, Scripta metallurgica. 14 (1980) 1233-1237.

[85] W.C. Johnson, J.E. Doherty, B.H. Kear, A.F. Giamei, Confirmation of S Embrittlement of Ni Alloys, Scr.Metall. 8 (1974) 971-974.

[86] S. Floreen, J.H. Westbrook, Grain boundary segregation and the grain size dependence of strength of nickel-sulphur alloys, 17 (1969) 1175-1181.

[87] J.E. Doherty, A.F. Giamei, B.H. Kear, Importance of grain boundary morphology and cohesion on intergranular strength, Can. Metall. Q. 13 (1974) 229-236.

[88] W. Wallace, R.T. Holt, T. Terada, The nature of the sulfo-carbides observed in nickel-base superalloys, Metallography. 6 (1973) 511-26.

[89] E.P. Whelan, M.S. Grzedzielski, H-Phase Sulphocarbides and S in Ni-Base Superalloys, Metals Technology. 1 (1974) 186-190.

[90] M.K. Miller, J.A. Horton, W.D. Cao, R.L. Kennedy, Characterization of the effects of boron and phosphorus additions to the nickel-based superalloy 718, Journal De Physique. IV : JP. 6 (1996) 241-246.

[91] R. Vincent, Precipitation Around Welds in the Nickel-Base Superalloy, Inconel 718, Acta Metall. 33 (1985) 1205-1216.

[92] H.R. Zhang, O.A. Ojo, M.C. Chaturvedi, Nanosize boride particles in heat-treated nickel base superalloys, Scr. Mater. 58 (2008) 167-170.

[93] H.D. Brody, Segregation and structurein the weld zone, (1986) 83-91.

[94] R. Nakkalil, N.L. Richards, M.C. Chaturvedi, Fusion zone microstructure of electron beam welded incoloy 903, Scripta metallurgica et materialia. 26 (1992) 545-550.

[95] P.N. Quested, M. Mclean, Effect of Variations in Temperature Gradient and Solidification Rate on Microstructure and Creep Behaviour of IN 738LC, Solidification Technology in the Foundry and Cast House; Coventry; England; 15-17 Sept.1980. (1980) 586-591.

[96] R. Nakkalil, N.L. Richards, M.C. Chaturvedi, Fusion zone microstructure of electron beam welded incoloy 903, Scripta metallurgica et materialia. 26 (1992) 545-550.

[97] O.A. Ojo, N.L. Richards, M.C. Chaturvedi, Study of the Fusion Zone and Heat-Affected Zone Microstructures in Tungsten Inert Gas-Welded INCONEL 738LC Superalloy, Meatllurgical and Materials Transactions A. 37A (2006) 421-433.

[98] L.O. Osoba, R.G. Ding, O.A. Ojo, Microstructural analysis of laser weld fusion zone in Haynes 282 superalloy, Mater Charact. 65 (2012) 93-9.

[99] L. Liu, B.L. Zhen, A. Banerji, W. Reif, F. Sommer, Effect of melt homogenization temperature on the cast structures of in 738 LC superalloy, Scripta metallurgica et materialia. 30 (1994) 593-598.

[100] R.G. Thompson, D.E. Mayo, B. Radhakrishnan, The relationship between carbon content, microstructure, and intergranular liquation cracking in cast nickel alloy 718, Metallurgical Transactions A (Physical Metallurgy and Materials Science). 22A (1991) 557-67.

[101] Y. Nakao, K. Shinozaki, Hot cracking susceptibility of Ni-base superalloy weld zones, Proceedings of a Conference on High Temperature Materials for Power Engineering 1990. (1990) 1461-1461.

[102] W.A. Owczarski, D.S. Duvall, C.P. Sullivan, A model of heat affected zone cracking in nickel -base superalloys, Weld J. 45 (1966) 145S155S.

[103] C.S. Smith, Grains, phases, and interfaces: Interpretation of microstructure, (1948) 37.

[104] H. Grimmer, W. Bollmann, D.H. Warrington, Coincidence-site lattices and complete pattern-shift lattices in cubic crystals, Acta Crystallographica, Section A (Crystal Physics, Diffraction, Theoretical and General Crystallography). (1974) 197-207.

[105] H. Guo, M.C. Chaturvedi, N.L. Richards, G.S. McMahon, Interdependence of character of grain boundaries, intergranular segregation of boron and grain boundary liquation in simulated weld heat-affected zone in Inconel 718, Scripta Materialia (USA). 40 (1999) 383-388.

[106] M. Rappaz, A. Jacot, W.J. Boettinger, Last-stage solidification of alloys: Theoretical model of dendrite-arm and grain coalescence, Metall Mat Trans A Phys Metall Mat Sci. 34 A (2003) 467-479.

[107] X. Huang, N.L. Richards, M.C. Chaturvedi, Effect of grain size on the weldability of cast alloy 718, Mater. Manuf. Process. 19 (2004) 285-311.

[108] R.K. Sidhu, O.A. Ojo, M.C. Chaturvedi, Weld cracking in directionally solidified inconel 738 superalloy, Canadian Metallurgical Quarterly. 46 (2007) 415-424.

[109] R.K. Sidhu, O.A. Ojo, N.L. Richards, M.C. Chaturvedi, Metallographic and OIM study of weld cracking in GTA weld build-up of polycrystalline, directionally solidified and single crystal Ni based superalloys, Science & Technology of Welding & Joining. 14 (2009) 125-131.

[110] S.A. David, J.M. Vitek, S.S. Babu, L.A. Boatner, R.W. Reed, Welding of nickel base superalloy single crystals, Science and Technology of Welding and Joining (UK). 2 (1997) 79-88.

[111] J.M. Vitek, S.S. Babu, J.-. Park, S.A. David, Analysis of stray grain formation in single-crystal nickel-based superalloy welds, (2004) 459-465.

[112] T.D. Anderson, J.N. Dupont, Stray grain formation and solidification cracking susceptibility of single crystal Ni-Based Superalloy CMSX-4, Weld J (Miami Fla). 90 (2011) 27s-31s.

[113] M. Gaumann, C. Bezencon, P. Canalis, W. Kurz, Single-crystal laser deposition of superalloys: processing-microstructure maps, Acta Materialia (USA). 49 (2001) 1051-1062.

[114] S. Mokadem, C. Bezencon, A. Hauert, A. Jacot, W. Kurz, Laser Repair of Superalloy Single Crystals with Varying Substrate Orientations, Metallurgical and Materials Transactions A.Physical Metallurgy and Materials Science. 38A (2007) 1500-1510.

[115] J.M. Vitek, The effect of welding conditions on stray grain formation in single crystal welds - theoretical analysis, Acta Materialia. 53 (2005) 53-67.

[116] J.C. Borland, Generalized Theory of Super-Solidus Cracking in Welds (and Castings), British Welding Journal. (August 1960) 508-512.

[117] J.N. DuPont, C.V. Robino, Influence of Nb and C on the solidification microstructures of Fe-Ni-Cr alloys, Scr. Mater. 41 (1999) 449-454.

[118] O.A. Ojo, N.L. Richards, M.C. Chaturvedi, Study of the fusion zone and heat-affected zone microstructures in tungsten inert gas-welded INCONEL 738LC superalloy, Metall Mat Trans A Phys Metall Mat Sci. 37 (2006) 421-433.

[119] L. Backerud, B. Carlsson, R. Oskarsson, M. Mikus, Study of nickel-rich and cobalt rich corners of the systems Ni-Ti-C and Co-Ti-C, Scand J Metall. 3 (1974) 225-235.

[120] R.K. Sidhu, O.A. Ojo, M.C. Chaturvedi, Microstructural Analysis of Laser-Beam-Welded Directionally Solidified INCONEL 738, Metallurgical and Materials Transactions A. 38 (2007) 858-870.

[121] A.T. Egbewande, On improving laser weldability of inconel 738 superalloy through microstructural modification, ProQuest Dissertations and Theses. (2009).

[122] X.A. Thakur, Microstructural responses of a nickel-base cast IN-738 superalloy to a variety of pre-weld heat-treatments, ProQuest Dissertations and Theses. (1998).

[123] W.A. Miller, G.A. Chadwick, On magnitude of solid/liquid interfacial energy of pure metals and its relation to grain boundary melting, Acta Metallurgica. 15 (1967) 607-614.

[124] M.C. Chaturvedi, W. Chen, A. Saranchuck, N.L. Richards, The effect of B segregation on heat-affected zone microfissuring in EB welded Inconel 718, Superalloys 718, 625, 706 and Various Derivatives; Pittsburgh, Pennsylvania; USA; 15-18 June 1997. (1997).

[125] R.K. Sidhu, N.L. Richards, M.C. Chaturvedi, Post-weld heat treatment cracking in autogenous GTA welded cast Inconel 738LC superalloy, Materials Science and Technology. 23 (2007) 203-213.